ABSTRACT

Title of Document: DETERMINING THE AIR-SIDE PERFORMANCE OF SMALL-DIAMETER, ENHANCED TUBE-FIN HEAT EXCHANGERS THROUGH NUMERICAL AND EXPERIMENTAL METHODS

Dennis Nasuta, Master of Science, 2017

Directed by: Research Professor Yunho Hwang, Ph.D.

Department of Mechanical Engineering

New correlations for the air-side pressure drop and heat transfer coefficient (HTC) of slit and louver fin heat exchangers with 3-5 mm outer diameter tubes were developed based on Computational Fluid Dynamics (CFD) simulations of small, symmetric fin sections using Design of Experiments (DOE) techniques. The prediction accuracy of these CFD-based correlations was validated by experimental testing of 16 unique 5 mm slit and louver fin heat exchangers under a range of air velocities. The experimental results indicate that the proposed CFD-based correlation with correction factors for air-side pressure drop can predict 100% of the experimental observations with 20% error or less. After a new data reduction procedure accounting for fin conduction was implemented and a single correction factor applied, the HTC correlations could predict 98% of accepted test data with 20% error or less regardless of fin type.

DETERMINING THE AIR-SIDE PERFORMANCE OF SMALL-DIAMETER, ENHANCED TUBE-FIN HEAT EXCHANGERS THROUGH NUMERICAL AND EXPERIMENTAL METHODS

By

Dennis Nasuta

Thesis submitted to the Faculty of the Graduate School of the

University of Maryland, College Park, in partial fulfillment

of the requirements for the degree of

Master of Science

2017

Advisory Committee:

Research Professor Yunho Hwang, Chair/Advisor

Professor Jungho Kim

Professor Bao Yang

Dedication

For Cara

Acknowledgements

I can’t even begin to express my deep gratitude for my partner, Cara Marcy, and my family for their encouragement, inspiration, and patience throughout this process. I want to thank my mentors at CEEE, Dr. Radermacher, Dr. Aute, and Dr. Hwang, who have provided me with invaluable guidance and opportunities to develop in my career.

This work was largely completed with funding from the International Copper Association (ICA) and I would like to thank Mr. Hal Stillman for his support throughout this effort. The entire team at Optimized Thermal Systems (OTS) has provided me with a great deal of assistance in completing this project. Dr. Shekhar Sarpotdar performed outstanding work developing CFD models of the slit and louver fins. This work would also not be possible without the expertise and efforts of Cara Martin, Song Li, Bo Hoffman. Additional thanks to all of my colleagues at Optimized Thermal Systems.

Table of Contents

List of Figures

List of Tables

1. Introduction

In recent years, the optimization of heat transfer and energy systems has been driven by increasing pressures to minimize environmental impacts while minimizing costs. Heat exchangers are critical to the performance of thermal systems across a wide range of industries including residential and commercial heating, ventilation, air conditioning, and refrigeration (HVAC&R); automotive cooling and heating; and energy generation and industrial processes, and their optimization can yield significant improvements in energy-efficiency and reductions in costs and environmental impacts.

The International Panel on Climate Change (IPCC) concluded that buildings account for 32% of global final energy use and 19% of energy-related greenhouse gas emissions (Lucon et al., 2014). Heating and cooling applications that utilize heat exchangers consume a substantial portion of that value; space heating alone is estimated to account for 32-34% of global building energy. Global energy consumption may double or triple by mid-century and space heating and cooling demands are expected to increase by approximately 180% by 2050 compared to 2010. In the US, space heating, water heating, air conditioning, and domestic refrigeration account for 7.1 quadrillion BTUs of energy consumption in residential homes, or about 70% of total residential energy consumption (US Energy Information Administration, 2009). Furthermore, direct emissions from these HVAC&R applications release greenhouse gases (GHGs) into the atmosphere; in 2011, hydrofluorocarbons (HFCs) accounted for the release of the equivalent of 129 million metric tons of CO_2, about 2% of US total GHG emissions (US EPA, 2013). Heat exchanger design and optimization can improve the energy-efficiency of HVAC&R

equipment to reduce indirect CO_2 emissions as well as reduce the charge of refrigerant to reduce direct emissions and enable low-GWP fluids.

Tube-fin heat exchangers, composed of round tubes through sheets of fins, are used in a variety of applications for transferring heat, including widespread use throughout the HVAC&R industry. Conventionally, tube-fin heat exchangers in these industries are constructed from tubes having outer diameters of 7 mm or more, but recent work has shown that heat exchangers with smaller diameter tubes (less than or equal to 5 mm) can achieve superior performance with reduced material costs. As an example, a 5 mm outer diameter (OD) tube-fin heat exchanger is shown in Figure 1.

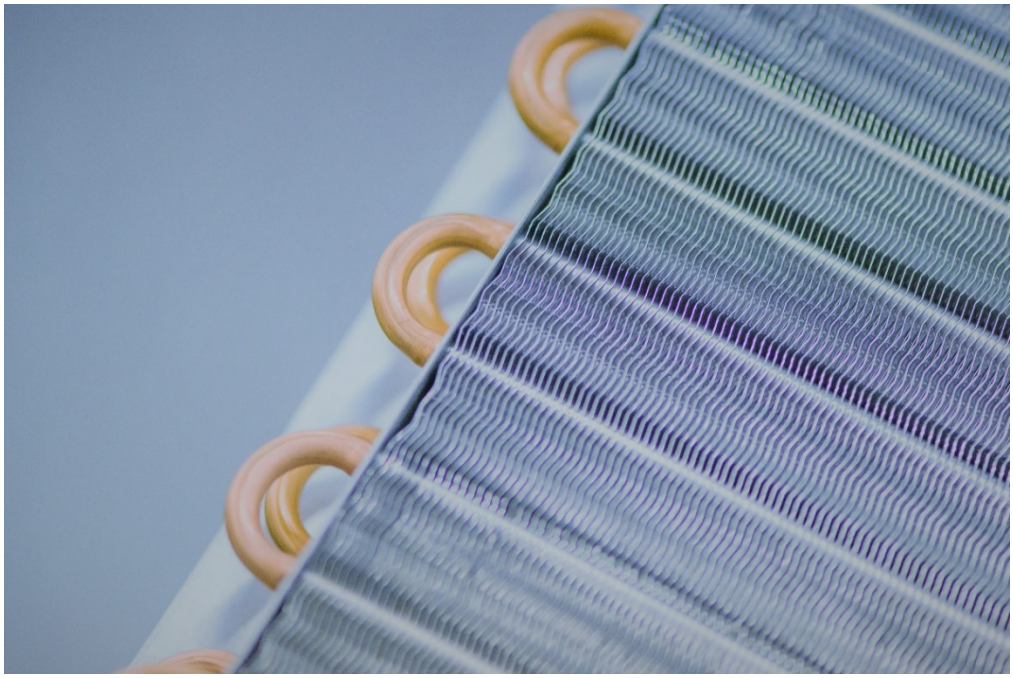

Figure 1: Tube-fin heat exchanger with 5 mm OD tubes

In the HVAC&R industry, enhancements to fin surfaces have been introduced for decades to improve the thermal-hydraulic performance of heat exchangers. Fins can be altered with wavy patterns, vortex generators, louvers, and slits, among many other configurations. This study focuses on heat exchangers with louver and slit enhancements.

The design of a new heat exchanger must often satisfy a number of performance, cost, safety, and manufacturing requirements and is interdependent with the other components of the vapor compression system. In order to prevent costly and time-consuming trial and error in the laboratory, simulation tools are utilized to predict the performance of heat exchangers. In order to predict overall heat exchanger performance, the heat transfer and pressure drop performance of the tube and fin surfaces must be known. For decades, researchers have developed correlations to predict the heat transfer coefficients and pressure drops of heat transfer surfaces from experimental testing. The goal of such studies is to test a wide range of different tube or fin geometries and operating conditions such that a mathematical model for the performance can be developed which can predict performance of not only the tested designs, but also other heat exchanger configurations within the tested range of parameters and conditions. Since many manufacturers produce very different geometries of tubes and fins, this generality is crucial for a correlation to be applicable to the heat exchanger designer.

In recent years, computational fluid dynamics (CFD) has been used increasingly to simulate heat transfer and fluid flow problems. While far more computationally expensive than calculating performance from an empirical correlation, CFD allows the user to determine the heat transfer and flow behavior of new, untested geometries. Due to the high cost and time-consuming nature of experimental correlation development, and

the ever-improving accuracy and speed of CFD simulations, it is desirable to develop new correlations based on CFD simulations to minimize experimental efforts and develop correlations that are applicable across a very wide range of geometry and operational parameters. However, because this process is relatively new, it is also necessary to validate the predictions made by the CFD simulations with experimental data to confirm their accuracy.

2. Objectives

This thesis aims to meet several key objectives with applications for researchers studying new air-side heat transfer surfaces as well as product designers in the industry.

1. The first objective of this work is to adequately summarize the procedure followed to develop CFD-based correlations for the air-side thermal-hydraulic performance of slit- and louver- fin heat exchangers. This process is documented here so that it can be used as a reference for developing future correlations in this manner.
2. A simple and automated procedure for developing new correlations using regression tools in MATLAB is also suggested. The aim is to demonstrate that the challenging and time-consuming approach using dimensional analysis can be replaced with a simpler linear regression model that requires little time to develop and can produce new correlations with a faster turnaround time.
3. Experimental results are presented to validate the predictions from these CFD simulations and demonstrate the accuracy of this approach for correlation development. Any deviations between theoretical predictions and observations may indicate shortcomings in the predictive accuracy of the CFD-based approach or uncertainties in experimental values.
4. The result of this effort is a set of correlations that professionals in the industry can use to evaluate the air-side performance of 3-5 mm slit- and louver-fin heat exchangers. These correlations can be used with a low computational cost, but were derived from a large number of accurate CFD simulations and were validated against experimental data. The goal is to provide the necessary tools for

heat exchanger designers to evaluate and optimize these heat exchanger types in order to meet goals of enhanced efficiency, reduced size and weight, reduced refrigerant charge, and reduced cost. The extensive range of these correlations is intended to allow for the evaluation of not only the current state of the art, but also future designs that are not currently manufactured.

3. Background

Accurate modeling of heat exchangers is often achieved through the use of published heat transfer and pressure drop correlations for the air- and refrigerant-side surfaces of the heat exchanger. Researchers have been experimentally testing and publishing these types of heat transfer and pressure drop correlations since the early to mid-20th century, however testing was usually limited to heat exchangers with tubes having greater than 7 mm outer diameter. Several researchers have conducted experiments and simulation studies to characterize the air- and refrigerant-side performance of small diameter tube-fin heat exchangers. While many publications establish the performance of some specific configurations of tubes and fins, most lack the generality required to evaluate and optimize the full range of potential designs.

3.1 Enhanced surfaces

For decades, heat exchangers have been designed with a variety of surface enhancements on both the interior of tubes and exterior surfaces of fins intended to increase heat transfer performance. The working principle of such enhancements is to alter the air or refrigerant flow behavior in order to achieve improved heat transfer without causing an unacceptable increase in pressure drop.

3.1.1 Tube enhancements

Internal enhancements are implemented in tubes to improve heat transfer performance and reduce heat exchanger costs. The basic working principle of such designs is that internal geometries such as fins or other protrusions will increase the internal surface area and increase turbulence in the flow, thereby increasing heat transfer. When two-phase refrigerant flows through enhanced tubes, they can extend the length of the heat

exchanger for which the refrigerant is in the annular flow regime, where heat transfer is greatest, resulting in improved performance (Liebenberg and Meyer, 2006). Tube-fin heat exchangers commonly use smooth tubes (no enhancements), as opposed to helical-microfin, and herringbone fins (shown in Figure 2). Smooth tubes are often the lowest cost, but helical microfin tubes can be extruded or drawn while herringbone fins must be welded along the tube length.

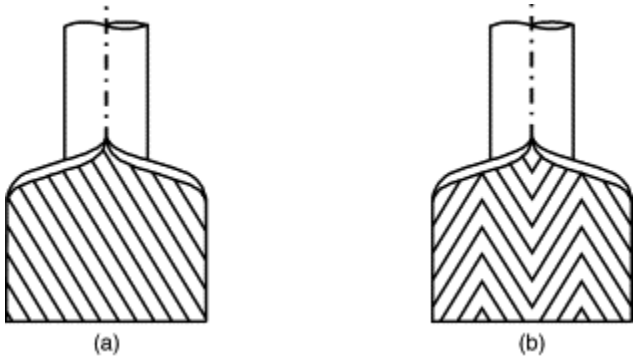

Figure 2: Helical microfin (left) and herringbone (right) enhanced tubes (Cavallini, 2003)

3.1.2 Fin enhancements

Tube-fin heat exchangers have been produced with enhanced fin geometries including wavy, slit, and louver fins (pictured in Figure 3) for many years. Surface enhancements like wavy fins increase fin surface area and turbulent heat transfer compared to flat fins by the nature of their geometry. Slit and louver fins are quite common in the modern HVAC&R industry due to their high heat transfer performance that results from the interruption and re-establishment of boundary layers along the surface of the fin. Air-side heat transfer and pressure drop correlations have been developed and published through experimental work. Wang (2000a, 2002) developed correlations for herringbone

and smooth wavy fins in inline and staggered arrangements. Slit fin (Wang et al., 2001) and louver fin (Wang et al., 1999) heat transfer and pressure drop correlations were also developed. However, all of these published correlations are limited to tube diameters approximately 7 mm and greater as summarized in Table 1. Air-side thermal resistances are much higher than those from conduction and refrigerant-side convection and therefore air-side performance is the most important factor in overall heat exchanger thermal performance. Accurate modeling of air-side heat transfer is essential for calculating overall heat transfer and air-side pressure drop is critical in fan/blower design. Heat exchangers with tube diameters of 5 mm or less cannot be reliably modeled using conventional correlations from the literature due to the lack of available data from small diameter tubes.

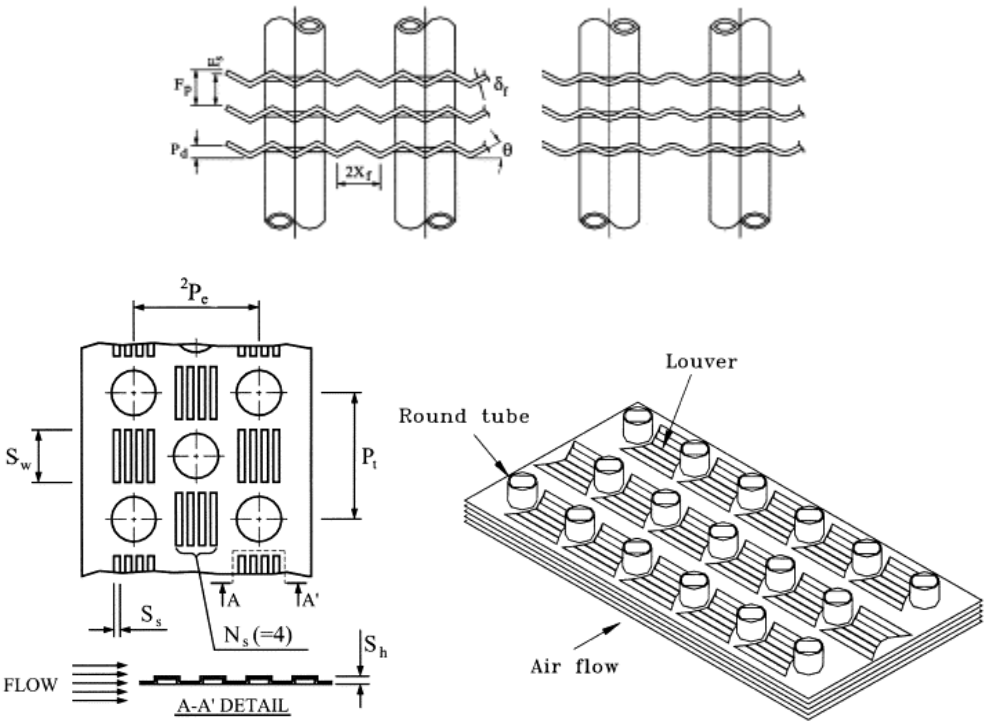

Figure 3: Enhanced fin surfaces; top left: wavy herringbone, top right: smooth/sine wavy (Wang, 2002), bottom left: slit, bottom right: louver (Wang, 1999)

Table 1: Range of sample conventional air-side correlations

Fin type	OD [mm]	Pt [mm]	Pl [mm]	N_{banks}
Wavy (Wang, 2002)	7.66-16.85	21-38	12-33	1-6
Slit (Wang, 2001)	7.52-16.4	20-39	12.7-33	1-6
Louver (Wang, 1999)	6.9-10.4	17.7-25.4	12.7-22.0	1-6

3.2 Refrigerant-side correlations

In order to accurately predict heat exchanger performance, heat transfer and pressure drop must be predicted for the single phase (liquid, vapor, or supercritical vapor) and two-phase (condensing or evaporating) refrigerant. The heat transfer performance of condensing and evaporating refrigerant in smooth tubes with diameters as small as 2 mm has already been characterized (for example, Shah (2013, 2014), respectively).

The performance of enhanced tubes had been well characterized by researchers including Cavallini (2003) and Miyara (2000) for conventional tube diameters of 7 mm and above. In recent years, several publications have been released attempting to characterize performance of enhanced microfin tubes for smaller diameter tubes. Many of these correlations have limited applicability, such as Huang's correlations (2010) developed from testing just one 5 mm and one 4 mm microfin tube with condensing R410A. Other examples of correlations for a single tube geometry exist throughout the literature, but are not generally applicable for a range of tube diameters and geometries. Wu's work (2015) is likely the most comprehensive review of heat transfer correlations at the time of writing for microfin tubes including a range of geometries in the small (≤5 mm) range. The author used five datasets for single-phase flow in tubes with inner diameters from 4.6 to 14.83 mm to identify the most accurate available correlation (Ravigururajan and Bergles, 1985). Nine published datasets of condensing refrigerant in tubes with inner

diameters from 3.56-8.98 mm were reviewed to identify the most suitable correlation for condensation (Yu and Koyama, 1998). Wu's correlation (2013) for evaporating refrigerant was found to predict 90% of points with ±30% error for 16 published datasets with inner tube diameters ranging from 2.1-14.85 mm.

3.3 Air-side correlations

While air-side correlations have been developed for conventional tube-fin heat exchangers with various enhanced geometries, no comprehensive experimentally-based publications have been produced to experimentally predict the performance of heat exchangers with small diameter tubes. Some publications include experimental performance data for a limited set of geometries; for example, Gao (2013) tested four 5 mm heat exchangers with louver fins (discussed further in the next section). However, these authors have not developed fully generic correlations for air-side performance of heat exchangers with small diameter tubes, meaning that designs with different tube pitches and louver geometries cannot be reliably predicted from the limited published results. Although many manufacturers already design and produce heat exchangers for HVAC equipment using 5 mm tubes, the air-side performance and details of these fin designs are not publicly available.

Conventionally, air-side heat transfer and pressure drop correlations would require experimental testing of a large number of heat exchangers in order to ensure accuracy across the entire range of design parameters. Taking for an example a well-cited and often-used correlation for louver fin heat exchangers (Wang et al., 1999): the author tested 49 unique heat exchangers each at 10 different points to develop a generic correlation. While the correlation covers 6 different louver fin geometries, 5 tube

diameters, 3 tube pitches, 3 louver heights, 4 louver pitches, and 5 different numbers of tube rows, the selection of tested geometries is limited to those that are commercially available. Production of unique fin geometries is extremely costly and as such, experimentally-developed correlations cannot be created for a prescribed design space with a full-range of fin designs.

3.4 Experimental methods and data reduction for correlation development

Numerous authors have prepared air-side correlations for tube-fin heat exchangers through experimental work. In general, the procedure requires that the heat exchanger is placed in a controlled wind tunnel and proper air and water flow rate, temperature, and pressure measurements are taken. Requirements for test procedures and measurement techniques are standardized by several organizations and the standards set by the American Society of Heating, Refrigerating, and Air-Conditioning Engineers (ASHRAE) are often followed for heat exchanger tests in the HVAC&R industry. ASHRAE Standard 41 (ANSI/ASHRAE, 1992) contains specifications for proper temperature, air flow, and pressure measurements among several other quantities. ASHRAE's Standard 33, (ANSI/ASHRAE, 2016) specifies a standardized testing procedure for heating and cooling coils. Once data is collected, it can be reduced through calculation to determine heat transfer coefficients.

Experimental techniques to measure heat transfer and pressure drop of heat exchangers date back over a century. Wilson (1915) published a technique, later referred to as the "Wilson plot method", for determining convective heat transfer coefficients of heat exchangers. The technique has since been modified by many authors for use in different types of heat exchangers but in its essence the technique remains the same. Heat transfer

measurements are made on a heat exchanger with two fluid streams while the velocity of one of the streams is modified and the other remains constant; this changes the heat transfer coefficient of one stream while maintaining the same conductive heat transfer and convective heat transfer of the unchanged fluid. When these results are plotted with the overall thermal resistance on the Y-axis and the $1/v_r^n$ (where v is velocity and n is a coefficient) on the x-axis, a linear regression can be used to determine the convective heat transfer coefficients.

Fernández-Seara et al. (2007) reviewed the history and summarized several modifications to the Wilson plot method, which typically replace the $1/v_r^n$ term with a functional form, or correlation, for the heat transfer coefficient of one fluid. Because the heat transfer of liquid flowing in smooth tubes is well-characterized by correlations, for example Gnielinski (1976), this approach can lead to a more accurate calculation of the air-side heat transfer coefficient from tube-fin heat exchanger tests. This modified Wilson plot method is a preferred technique in the industry for testing air-to-refrigerant heat exchangers.

Wang et al. (2000b) outlined a data reduction technique for air-side heat transfer of tube-fin heat exchangers. The approach relies on generalized ε-NTU relations to determine the overall UA of the heat exchanger and estimates the refrigerant-side resistance using the Gnielinski correlation (1976). This approach has been utilized to develop several well-cited correlations for tube-fin heat exchangers of various fin geometries.

3.5 CFD-based correlations

In recent years, advancements in both the reliability and speed of computational fluid dynamics (CFD) have allowed for its use in evaluating the performance of heat

exchangers. Compared with conventional experimental techniques, CFD simulations have the potential to deliver results more quickly and at a lower cost. Another major advantage is the ability to simulate any arbitrary geometry; this allows for the development of correlations that cover wide ranges of geometry parameters in increments that cannot be conveniently prototyped and tested.

Simulations of heat exchangers have been attempted since the 1990s (Bestani et al., 1990). Since then, CFD was used as a tool to evaluate heat transfer and pressure drop performance for particular heat exchanger designs including novel geometries such as oval / elliptical tubes (Sun et al., 2014 and Taler and Ocłoń, 2014). Recently, CFD has been utilized to extend or supplement correlations beyond the ranges for which they were tested. Heat exchangers with large diameter tubes, exceeding the values tested by Wang (2000), were simulated through CFD and found to vary significantly from Wang's predictions (Xie et al., 2009).

CFD has been used as a tool for fin design and soft-optimization in several publications (Wu et al., 2012 and Gao, 2013). These authors presented an approach to evaluate trends in fin performance and select values of louver dimensions and tube pitches with good performance. Four prototype heat exchangers were constructed and tested based on this optimization study and a correlation was developed for air-side heat transfer and pressure drop (Gao, 2013). This approach leverages the strengths of CFD to evaluate varying fin designs and correlate performance. However, the dataset is extremely limited and the correlation is not applicable across a wide range of operating conditions. Similarly, Kong et al. (2016) studied slit fin heat exchangers with 25 mm diameter tubes through a range

of CFD simulations; the publication included experimental validation and the development of heat transfer and pressure drop correlations.

Abdelaziz et al. (2010) published an approach to optimize a novel type of heat exchanger using CFD simulations. The construction of the heat exchanger consists of a “webbed” set of tubes connected by a fin material as shown in Figure 4. The authors explored a wide range of port diameters, number of ports, horizontal and vertical spacing, offset, tube length, number of tubes, and velocity by applying Design of Experiments (DOE) techniques and developing a metamodel. The design space was sampled with the Maximum Entropy Design (MED) technique (Shewry and Wynn, 1987) and space-filling cross validation trade-off (SFCVT) adaptive approximation technique (Aute et al., 2013). The Kriging technique was used to build a metamodel to predict performance within the design space and then the multiobjective genetic algorithm (MOGA) solver was used to identify optimal designs. The authors optimized designs for an example radiator application which could provide a 61% volume reduction and 84% material volume reduction or a 95% reduction in air-side pressure drop, 69% reduction in material volume, and 5% reduction in heat exchanger volume when compared to a conventional baseline heat exchanger. The applications of Parallel Parameterized Computational Fluid Dynamics (PPCFD), DOE, metamodeling, and optimization described in this work are adopted in several later publications including this thesis.

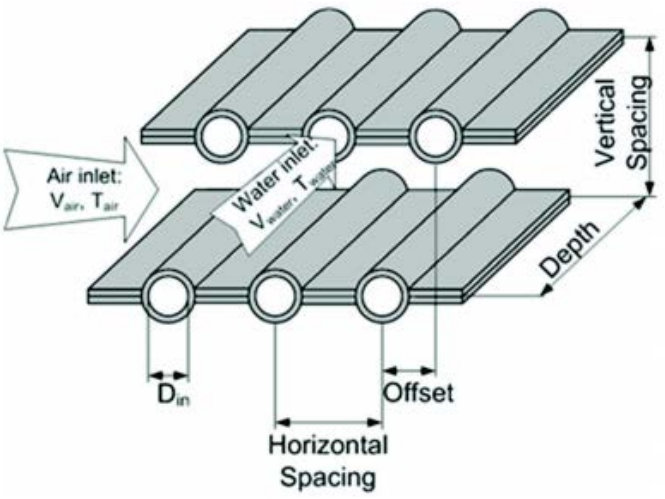

Figure 4: Heat exchanger design studied by Abdelaziz et al. (2010)

Bacellar (2014) presented an approach to develop air-side heat transfer and pressure drop correlations directly from CFD data for plain fin and finless tube bundles. Unlike past work, this effort systematically generated simulation results for an entire design space of tube/fin surfaces. The work leverages the PPCFD method to automate the geometry generation, meshing, simulation, and data reduction from multiple parallel CFD simulations. Bacellar was able to simulate 500 geometries for each heat exchanger type using the Maximum Entropy Design (MED) method for DOE to fill the design space. This space-filling technique allows for non-biased exploration of the entire design space based on a limited number of CFD simulations whereas past publications often relied on limited experimental test data from commercially-available fin geometries. As such, the approach outlined by Bacellar can characterize a design space in much greater detail than would be feasible through an experimental effort. The size of the design space underscores the importance of the use of DOE for sampling the design space; if an exhaustive search were to be performed with only 5 values for each of the 7 variables, 5^7=78,125 simulations would need to be conducted which would require 34 days to

compute on 8 parallel processors assuming a conservative 5 minutes per simulation (Bacellar observed 5-15 minutes each). If a greater resolution were desired or a larger design space (such as an enhanced fin geometry) were considered, the processing time would be even less feasible. The use of DOE allowed the author to sample the design space with only 500 simulations.

In the following year, Bacellar (2015) presented results for a sinusoidal wavy fin surface using the same technique. In this work, the author explored a large parameter set of 2-5 mm OD fin designs with varying wavelength and pattern depth (amplitude) and sampled the design space using 1,000 simulations selected using the Latin Hypercubes method for DOE. This was the first of such publications to thoroughly explore the design space of an enhanced fin geometry. To correlate the results of these simulations, Bacellar adopted a modified version of the wavy fin correlation developed by Wang (2002) and solved for new coefficients that would minimize the error in predicting the new dataset. Within this publication, the authors ultimately found that the proposed correlations for dimensionless j and f factors can predict only 64% and 66% of the data respectively with 20% error or less. These correlations were further refined such that the Nusselt numbers of 94% of the data could be predicted with 15% error or less and 93% of the friction factors were predicted with 15% error or less (Bacellar et al., 2016a). The same publication includes correlations for the herringbone wavy surface and was able to predict 96% of simulated Nusselt numbers with 15% error or less and 94% of friction factors with 15% error or less.

Bacellar (2016b) also expanded the correlation for bare (finless) tubes to include the diameter range of 0.5-2.0 mm and a larger range of tube pitches and tube banks in the

airflow direction. This work provides an unprecedented correlation for airside heat transfer coefficient and pressure drop of very small diameter tubes and follows essentially the same approach as the previous publications. In this study, Bacellar showed, through validation against 100 additional random data points, that the DOE sampling technique was sufficient to produce correlations that would accurately predict the performance of random points throughout the entire design space. The results of the CFD correlations were validated against an experiment for a heat exchanger constructed from 0.8 mm diameter tubes at 15 operating points (5 airflow rates and 3 water flow rates). The experimental results showed that while many existing correlations from other authors failed to accurately predict the performance, the CFD simulations and the resulting correlations predicted the experimental heat transfer coefficients with less than 15% error and pressure drop with less than 7% error. Overall the effort produced new correlations capable of predicting performance of more than 90% of data within 20% error in this previously un-correlated space. The contributions of Bacellar are summarized in Table 2 to illustrate the range of applicability of the newly developed correlations. It is important to note that the range of tubes in the airflow direction, fin densities, and fin thickness is greater than is typically explored through most experimental work. While the work is extensive, it does not characterize the performance of designs outside this range or using other enhanced surfaces and the author is not seeking to extend the work to include enhancements such as slit and louver fins which are typical in the HVAC industry.

Table 2: Summary of contributions by Bacellar

Parameter / Range	Bare Tubes (Bacellar, 2014)	Plain Fins (Bacellar, 2014)	Smooth and Herringbone Wavy Fins (Bacellar, 2016)	Small Bare Tubes (Bacellar, 2016)
Outer diameter, D_o [mm]	2.0 – 5.0	2.0 – 5.0	2.0 – 5.0	0.5-2.0
Longitudinal tube pitch, P_l [mm]	$1.5D_o$-$3.0D_o$	$1.5D_o$-$3.0D_o$	$1.25D_o$-$4.0D_o$	$1.2D_o$-$4.0D_o$
Transverse tube pitch, P_t [mm]	$1.5D_o$-$3.0D_o$	$1.5D_o$-$3.0D_o$	$1.25D_o$-$4.0D_o$	$1.2D_o$-$4.0D_o$
FPI [in^{-1}]	-	8-24	5-50	-
Number of rows in airflow direction, N [-]	2-20	2-10	2-20	2-40
Velocity, u [m/s]	0.5-7.0	0.5-7.0	0.5-7.0	0.5-7.0
Fin thickness, Ft [mm]	-	0.115	0.05-0.1	-
Pattern Depth /Half Wavelength Pd/Xf	-	-	0.088-0.84	-

4. CFD-based correlation

Within the HVAC&R industry, a shift to smaller diameter tube heat exchangers is already taking place, due to increasing performance and economic pressures. In such applications, the use of enhanced fin surfaces, especially louver and slit fins, is quite common, yet comprehensive correlations for their performance are not available. The approach developed by Bacellar et al. (2014, 2015, 2016) has been demonstrated to be both computationally-efficient and sufficiently accurate when compared to random CFD simulations and experimental data. A similar approach was taken in this work in order to simulate the performance of a large design space of both slit fin and louver fin heat exchangers with outer diameters ranging from 3-5 mm. The approach and results of the correlation development effort for louver- and slit-fin heat exchangers were published by Sarpotdar and Nasuta (2016a and 2016b).

4.1 Design space

For each fin type, a parameterized CFD model was developed, allowing the geometry variables to be modified externally, then meshed, and simulated automatically. Since innumerable designs can be conceived, the design space must be selected to include parameters that are important for performance and also ranges of geometries which are feasible from a manufacturing perspective (or may be feasible in the future as manufacturing technologies improve).

4.1.1 Louver fin

Several key parameters that have impacts on the performance of a louver fin were identified and selected for study. Ranges of important tube-and-fin geometry parameters were selected based on past correlations and manufacturer feedback provided by Burr

Oak Tool, Inc. and Heat Transfer Technologies, LLC. The louver angle was kept constant at 27° based on manufacturer feedback and research indicating that optimal performance is found at similar values of louver angle and significant performance differences are not seen through small changes in louver angle (Gao, 2013 and Jang and Chen, 2015). Additionally, fin thickness is not varied throughout the simulations because most currently-manufactured fins do not vary in thickness significantly and the impact of changing fin thickness within typical ranges is expected to have little significance on performance. Selecting these 8 variables allowed for successful mapping of the parameter space through 1,256 simulations, whereas inclusion of additional variables would increase the required number of samples significantly which was found to be infeasible in this work. Table 3 summarizes the design space studied in this work and Figure 5 provides an illustration of the geometry parameters for the louver fin. Parameters Cl and Ct are multipliers that define the longitudinal pitch (Pl) as proportional to tube diameter (D_n) and the transverse pitch (P_t) as proportional to (and always greater than or equal to) the longitudinal pitch (P_l), respectively.

Table 3: Louver fin parameter space (Sarpotdar et al., 2016a)

Design Variable	**unit**	**Min to Max**
D_n	mm	3 to 5
D_c	mm	$(1.023D_n+0.1)+2\delta_f$
$C_l = P_l / D_n$	--	2 to 4
$C_t = P_t/P_l$	--	1 to 2
N	--	1 to 6
N_l	--	2 to 8
FPI	in^{-1}	14 to 40
L_p	mm	0.8 to 1.8
θ	degrees	27
u	m/s	0.75 to 5
δ_f	mm	0.125

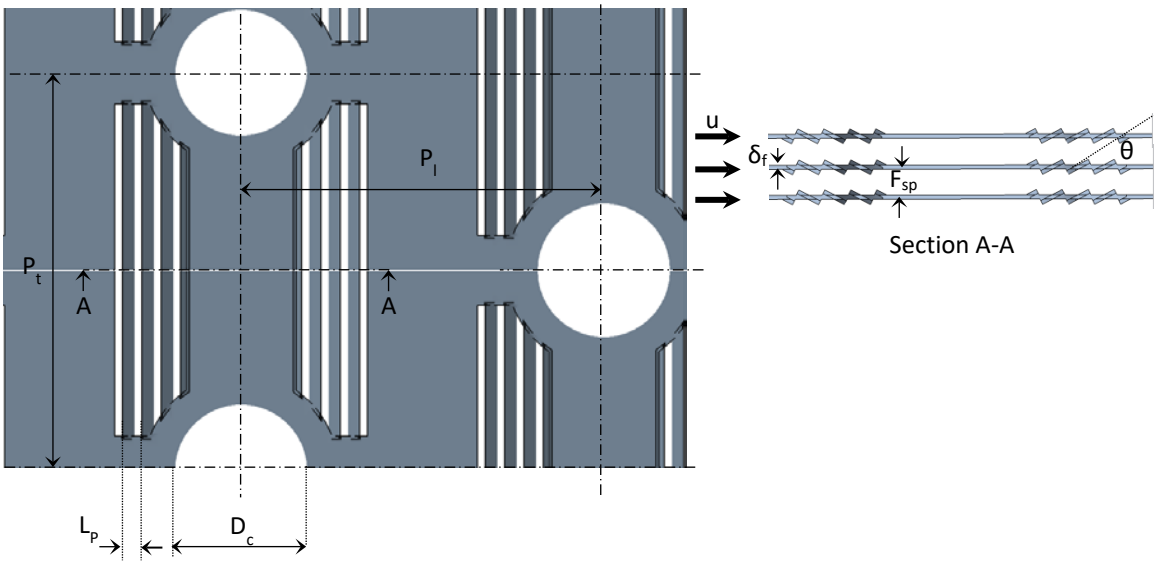

Figure 5: Louver fin geometry (Sarpotdar et al., 2016a)

4.1.2 Slit fin

Slit fin performance is impacted by geometry parameters including the tube diameter, number, and pitches; fin density and thickness; slit height and width; and air velocity. Again, in the interest of ensuring manufacturing feasibility and developing a design space that can be explored computationally within a reasonable timeframe, some variables must be omitted. The fin thickness is fixed at a single value as is the slit width. The slit width is an important parameter from a performance perspective and small values perform well, however current manufacturing limitations make it very difficult or impossible to produce slits with a width less than 1 mm.

Table 4 summarizes the design space selected for this work and Figure 6 shows the relevant geometry parameters graphically.

Table 4: Slit fin parameter space (Sarpotdar et al., 2016b)

Design Variable	unit	Min to Max
D_n	mm	3 to 5
D_c	mm	$(1.023D_n+0.1)+2\delta_f$
$C_l = P_l/ D_n$	--	2 to 4
$C_t = P_t/P_l$	--	1 to 2
N	--	1 to 6
N_s	--	2 to 6
FPI	in^{-1}	14 to 40
$C_h= S_h/F_{sp}$	--	0.3 to 0.7
S_w	mm	1
u	m/s	0.75 to 5
δ_f	mm	0.098

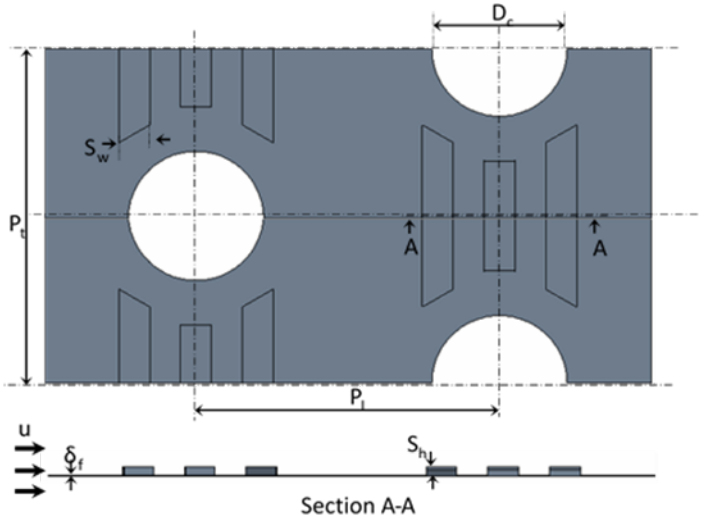

Figure 6: Slit fin geometry (Sarpotdar et al., 2016b)

4.2 CFD model

CFD Simulations were conducted using the Star CCM+® CFD package and are described in the prior publications (Sarpotdar and Nasuta, 2016a,b). This section provides high-level summary information on the CFD modeling approach.

Within most commercially-available CFD tools, it is now possible to parameterize a model such that a geometry can be modified programmatically, similarly to the PPCFD

technique. Louver and slit geometries were developed within Star CCM+® with the parameterization of geometry variables described in Table 3 and

Table 4. Meshing is also automated through the software for each new geometry generated within the design of experiments sample as illustrated in Figure 7 (b). A polyhedral mesh was used for the bulk of the model with a refined boundary layer mesh along the tube and fin walls. The two-layer SST K-ω turbulence model was used. The boundary conditions of the model are depicted in Figure 7 (a). The domain consists of two fins, each cut in half, placed side by side with airflow traveling past; on each side is a periodic boundary condition to approximate the effect of the additional fins that would exist in both directions. The top and bottom boundaries are cut halfway through the tubes and modeled with symmetry boundary conditions. Air flows in through a velocity inlet (which is parameterized) and exits through a pressure outlet. The air inlet temperature is fixed at 35°C and the tube wall (inner collar) temperature is set as 65°C. This large temperature difference is important for ensuring that the results are not “pinched” (when air leaves at very nearly the same temperature as the tube wall).

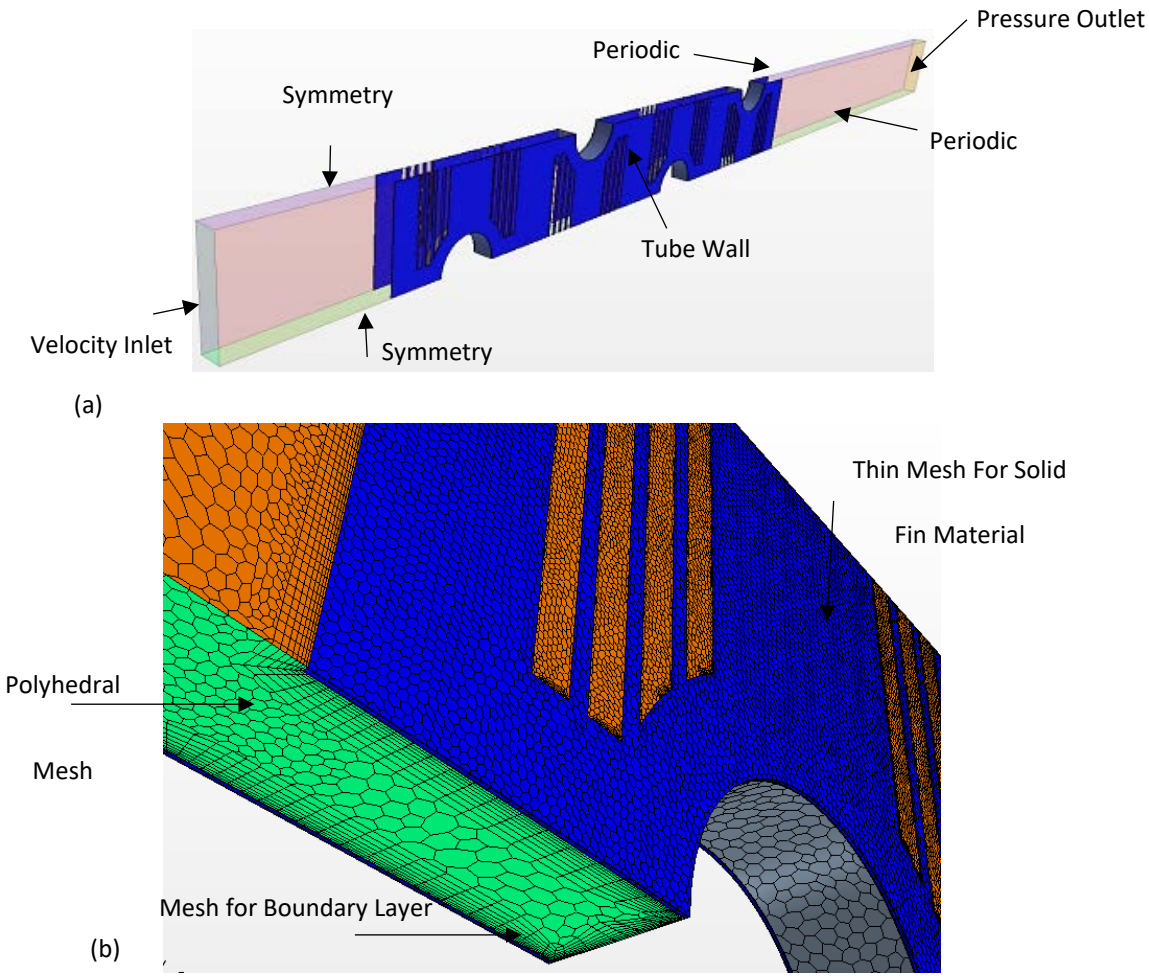

Figure 7: CFD (a) boundary conditions and (b) mesh. (Sarpotdar et al., 2016)

A mesh independence study was conducted to ensure that mesh size does not impact the results. The Richardson Extrapolation method (Roache, 1997) was used to calculate Grid Convergence Index (GCI). For 33 configurations on the boundaries of the design space, simulations were carried out with three grid sizes, each having element sizes 1.35 times larger than the previous finer mesh. The mean uncertainty in pressure drop and HTC

were found to be 1.5% and 1.1%, respectively, and the size of the selected mesh was found to be adequate.

4.3 Data reduction

Data reduction from the CFD results followed the technique described by (Bacellar et al., 2014), which is based on Wang et al. (2000b) approach and is summarized in equations (1-4) below. In essence, the simulations are treated in the same manner an experiment would be, and the heat transfer coefficients and j factors are determined from the observed inlet and outlet temperatures. The Schmidt fin efficiency correlation is used as recommended by Wang (and shown in equations (5-11)); although this correlation is intended for plain fins, an accurate overall air-side heat transfer coefficient will still be achieved when the same model is used for both data reduction and subsequent predictions in a heat exchanger simulation tool (in this case CoilDesigner®).

$$\dot{Q}=\dot{m}\cdot c_{p_{0lr}}\cdot(T_{air,out}-T_{air,in}) \quad (1)$$

$$\dot{Q}=UA_o.\ LMTD \quad (2)$$

$$LMTD=\frac{(T_w-T_{air,in})-(T_w-T_{air,out})}{ln\left(\frac{T_w-T_{air,in}}{T_w-T_{airout}}\right)} \quad (3)$$

$$\frac{1}{UA_o}=\frac{1}{\eta_0 h_{air} A_o}+\frac{\delta_w}{k_w A_w}+\frac{1}{h_{ref} A_{ref}} \quad (4)$$

$$h_{air}=\frac{U}{\eta_o} \quad (5)$$

$$\eta_0 = 1-\frac{A_f}{A_o}(1-\eta) \quad (6)$$

$$\eta = \frac{tanh(mr\Phi)}{mr\Phi} \quad (7)$$

$$m = \sqrt{\frac{2h_o}{k_f \delta_f}} \quad (8)$$

$$\Phi = \left(\frac{R_{eq}}{r}-1\right)\left[1+0.35*ln\left(\frac{R_{eq}}{r}\right)\right] \quad (9)$$

$$\frac{R_{eq}}{r} = 1.27*\frac{X_M}{r}\left[\frac{X_L}{X_M}-0.3\right]^{\frac{1}{2}} \quad \text{for staggered tubes} \quad (10)$$

$$\frac{R_{eq}}{r} = 1.28*\frac{X_M}{r}\left[\frac{X_L}{X_M}-0.2\right]^{\frac{1}{2}} \quad \text{for inlet/ 1-row coils} \quad (11)$$

The Colburn j factor and the friction factor, f, are defined based on the maximum air velocity as shown in equations (12) and (13).

$$j=\frac{h_{air}\,Pr^{\frac{2}{3}}}{\rho_m u_{max} c_{p_m}} \tag{12}$$

$$f=\frac{A_{min}}{A_o}\frac{\rho_m}{\rho_1}\left[\frac{2\Delta P\rho_1}{G_{max}^2}(1+\sigma^2)\left(\frac{\rho_1}{\rho_2}-1\right)\right] \tag{13}$$

Two additional parameters, j_{simple} and f_{simple} are defined in equations (14) and (15) for convenient integration with software such as CoilDesigner®. These parameters are identical to those defined in equations (12) and (13), but average thermophysical properties are replaced with the properties at the inlet state. This simplification is made because software such as CoilDesigner does not iterate to use both inlet and outlet properties in the calculation of the HTC or ΔP, instead, only the inlet air properties are used when determining these parameters. This approach later shows satisfactory ability to predict HTC and ΔP values without the need for additional iteration.

$$j_{simple}=\frac{h_{air}\,Pr^{\frac{2}{3}}}{\rho_{in} u_{max} c_{p_{in}}} \tag{14}$$

$$f_{simple}=\frac{A_{min}}{A_o}\left[\frac{2\Delta P\rho_1}{G_{max}^2}(1+\sigma^2)\right] \tag{15}$$

4.4 Correlation development

Initial correlations were developed based on this work (Sarpotdar et al., 2016b, 2016a). Initial attempts to fit the reduced CFD data to existing forms of correlations for slit and louver fins by Wang et al. (2000a, 1999) failed to produce satisfactory predictions of the source data. Instead, the stepwiselm regression approach was used to develop a regression model for the data (MathWorks Inc., 2016). This tool can evaluate the

significance of all independent variables, their squares, and their interactions and discards all terms with p-values greater than 0.05. In order to produce a satisfactory fit and avoid negative predictions, all independent variables and response functions are transformed by the natural log function. The details of the proposed correlations are outlined in Sarpotdar et al. (2016a). The general form of the equation is illustrated in equation (16), where the log-transformed functions are predicted by the summation of all log-transformed variables, their squares, and their interactions, noting that the redundant and statistically insignificant terms are omitted by the stepwiselm algorithm.

$$\boldsymbol{ln(f)} = \sum_{i=1}^{n}\sum_{j=1}^{n} \boldsymbol{c_{ij}} * \boldsymbol{ln(X_i)} * \boldsymbol{ln(X_j)} \quad (16)$$

The variables selected for the correlation are important in ensuring its applicability for future designs and operating conditions. The correlations should be based on geometry variables that are available and operating conditions that are not dependent on fluid properties. The Reynold's number is the preferred dimensionless term to characterize the flow as opposed to the dimensioned velocity, which may change with air properties. The Reynold's number based on the collar diameter and maximum, or "core", velocity was selected. This parameter is more representative of the actual flow conditions within the heat exchanger as it is affected by the fin geometry parameters that determine the minimum free flow area and thus yielded a more accurate correlation.

The regression models predict source data with a high degree of accuracy, summarized in Table 5. Furthermore, the louver fin correlations were verified against a set of randomly generated data, not included in the regression models. In 117 random simulations, the proposed correlations predicted 93.7% and 83.8% of pressure drops and air-side heat

transfer coefficients with 90% accuracy or better, similar to the predictions of the source data in Table 5.

Table 5: Regression accuracy of original CFD correlation

Fin Type:	Slit Fin		Louver Fin	
Predicted parameter:	ΔP	HTC	ΔP	HTC
Percentage of data with 10% error or less	98.1%	84.7%	93.1%	84.7%
Percentage of data with 20% error or less	100%	97%	99.8%	97.4%

4.4.1 Alternate slit pressure drop correlation

Despite the high quality of the correlations presented in the 2016 work, one shortcoming was uncovered after implementing the models into the CoilDesigner environment. Although the correlations were not developed for vastly different fin thicknesses and should not be interpreted as being broadly applicable for fins with significantly different thicknesses, they should be suitable for fins of comparable thickness. When conducting simulations with the slit fin correlation, it was observed that air pressure drop values decreased as fin thickness increased; this result is contrary to the expected physical result and may indicate some flaw in the proposed correlations. A simplified form of the slit fin air pressure drop correlation was developed and is outlined in

Appendix C: Modified Slit fin DP correlation. This correlation predicts 85.7% and 97.1% of CFD source data with 10% and 20% error or less and contains considerably less terms. This form is recommended because it shows the correct trend of increasing air pressure drop with increasing fin thickness.

5. Experimental validation

In order to validate the performance of the CFD-based correlations with experimental observations, extensive testing was carried out on a representative sample of heat exchangers. At the time of writing, heat exchangers with 3 and 4 mm OD tubes were not readily available commercially, but 5 mm designs were prevalent. Prototype heat exchangers with 5 mm tube diameters were purchased from five manufacturers, each with different enhanced fin designs. Dry coil tests were conducted using hot water as the working fluid to determine the air-side heat transfer coefficients and pressure drops under a range of operating conditions.

5.1 Test facility

A closed-loop wind tunnel facility operated by Optimized Thermal Systems, Inc. (OTS) was used for heat exchanger testing. Figure 8 shows the schematic of the test facility. Air is forced through a closed-loop wind tunnel, it is cooled by a cooling coil and heated by a duct heater as needed, and mixed before entering the test section. The duct throughout the loop is 36x36” (below M is 36”) and is reduced to the size of the test section, approximately 22x22”. The facility was constructed to comply with the requirements of the industry-accepted test standards for airflow measurement (ANSI/ASHRAE Standard 41.2, 1992) and heat exchanger testing (ANSI/ASHRAE Standard 33, 2016). Measures were taken to ensure the uniformity of airflow, namely an air mixer and several perforated sheets which act as settling means. Water mass flow rate is measured with a Coriolis flowmeter and inlet and outlet temperatures are taken with resistive temperature devices (RTDs). A differential pressure measurement is taken across the coil on the air-side and the inlet and outlet temperatures are measured using a grid of thermocouples.

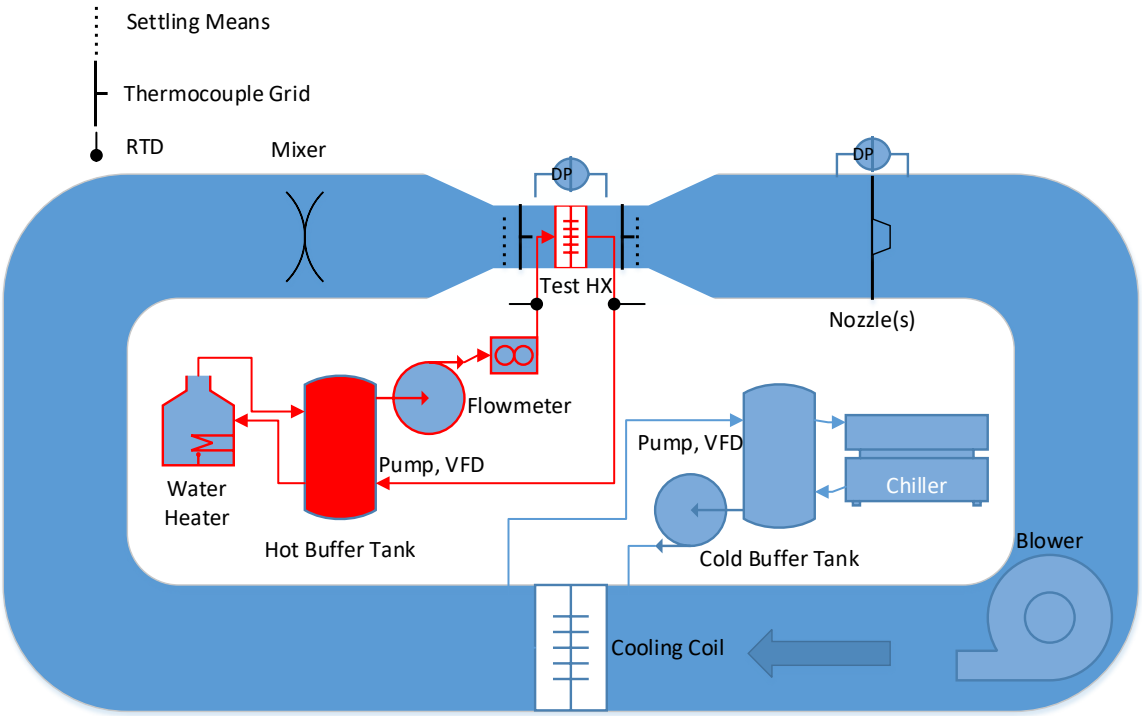

Figure 8: Schematic of experimental setup

Several key considerations were addressed in the construction of the facility to ensure compliance with ASHRAE Standard 41.2 (ANSI/ASHRAE, 1992) for air flow measurement (Figure 9):

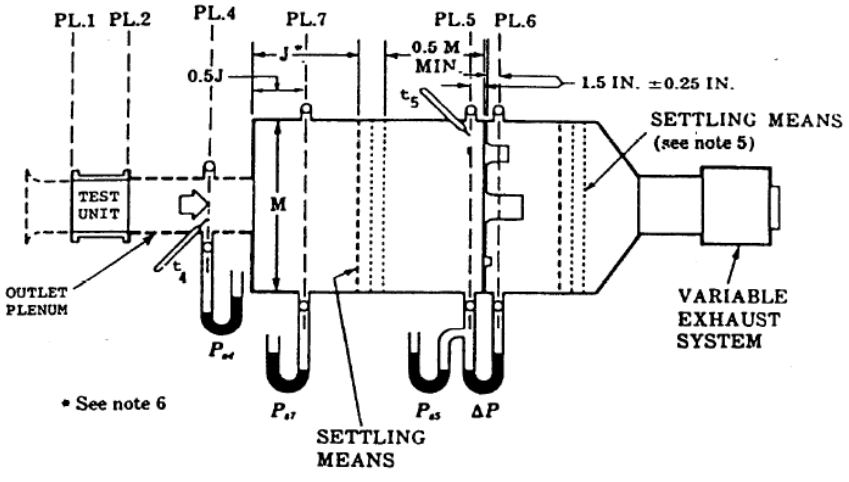

Figure 9: Schematic from ANSI/ASHRAE Standard 41.2 (1992)

- Pressure drop across the calibrated nozzle is measured 1.5 inches before and after the plane of the nozzle
- Settling means are installed at least 0.5*M before the nozzle plane and 2.5 times the throat diameter of the largest nozzle (7 inch nozzle) from the exit face of the largest nozzle
- J is larger than M (36”)
- Exiting air dry-bulb temperature is taken with a 9-point thermocouple grid on the settling means before the nozzle

Additional considerations for following Standard 33 for coil testing (ANSI/ASHRAE, 2016) are listed below and in Figure 10:

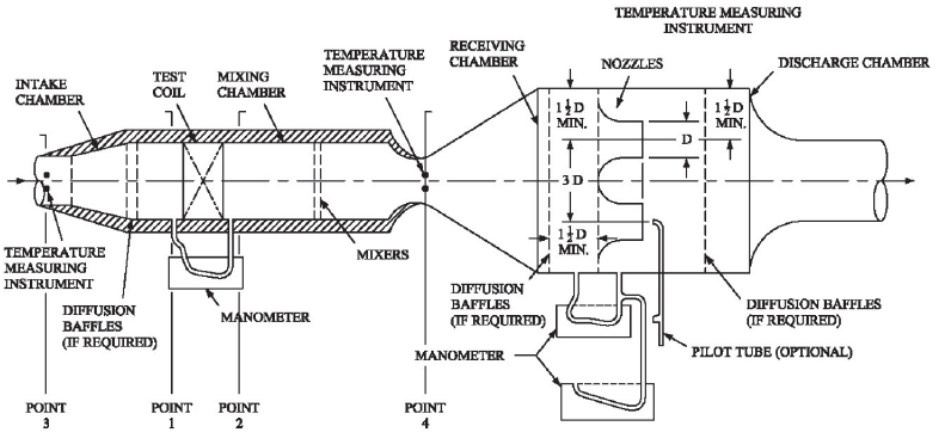

Figure 10: Schematic from ANSI/ASHRAE Standard 33 (2016)

- Entering air dry-bulb temperature is measured using a 9-point thermocouple grid approximately 1 inch from the face of the test coil. The thermocouple grid has a negligible effect on air-side pressure drop
- Four static pressure taps are located 12 inches before and after the test coil, to measure absolute barometric pressure and pressure drop

- Diffusion baffles (settling means) are used before the inlet pressure tap and after the outlet pressure tap
- Air relative humidity is measured before the test coil, after the diffusion baffles, and before the nozzle array
- An array of nozzles (one 4”, two 5” and one 7”) are oriented based on the required clearance

This facility allows for collection of air-side performance data of the heat exchangers with an appropriate degree of accuracy. For several decades, researchers have implemented similar experimental setups to collect data for the development of air-side heat transfer and pressure drop correlations; the facility and instrumentation closely resemble those of Wang et al. (1999) and Kim et al. (1999) among many others.

5.2 Uncertainty propagation

Table 6 provides a summary of the equipment used for heat exchanger testing along with the published ranges and accuracies of each primary measurement. In addition to systematic uncertainties of the measurement equipment, random errors exist within the data and can be determined from the standard deviation of values collected for 30 minutes at steady state for each measurement.

Table 6: Instrumentation and systematic uncertainties

Measurement	Type	Model #	Range	Accuracy
Air Temperature	Thermocouple	Omega TT-T-24-SLE-100	-200 - 200°C	±0.5 K (0.17 K for 9-point grid)
Air Relative Humidity	Relative Humidity	Dwyer RHP-2D11	0-100%	±2%
Air Pressure	Barometric Pressure	Setra 2701800MA1F2B02N	800-1100 mbar	±0.55 mbar
Nozzle Pressure Drop	Differential Pressure	Setra 2641005WD11A1F	0-1245 Pa	±3.1 Pa
Coil Pressure Drop	Differential Pressure	Setra 2641001WD11A1F	0-249 Pa	±0.6 Pa
Refrigerant Temperature	RTD	Omega P-M-1/10-1/4-6-0-P-15	-100°C – 400°C	±0.03 K
Refrigerant Mass Flow Rate	Coriolis Flow Meter	Micromotion R050S239NQBMEZYZZ	0-150 g/s	±0.5% of reading
Refrigerant Pressure	Absolute Pressure	Omega PX409-750AI	0-5170 kPa	±4.1 kPa

For each measurement, the systematic and random uncertainties should be added because the observed value can be as much as the sum of the maxes of these two types of uncertainty. The two key parameters output by this research are the air-side pressure drop and the air-side heat transfer coefficient. While the air-side pressure drop is observed directly, the heat transfer coefficient must be determined from the combination of several measurements. Generally, the classical approach defined by Kline et al. (1953), and summarized in equation (17), is followed to propagate uncertainties in the calculation of the key output quantities. However, because the heat transfer coefficient is determined through external software, as later described in section 5.5.3, the partial derivatives must be taken numerically within the CoilDesigner data reduction tool.

$$w_R = \sqrt{\left(\frac{\partial R}{\partial v_1} w_1\right)^2 + \left(\frac{\partial R}{\partial 2} w_2\right)^2 \ldots \left(\frac{\partial R}{\partial v_n} w_n\right)^2} \quad (17)$$

Example systematic and random uncertainties for each measurement used in the calculation of the air-side pressure drop and heat transfer coefficient are listed in Table 7. These values are obtained from test data for coil #1, but the random uncertainties are comparable for all other tests. The average value and uncertainties of some secondary quantities including air flowrate and capacity are calculated using Engineering Equation Solver (Klein, 2017) and to propagate the uncertainties of all instruments used in their calculation. After numerically calculating the derivatives and propagating the results for this example, the overall uncertainty in air-side pressure drop is determined to be ±1.78Pa or 1.68% and the heat transfer coefficient has an uncertainty of ±2.5 W/m^{2}K or 2.42% when using the tube-side heatload and 4.72% when using the average heatload.

Table 7: Typical measurement uncertainties: Coil #1, test point 4

Measurement [units]	Mean Value	Systematic Uncertainty	Random Uncertainty	Total Uncertainty / (average of 9 measurements)	Total Relative Uncertainty [%]
Air Pressure Drop [Pa]	105.77	0.623	1.157	1.780	1.68
T air out [°C]	25.27	0.500	0.046	0.546 (0.182)	2.16 (0.72)
Nozzle RH [%]	43.41	0.500	0.063	0.563	1.30
Nozzle ΔP [Pa]	224.99	3.125	2.976	6.101	2.71
Air flowrate [m^3/s]	0.97	-	-	0.0132	1.36
RTD Water in [°C]	50.04	0.030	0.038	0.068	0.14
RTD Water out [°C]	23.96	0.030	0.046	0.076	0.32
Mass flowrate water [g/s]	97.00	0.291	0.048	0.339	0.35
Air RH in [%]	78.53	-	-	1.735	2.21
Air T in [°C]	16.11	0.500	0.056	0.556 (0.185)	3.45 (1.15)
Q_{air} [kW]	10.65	-	-	0.329	3.09
Q_{water} [kW]	10.59	-	-	0.056	0.53

As is later discussed in Section 5.5.3, the data reduction to determine air-side HTC can be performed based on the average heat load (both tube- and air-side) or only on the tube-side. After performing the numerical uncertainty propagation using both techniques, the results were found to be comparable as shown in the examples in Table 8, however, the average heatload is used to determine HTC in final results presented in this thesis. The reason why one technique does not always produce lower uncertainty than another is because the uncertainties of individual measurements can change significantly across different operating conditions. For example, the uncertainty of the air flow rate can sometimes be higher at high air flow rates depending on the diameter of nozzles and range (switchable) of the differential pressure transducer used for air flow measurement; in such cases, the overall uncertainty in HTC suffers when using the average capacity due to the introduction of this less certain term. In some scenarios with low air flow rates, where just one small nozzle is used for flow measurement and the pressure drop is low, the air flow uncertainty is lower and its inclusion in the air-side HTC calculation improves the overall confidence. Ultimately, both approaches produce acceptable results and the choice to use the average heat load was made at the recommendation of existing literature (Wang et al., 2000). When using tube-side heat load only, the sample analyses show that the highest uncertainty in air-side HTC occurs in the tests with the lowest HTCs and flow rates. This finding is intuitive because the primary contributors to uncertainty are the inlet and outlet temperature measurements; when air flow is low and water flow is high, the water temperature difference is small and the uncertainty is greater. Conversely, the averaging approach yields a higher uncertainty at high air flow rates due to the nature of the air flow rate measurement. The use of the average heat load

is also preferred because some numerical issues can arise when using only the tube-side heat load. In some instances, the use of refrigerant heat load to calculate HTC resulted in a very high sensitivity to refrigerant outlet temperature which led to cases where an impossibly large HTC value was required to replicate the reported refrigerant outlet state. Often, when using refrigerant heat load to determine HTC, the data reduction procedure yielded very different air HTCs at constant air velocity. These issues were avoided by using the average heat load to calculate air-side HTC.

Table 8: HTC uncertainties in Coil #1 tests

Air frontal velocity [m/s]	Refrigerant flow rate [g/s]	Average air HTC (using tube-side / avg. heat load) [W/m^{2}K]	HTC uncertainty (tube-side heat load) [W/m^{2}K]	HTC uncertainty % (tube-side heat load)	HTC uncertainty (avg. heat load) [W/m^{2}K]	HTC uncertainty % (avg. heat load)
3.80	97.0	102.84/101.52	2.49	2.42	4.79	4.72
1.05	97.0	69.87/71.54	3.58	5.13	1.69	2.35

5.3 Prototype heat exchangers

Heat exchangers were designed specifically for operation within the OTS wind tunnel and were purchased after coordinating with several manufacturers in China, India, and the United States. The goal of the prototype selection was to ensure that at least two different slit fin and two louver fin patterns were included, each with at least two different fin densities and two different numbers of tube rows in the airflow direction. In order to minimize edge effects, it was decided that each coil must have at least 20 tubes in the transverse direction.

Table 9 and Table 10 contain all geometric details of the slit- and louver-fin prototype coils, respectively. The finned lengths of all heat exchangers are designed to ensure that all coils have equivalent face area. All prototype heat exchangers for air-side testing were constructed using smooth (not internally-enhanced) copper tubes to produce predictable water-side performance and allow for accurate data reduction of air-side heat transfer coefficients. Additional heat exchangers with internally-enhanced tubes were also procured for two-phase refrigerant testing. Final inspection of all delivered coils confirmed that all heat exchangers were built within the provide specifications to an acceptable level of quality. Actual measurements of dimensions, including averaged values of fin density deviate only slightly from the original specifications but are provided in the tables below.

Table 9: Sample slit fin heat exchangers

PN	Manufacturer	Tube OD [mm]	Pl [mm]	Pt [mm]	Banks	Circuits	Tubes Per Bank	FPI [-/in]	Finned length [mm]	Coil height [mm]	Coil Depth [mm]	Fin thickness [mm]	Slit height [mm]	Slit width [mm]	Number of slits
1	1	5.2	11.60	19.50	2	2	24	23.2	534.19	468.00	23.20	0.105	0.7	1.00	5
2	1	5.2	11.60	19.50	1	2	24	23.4	534.19	468.00	11.60	0.105	0.7	1.00	5
3	1	5.2	11.60	19.50	2	2	24	16.9	534.19	468.00	23.20	0.105	0.7	1.00	5
4	1	5.2	11.60	19.50	1	2	24	17.9	534.19	468.00	11.60	0.105	0.7	1.00	5
5	2	5.2	13.86	16.00	1	2	30	22.0	520.83	480.00	13.86	0.098	0.5	1.00	5
6	2	5.2	13.86	16.00	2	3	30	22.0	520.83	480.00	27.72	0.098	0.5	1.00	5
7	2	5.2	13.86	16.00	1	2	30	29.8	520.83	480.00	13.86	0.098	0.5	1.00	5
8	2	5.2	13.86	16.00	2	3	30	29.8	520.83	480.00	27.72	0.098	0.5	1.00	5

Table 10: Sample louver fin heat exchangers

PN	Manufacturer	Tube OD [mm]	Pl [mm]	Pt [mm]	Banks	Circuits	Tubes Per Bank	FPI [-/in]	Finned length [mm]	Coil height [mm]	Coil Depth [mm]	Fin thickness [mm]	Louver pitch [mm]	Louver height [mm]	Number of louvers
9	3	5.2	16.50	19.05	1	2	24	15.1	546.81	457.20	16.5	0.100	1.67	1.00	6
10	3	5.2	16.50	19.05	2	2	24	15.1	546.81	457.20	33.0	0.100	1.67	1.00	6
11	3	5.2	16.50	19.05	1	2	24	20.1	546.81	457.20	16.5	0.100	1.67	1.00	6
12	3	5.2	16.50	19.05	2	2	24	20.3	546.81	457.20	33.0	0.100	1.67	1.00	6
13	4	5.2	13.60	19.00	2	2	24	21.0	548.25	456.00	27.2	0.095	1.20	0.66	4
14	5	5.2	10.90	21.00	1	2	24	19.1	496.03	504.00	10.9	0.095	1.30	0.80	4
15	4	5.2	13.60	19.00	2	2	24	19.5	548.25	456.00	27.2	0.095	1.20	0.66	4
16	5	5.2	10.90	21.00	1	2	24	18.5	496.03	504.00	10.9	0.095	1.30	0.80	4

5.4 Test matrix

Testing was performed under a range of operating conditions in order to determine accurate air-side heat transfer coefficients under a range of air velocities. Air velocities range from approximately 1 to 4 m/s, which is typical of heat exchangers of this type in many HVAC&R applications. Other conditions of the experiments must be controlled to ensure that heat transfer coefficients can be accurately determined. As indicated by Wang et al. (2000b), at least a 2°C ΔT is required on the water side and water Reynold's numbers should be sufficiently high to produce a water-side resistance which is much smaller than the air-side resistance. Table 11 shows a summary of the test matrix for air-side testing; the variation of air and water velocities allows for the determination of air-side heat transfer coefficients across a wide range of air velocities. Typical water mass flux values range from approximately 1,550 to 4,600 kg/m^{2}s and Reynolds numbers range from 12,000 to 37,000. These test conditions ensure fully turbulent flow within the tubes which allows for more accurate water HTC predictions and subsequently more accurate air-side HTC calculations.

Table 11: Coil test matrix

Test no.	Air velocity [m/s]	Water flow rate [g/s]	Air Inlet Temp [°C]	Water Inlet Temp [°C]
1	1	70~80	16	50
2	1	70~90	16	50
3	1	90~140	16	50
4	2.5	70~80	16	50
5	2.5	70~90	16	50
6	2.5	90~140	16	50
7	4	70~80	16	50
8	4	70~90	16	50
9	4	90~140	16	50

5.5 Data reduction

While observations of air-side pressure drop are directly made using a differential pressure transducer, the calculation of the air-side heat transfer coefficient relies on a data reduction technique to approximate the average convective heat transfer coefficient from primary measurements of temperatures and flowrates. Several techniques, summarized in section 3.4, have been used in the industry to determine heat transfer coefficients from experimental data. Throughout the course of this effort, these different techniques were used and compared in order to verify their accuracy and select the best approach.

5.5.1 Wilson plot method

The original Wilson plot method was implemented on a sample heat exchanger to assess its suitability for this application (Wilson, 1915) . The desirable feature of the original method is that it does not require knowledge of the heat transfer performance of either fluid to determine the heat transfer coefficients. However, without knowledge of the tube-side heat transfer, the fitting approach is somewhat rudimentary and can lead to highly uncertain results.

Figure 11 and Figure 12 show the Wilson plots for one sample heat exchanger tested in this study with two different fitting parameters of 0.82 (originally assumed by Wilson in 1915) and 1.0 (shown for the sake of illustration). It is evident that both parameters allow for a satisfactory linear fit of the data, however, the fitting parameter of 1.0 yields a slightly greater R^2 value for all series. While the difference in the quality of fit and the values of the intercepts may appear marginal, the resulting air-side heat transfer coefficients are quite different from one another, differing by nearly 50% in one case (as summarized in Table 12).

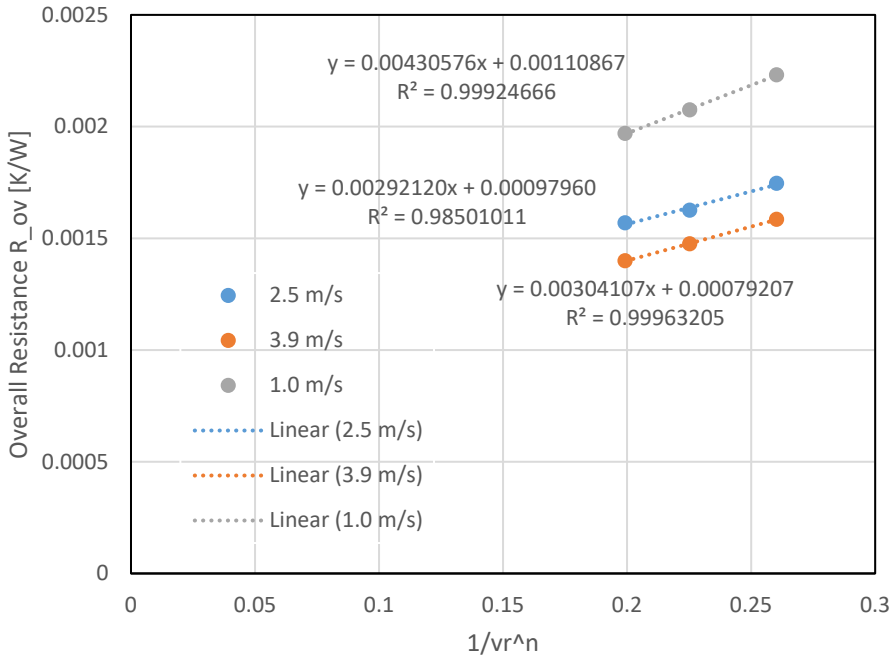

Figure 11: Original Wilson plot method with n=0.82

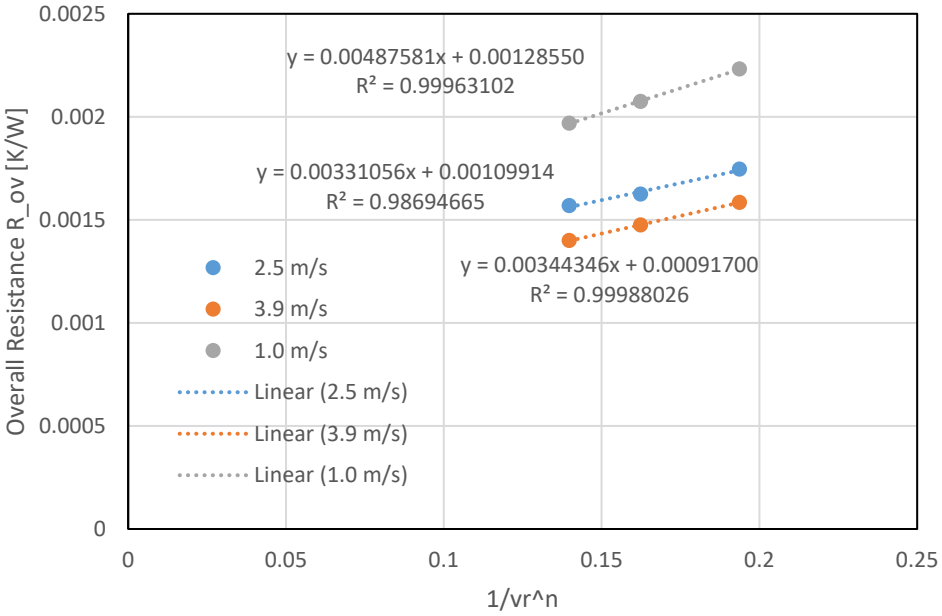

Figure 12: Original Wilson plot method with n=1

Table 12: Overall air HTCs (η^*h_o) determined by original Wilson plot method

Air frontal velocity [m/s]	Wilson plot with n=0.82 [W/m^{2}K]	Wilson plot with n=1 [W/m^{2}K]
2.5	77.7	113.9
3.9	109.0	126.2
1.0	98.5	90.1

5.5.2 Wang ε-NTU method

As discussed previously, further modifications were made to the Wilson plot method, which utilized a functional form, or correlation, for the refrigerant-side heat transfer coefficient. Beyond this improvement, Wang et al. (2000b) outlined a technique for determining air-side heat transfer coefficients from experimental data using ε-NTU relations. In this approach, the Gnielinski correlation for single-phase in-tube heat transfer (Gnielinski, 1976) is used along with details of the heat exchanger geometry in order to determine the air-side heat transfer coefficients. A thorough study of this approach was conducted for several heat exchangers. The following section describes the data reduction approach using CoilDesigner to back-calculate heat transfer coefficients using a detailed finite-volume model of each heat exchanger. Using the experimental data for Coils #2 and #5, the data reduction approach proposed by Wang and the CoilDesigner approach were compared. While the approach from Wang uses approximate NTU relations, the CoilDesigner approach accounts for the actual details of the coil geometry and circuitry. The results in Figure 13 show that both approaches produce nearly identical values of heat transfer coefficient, thereby adding confidence to the selected method. This result also indicates that, at least in these cases of simple cross-counterflow geometries, the NTU method is quite accurate at expressing heat exchanger performance and is comparable with a more complex model. The same studies were conducted replacing the

Gnielinski correlation, recommended by Wang, with the more recent AHRI standard correlations (AHRI, 2001). As might be expected, the results are nearly identical as shown in Figure 14. Figure 15 shows that when using these calculated values of heat transfer coefficient from the experiments, both techniques predict an overall capacity that matches well with the experimental value.

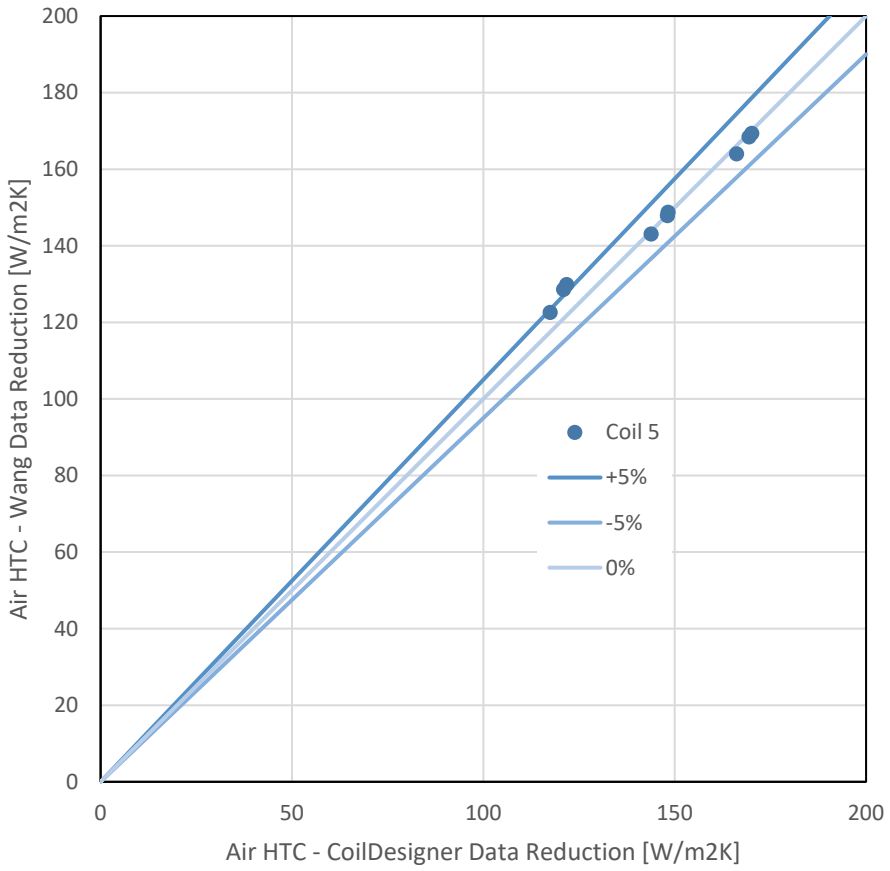

Figure 13: Comparison of data reduction techniques, both using Gnielinski correlation for refrigerant heat transfer

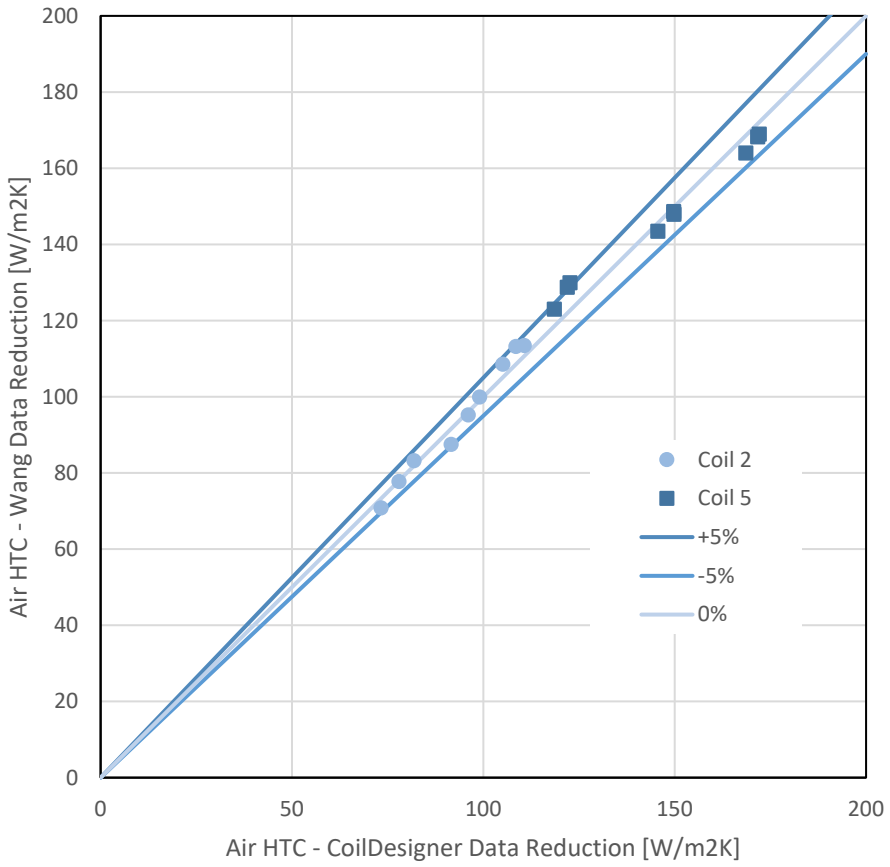

Figure 14: Comparison of data reduction techniques, using AHRI correlation for refrigerant heat transfer

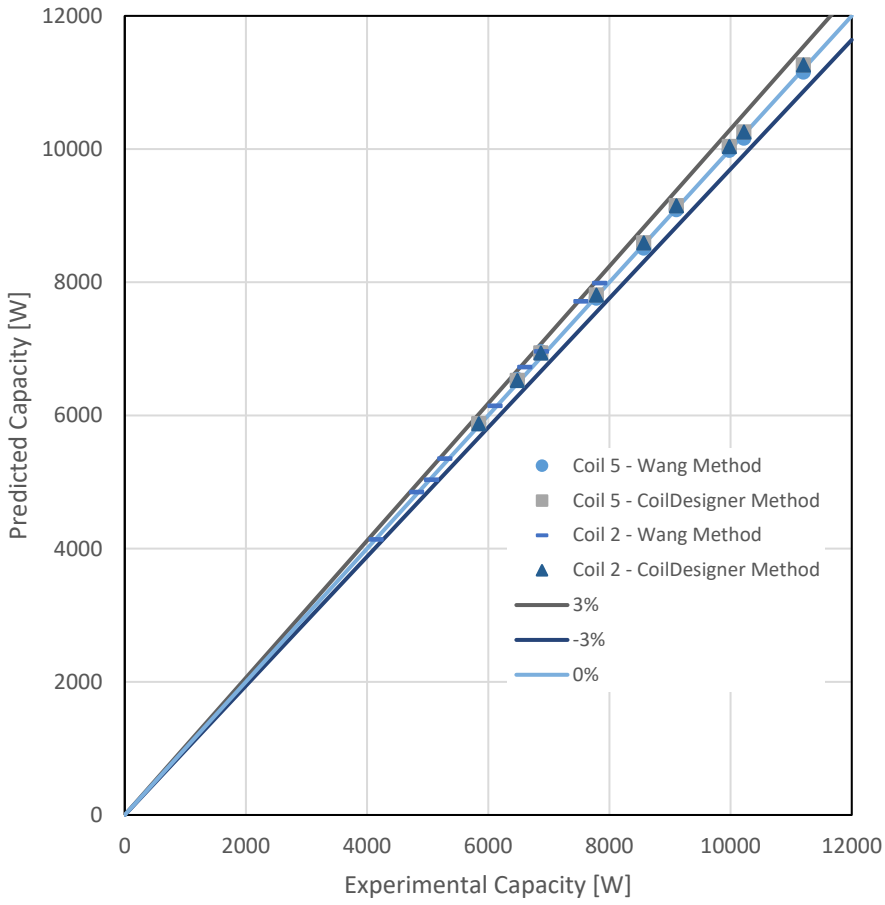

Figure 15: Comparison of predicted capacities using two data reduction techniques

5.5.3 CoilDesigner data reduction tool

The ultimate objective of this research is to provide correlations for the prediction of air-side heat transfer coefficients and pressure drops within the context of a heat exchanger simulation tool such as CoilDesigner. As such, the most rational approach for determining heat transfer coefficients from an experiment, is to back-calculate them using the exact modeling software that will be used subsequently for simulations. The CoilDesigner data reduction tool uses a detailed heat exchanger model to iteratively solve

for the air-side heat transfer coefficient that will produce the results observed experimentally. The tool also calculates non-dimensional terms including j, f, and several variations of Reynolds number; the result is a very convenient environment for quickly determining heat transfer coefficients that allow simulation results to match experimental findings.

The tool was utilized to deduce the air-side heat transfer coefficients, j, and f factors from 144 experimental observations. It was decided that data reduction should be conducted using the average heat load, as opposed to the tube-side capacity only. Using these exact values of air-side heat transfer coefficients within each CoilDesigner simulation can reliably reproduce the observed outlet conditions. In section 6.3.3, a similar technique is employed to iteratively solve for the heat transfer coefficient in the model, including effects of fin conduction, that replicates the observed capacity.

5.5.4 Experimental results

Following the above data reduction procedure, a satisfactory dataset was produced from the experimental results. Figure 18 shows the j and f factors plotted against Reynolds number for slit fin coils and Figure 19 shows the same plot for louver fin coils.

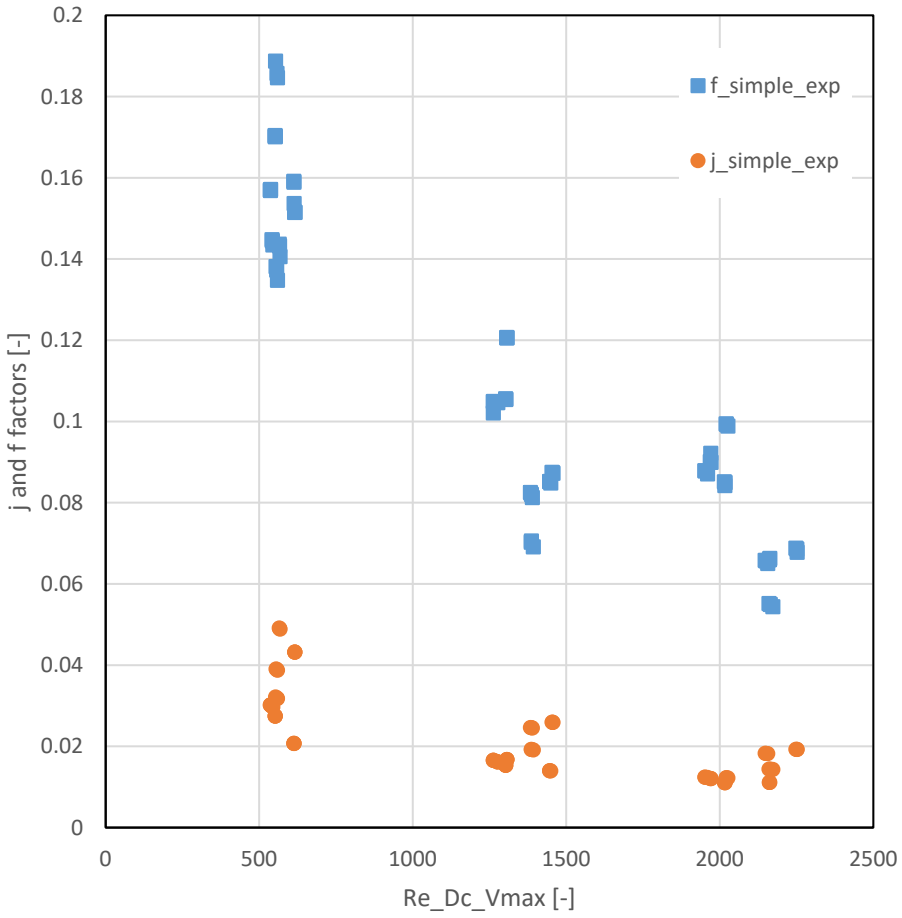

Figure 16: j and f factors for slit fin heat exchanger experiments

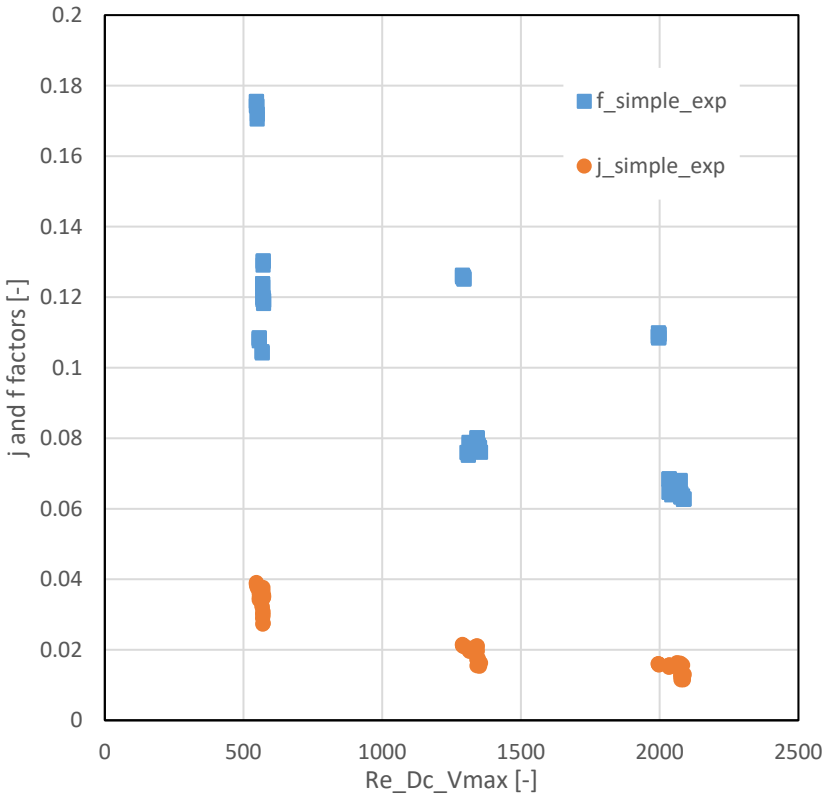

Figure 17: j and j factors for louver fin heat exchanger experiments

5.6 Refrigerant testing validation

The ultimate goal of this effort is to accurately characterize the performance of this new generation of small-diameter tube-fin heat exchangers to aid in their design for HVAC&R applications. Following the completion of testing and the development of new air-side correlations, it is therefore also necessary to ensure that the available models are able to accurately predict the performance on the refrigerant side. While the behavior inside smooth tubes is well-predicted by existing correlations, there is greater uncertainty in the accuracy of correlations for internally-enhanced tubes. For this reason, and because internally-enhanced tubes are more prevalent in 5 mm heat exchangers, a series of tests were conducted using a 5 mm heat exchanger with internally-enhanced tubes and several refrigerants. R-410A and R-404A were selected due to their wide acceptance in modern

HVAC and refrigeration applications, respectively. Additionally, R-407C was tested due to its large temperature glide. These refrigerant tests were conducted to ensure that the new air-side correlations, along with existing refrigerant-side correlations could produce accurate predictions of the overall heat exchanger performance. Particularly, it is important to ensure that the overall capacity, refrigerant pressure drop, and degree of subcooling/superheat can be predicted accurately when designing heat exchangers for real applications. Table 13 shows the test conditions chosen for refrigerant-side validation. The test matrix includes multiple values of air velocity, refrigerant saturation temperature, and refrigerant mass flow rate, to evaluate the range of applicability of the proposed correlations across many applications. This test matrix of 12 points was repeated for each of the three refrigerants, R-410A, R-404A, and R-407C.

Table 13: Refrigerant-side test matrix

Test number	Air velocity [m/s]	Refrigerant saturation temperature [K]	Degree subcooling [K]
1	1.5	318	5
2	1.5	318	10
3	1.5	318	15
4	1.5	321	5
5	1.5	321	10
6	1.5	321	15
7	4	318	5
8	4	318	10
9	4	318	15
10	4	321	5
11	4	321	10
12	4	321	15

6. Results and correlation development

With complete datasets from both CFD simulations and experimentation, it is desirable to generalize these findings through the use of correlations for air-side heat transfer and pressure drop. In the following sections, the experimental results are compared against predictions made by existing correlations from the literature (developed for larger diameter tubes), the originally published CFD-based correlations (Sarpotdar et al., 2016a, 2016b), and several new models.

6.1 Accuracy of existing correlations

This research was prefaced with a perceived need for new correlations due to the lack of available correlations developed for tube-fin heat exchangers with diameters of 5 mm and less. Existing correlations for slit and louver fins have been developed by Wang et al., (2001, 1999), but these models included experimental data for designs having diameters of 7.52 and 6.9 mm and greater respectively. The following figures compare the predictions of the correlations by Wang et al. against the experimental results from this study.

Figure 18 and Figure 19 show comparisons of the air-side pressure drop and heat transfer coefficient prediction versus experimental results for the louver fin heat exchangers tested in this study. The results show that existing correlation (Wang et al., 1999) for pressure drop can predict 15% of the experimental data with ±10% error or less and 57% of the data with ±20% error or less. The same author's correlation can predict the heat transfer coefficient within ±20% error for 25% of the data points.

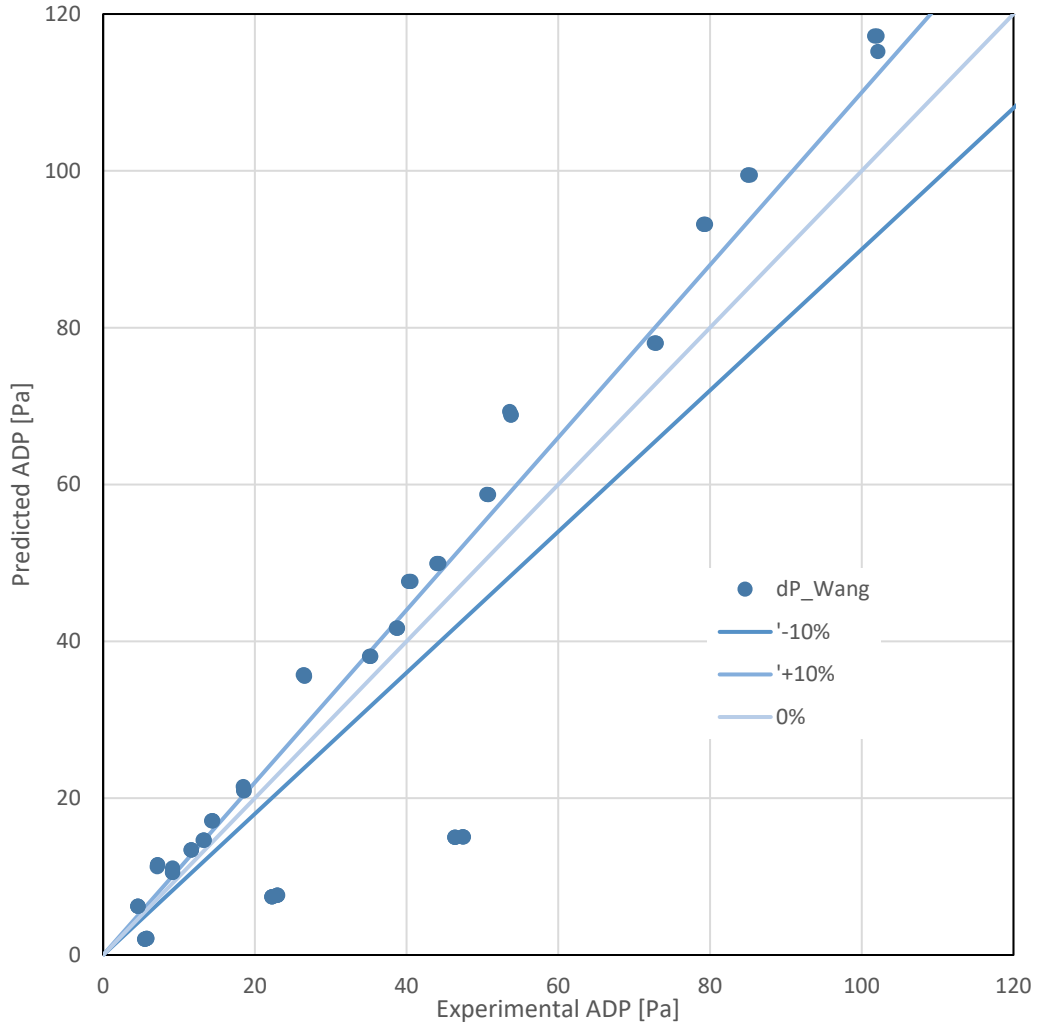

Figure 18: Predicted (Wang et al., 1999) versus experimental air pressure drop for louver fin heat exchangers

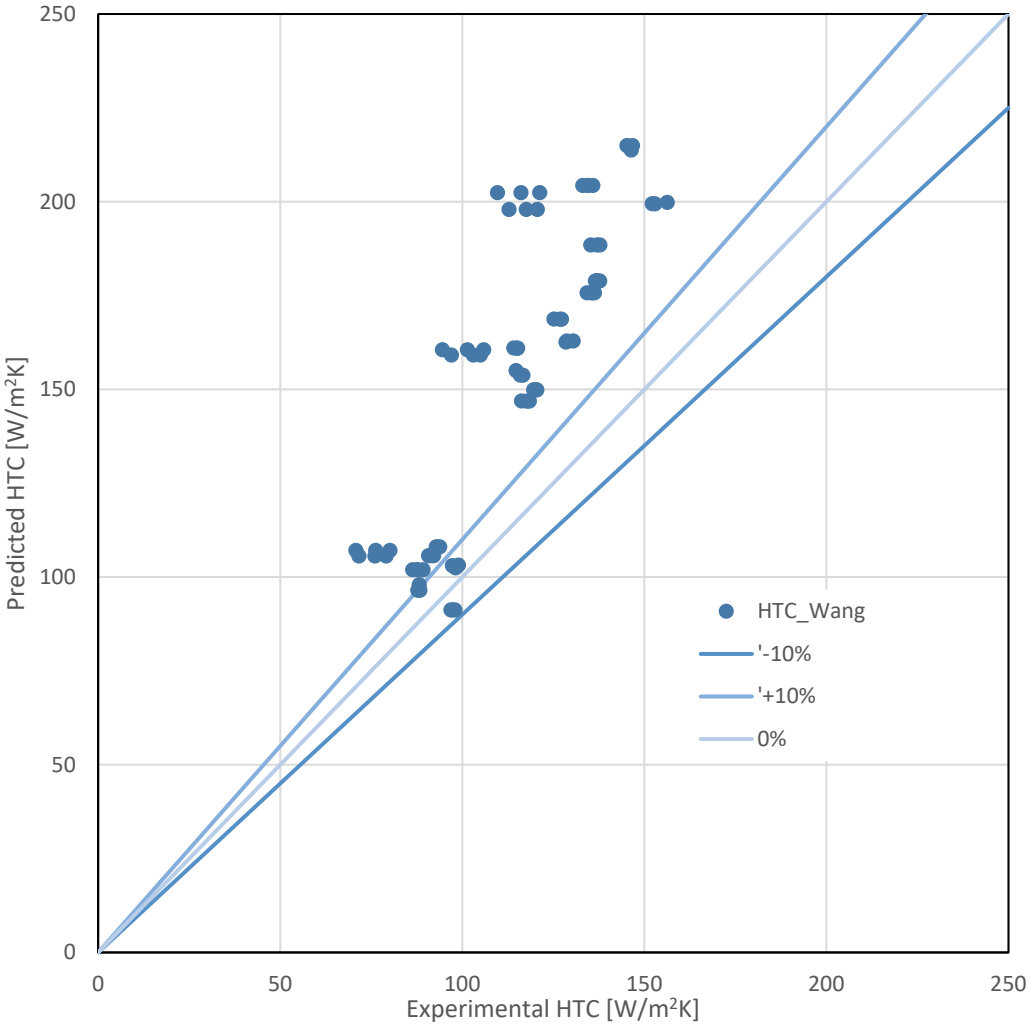

Figure 19: Predicted (Wang et al., 1999) versus experimental air heat transfer coefficient for louver fin heat exchangers

Figure 20 and Figure 21 show comparisons of predicted and experimental air pressure drops and heat transfer coefficients for the slit fin heat exchangers tested in this study. The average error for pressure drop using Wang's correlation is -37% with a standard deviation of 11%. None of the predicted data fall within the 10% error bars. The same correlation for heat transfer coefficient is has an average error of +37% with a standard deviation of 21%. 33% of the predicted heat transfer data are within 10% error or less.

In general, the existing correlations from Wang et al. do not provide satisfactory accuracy for predicting the performance of the observed 5 mm OD heat exchangers.

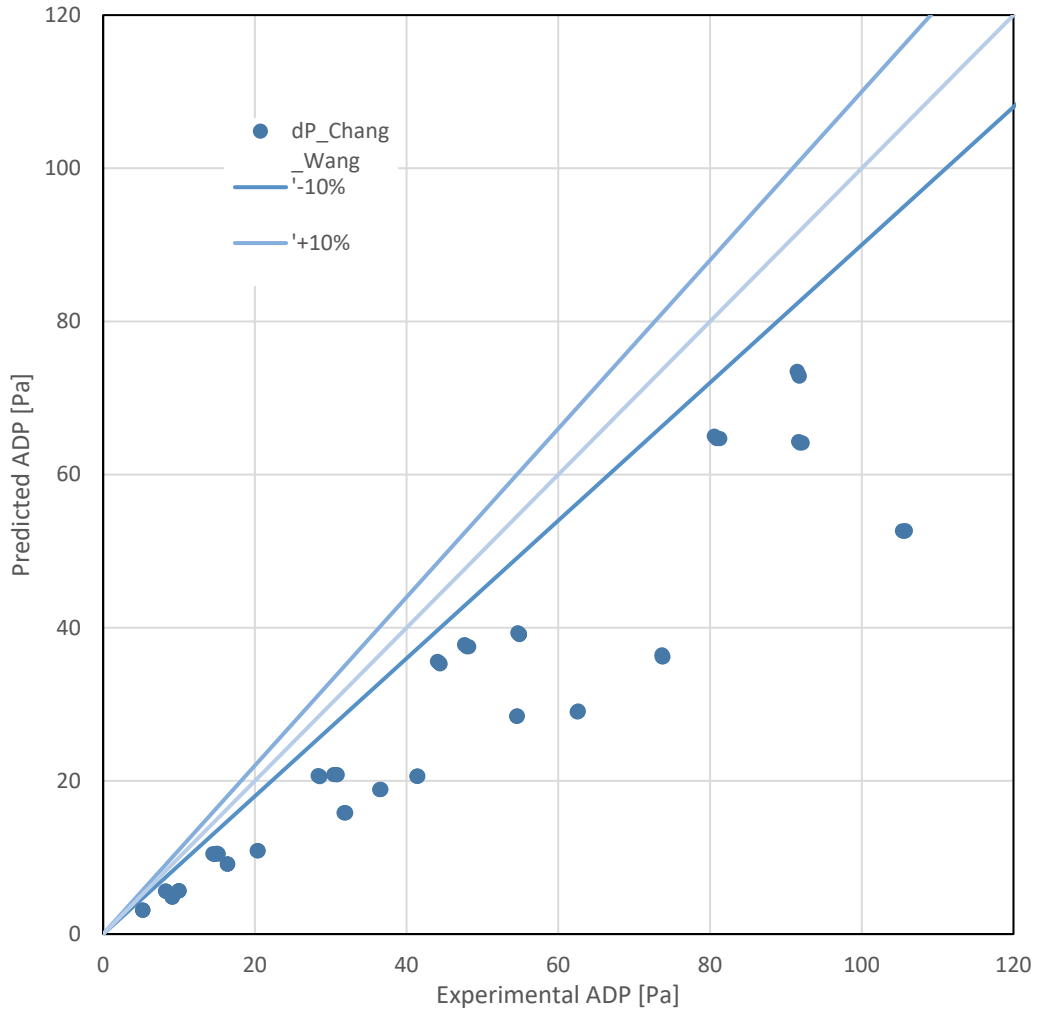

Figure 20: Predicted (Wang et al., 2001) versus experimental air-side pressure drop for slit fin heat exchangers

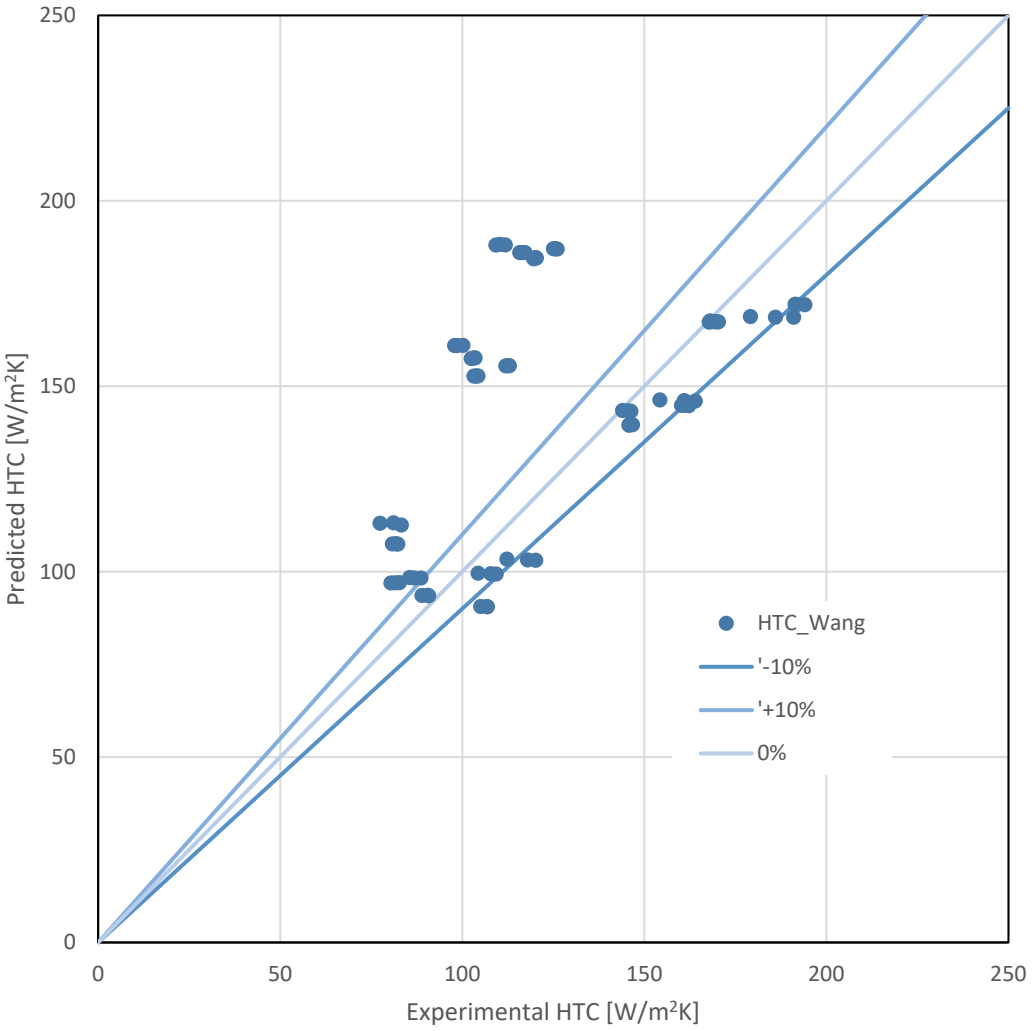

Figure 21: Predicted (Wang et al., 2001) versus experimental air-side heat transfer coefficient for slit fin heat exchangers

6.2 Original CFD-based correlations and proposed corrections

The previous section provides the motivation for developing new correlations for heat transfer and pressure drop for both slit and louver fin heat exchangers with tube diameters of 5 mm and less. Initial correlations were developed based on the work described in section 4. The following section summarizes the ability of these CFD-based correlations

to predict the experimentally-observed performance of 5 mm heat exchangers within this study.

Figure 22 and Figure 23 show the predictions (using the original CFD-based correlations) and experimental results for the louver fin heat exchangers. The air pressure drop correlation predicts the data well without any modifications; 57% of the points are predicted with 10% error or less and 100% of the data are predicted with 20% error or less. The heat transfer coefficient correlation, without alteration, predicts only 43% of the experimental data within 20% or less error. However, it should not be expected that CFD results will exactly match the observed experimental heat transfer. A single correction factor of 0.793 was determined via least squares regression; when applied to all predictions, the heat transfer coefficient correlation can predict 63% of the experimental data with 10% error or less and 99% with 20% error or less. A minor correction factor of 0.984 applied to the air pressure drop correlation improves the fit such that 68% of the data is predicted with 10% error or less.

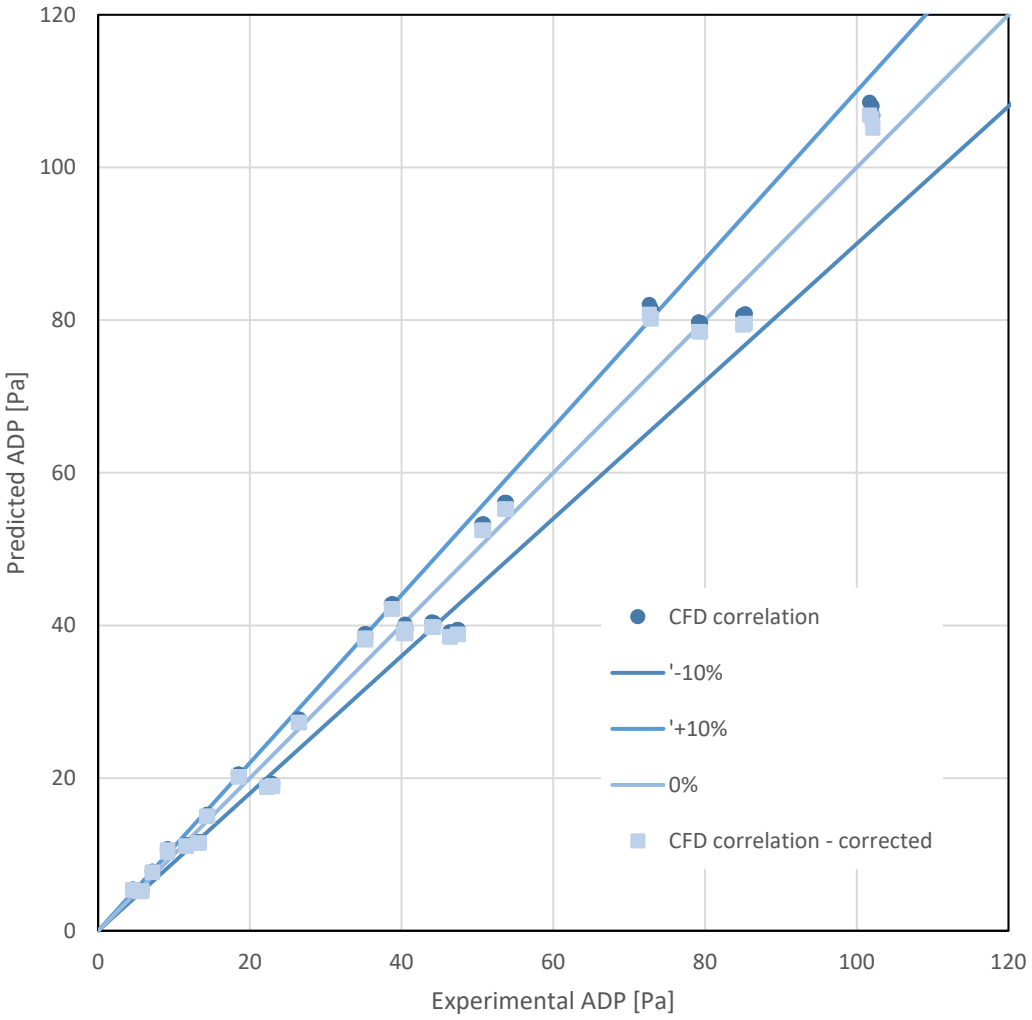

Figure 22: Predicted (Sarpotdar et al., 2016a) versus experimental air pressure drop for louver fin heat exchangers

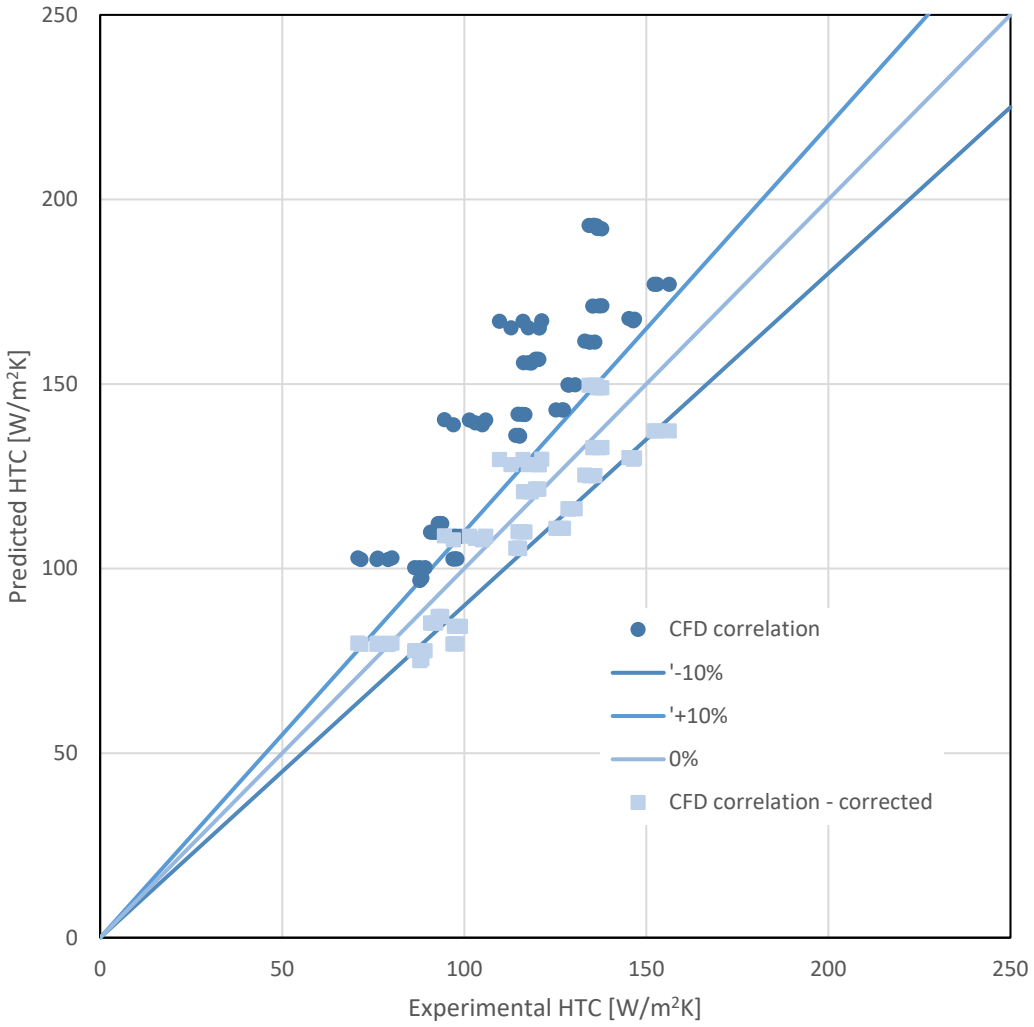

Figure 23: Predicted (Sarpotdar et al., 2016a) versus experimental air-side heat transfer coefficient for louver fin heat exchangers

The same comparison is again conducted for the slit fin heat exchangers and summarized below. Figure 24 shows an assessment of the new correlation's ability to predict air-side pressure drop in the slit fin heat exchangers and Figure 25 shows the comparison of air-side heat transfer coefficient. The proposed CFD-based air pressure drop correlation is about to predict 11% and 63% of the data with 10% and 20% error or less, respectively

without any modification. With a correction factor of 0.834 applied, the correlation can predict 92% and 100% of the data with 10% and 20% error or less, respectively.

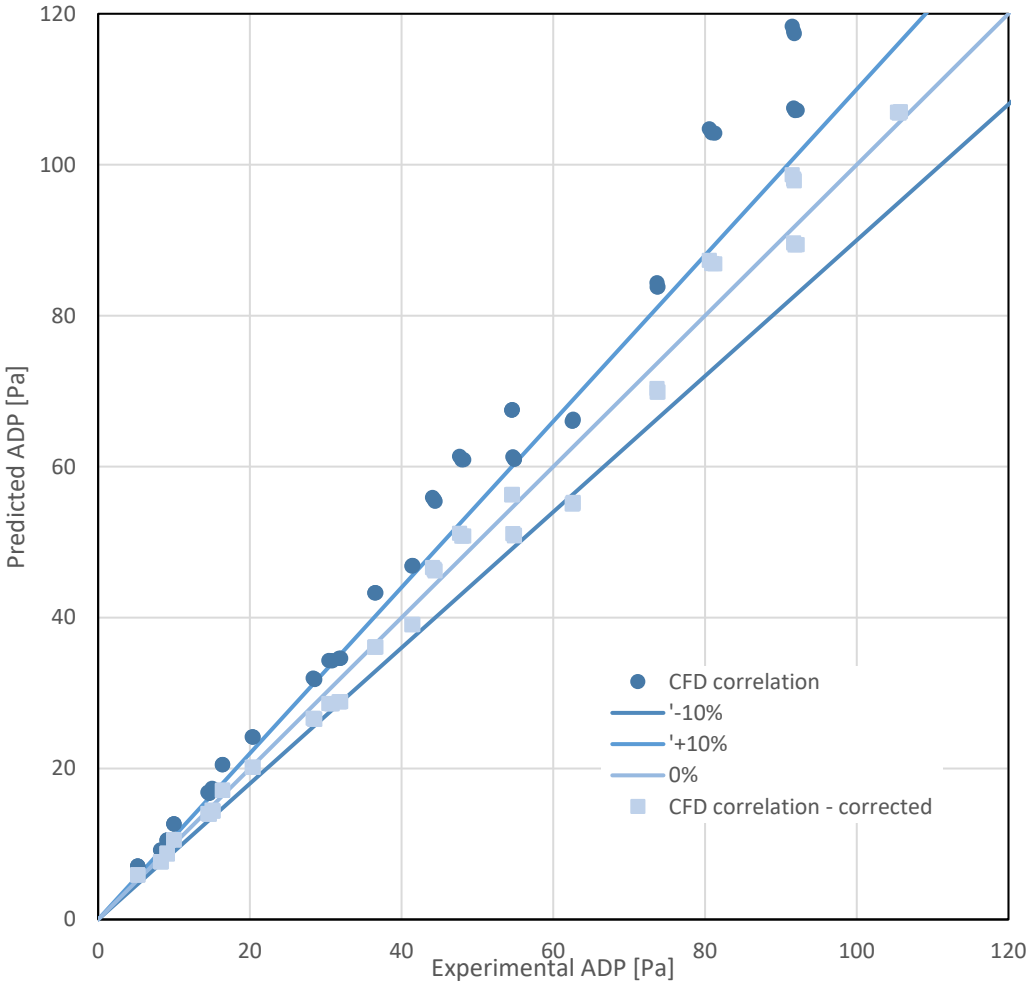

Figure 24: Predicted (modified correlation from Appendix C) versus experimental air pressure drop for slit fin heat exchangers

The CFD-based correlation for air-side HTC does not provide a good fit of the data and is only able to predict 25% of the points with 20% error or less. A correction factor of 0.6374 is proposed to improve the level of fit; the corrected correlation is able to predict

42% and 50% of the data points with 10% and 20% error or less, respectively.

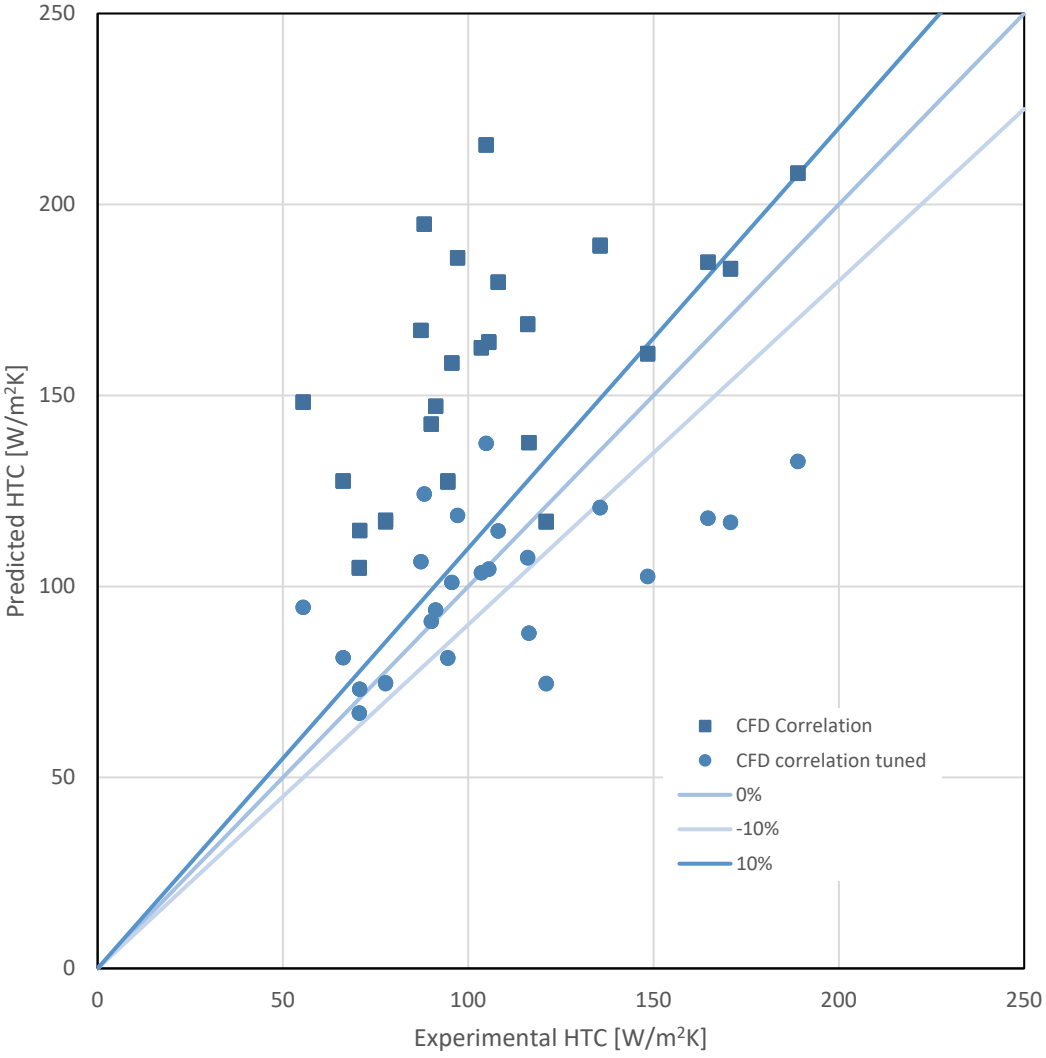

Figure 25:Predicted (Sarpotdar et al., 2016b) versus initial experimental air heat transfer coefficient for slit fin heat exchangers

6.3 Additional analysis and testing

The results in section 6.2 indicate that the newly-developed and tuned CFD-based correlations are capable of providing satisfactory predictions of air-side HTC and pressure drop for actual 5 mm louver fin heat exchangers and can also accurately predict the pressure drop of slit fin coils. However, the experimental results for the slit fin HTCs

are not well-predicted by the correlation. Additional steps were taken to understand the cause of these discrepancies and determine if the differences were a result of flaws in the correlation, experiments, or both.

6.3.1 Kriging methodology

In order to demonstrate a high-accuracy fitting technique, a model was developed using Kriging to interpolate air-side pressure drops and heat transfer coefficients from the CFD source data. This model is inherently able to reproduce all source data exactly, and is also able to reproduce random results (which it was not trained on) with greater accuracy than the linear regression models presented in previous work. Practical considerations make the implementation of a Kriging model difficult in heat exchanger simulation software, but the results are presented to demonstrate the existence of a more accurate fitting technique. The DACE toolbox for MATLAB was used to develop the model shown below for slit fin pressure drop and heat transfer coefficient (Lophaven et al., 2002).

The model was fitted to the natural log of the parameters listed in Table 14 using second-order polynomial regression and spherical correlation functions; the resulting $sigma^2$ values for log(f) and log(j) were 0.0014 and 0.0032. This model can predict the randomly generated CFD data well, as summarized in Table 15. When used to predict experimental data, the model is more accurate than the regression, but the experimental data are still not as well-matched as the CFD simulations (here the MASXX terminology is used to indicate the percentage of points predicted within XX% error or less). This evidence supports the conclusion that the CFD-based HTC correlation (regression-based) is not the source of the errors; instead, there may be flaws in the CFD simulation results and/or the experiments.

Table 14: Fitting parameters for Kriging model

Variable	Dc	Pl	Pt	N	Sh	Ns	Fp	$Re_{Dc,Vmax}$
Theta	1	5.14	10.56	0.18	0.14	0.11	0.065	103.07

Table 15: Kriging model performance for slit fin heat exchangers

	MAS5	**MAS10**	**MAS20**
Random CFD ΔP	80.6%	94.6%	98.9%
Random CFD HTC	75.3%	96.8%	98.9%
Experimental ΔP*	45.8%	87.5%	100%
Experimental HTC**	16.7%	37.5%	58.3%

*after application of 0.884
**after application of 0.574 correction factor

The Kriging approach was also used to examine the impact the number of source data points on the overall performance of the correlation. Separate Kriging models were developed using less than the total number of source data points simulated within CFD. The total slit fin dataset used for Kriging contains a total of 872 points after removing infeasible designs and designs with small temperature differences where "pinching" may occur. Reducing the design space to use only the feasible full-factorial designs and 500 Latin hypercube samples results in a correlation with greater error in predicting the random data set, however the agreement is still very good, as shown in Table 16 and Table 17. Reducing the number of Latin hypercube (LHC) samples to 200 yields further degradation of the model performance, but the results may still be satisfactory in a number of applications. These findings indicate that the number of CFD simulations conducted may have been excessive and a lesser number of runs could have characterized performance within the design space with comparable accuracy. This is particularly important due to the high computational cost of CFD simulations.

Table 16: Performance comparison of slit fin Kriging models for j factor

	MAS5	MAS10	MAS20
738 LHC samples	75.3%	96.8%	98.9%
500 LHC samples	65.6%	93.5%	98.9%
200 LHC samples	52.7%	75.3%	98.9%

Table 17: Performance comparison of slit fin Kriging models for f factor

	MAS5	MAS10	MAS20
738 LHC samples	80.6%	94.6%	98.9%
500 LHC samples	72.0%	94.6%	98.9%
200 LHC samples	65.6%	94.6%	98.9%

6.3.2 Alternate correlation forms

The level of fit achieved by the correlations shown above is still not satisfactory for the slit fin heat transfer coefficient predictions. Using experimental data only, a new correlation for j factor was developed using the form proposed by Wang et al. (2001). The form of this equation is presented in equations (18-22) and separate coefficients are prepared for 1 row and 2 row coils and summarized in Table 18. The resulting correlations can predict the 1 and 2 row coil j factors as described in Table 19.

$$j = C_4 Re_{Dc}^{j_4} \left(\frac{F_s}{D_c}\right)^{j_5} \left(\frac{S_s}{S_h}\right)^{j_6} N^{j_7} \tag{18}$$

$$j_4 = C_{14} + C_{15}\left(\frac{P_t}{P_l}\right) - C_{15}N \tag{19}$$

$$j_5 = C_{16} + C_{17}\sqrt{\frac{N}{Re_{Dc}}}\ln\left(\frac{N}{Re_{Dc}}\right) + C_{18}\sqrt{\frac{N}{Re_{Dc}}} \tag{20}$$

$$j_6 = C_{19} + C_{20}\left(\frac{S_s}{S_h}\right)\ln\left(\frac{S_s}{S_h}\right) - C_{21}\left(\frac{S_s}{S_h}\right)^3 \tag{21}$$

$$j_7 = C_{22} + C_{23}\sqrt{Re_{Dc}}\ln(Re_{Dc}) - C_{24}\sqrt{Re_{Dc}} \tag{22}$$

Table 18: Coefficients for experimental slit fin correlation

Coefficient number	Fitted for 1 row coils	Fitted for 2 row coils
4	1.069788	1.069084
14	-0.52982	-0.53512
15	-0.04054	0.016804
16	-0.00552	-0.01094
17	0.405993	0.411528
18	5.576799	5.575592
19	24.20262	24.2028
20	0.270963	0.264593
21	1.063362	1.049096
22	-0.13354	-0.21602
23	0.3749	0.374888
24	0.0046	0.001932
25	-0.0433	-0.04368

Table 19: Performance of modified Wang correlation for slit fin heat transfer coefficient

Data points within XX% error	1 row coils	2 row coils
5%	72%	25%
10%	100%	49%
20%	100%	66%

The correlation form presented by Wang appears to provide a satisfactory fit for the tested heat exchangers, especially for 1 row coils. It was necessary to develop two separate correlations for 1 and 2 row coils because a combined correlation had very poor accuracy. The poor level of fit that is achieved for 2-row heat exchangers raises suspicions about the accuracy of experimental results for these heat exchangers.

6.3.3 Fin conduction

Another important phenomenon was identified in further analysis of the slit fin experimental results. The data reduction approach was repeated after enabling CoilDesigner's fin conduction model (Singh, 2009),. This solver allows for the

calculation of conductive heat transfer along fins between adjacent tubes and was validated against experimental data. It was observed that the air HTC calculated using the fin conduction solver differed from the HTC calculated using the standard “fast” solver in some cases. Examining these differences further led to additional insights.

Test #1 for coil #8 is taken as an example to illustrate this point. In this case, with an air velocity of 3.65 m/s, the proposed CFD-based correlation predicts an air-side HTC of 250.5 W/m^2K, but initial experiments suggested an observed HTC of just 104.9 W/m^2K. However, closer examination reveals that the large refrigerant ΔT between inlet and outlets of the counterflow circuitry and the high density of fins, result in significant conductive heat transfer from tube to tube along the fins. Figure 26 shows the counterflow circuitry and Figure 27 shows the average tube temperature along each of the three circuits, calculated using the CoilDesigner conduction solver. The figure shows that the tubes in the first row of the coil (at the ends of the circuits) are actually increasing in water temperature, due to this conduction effect. The large temperature difference between rows can result in more than 300 W of heat entering some individual tubes in the first row solely through conduction, reducing the net heat transfer in the first row and in some cases creating tubes that have a net positive heat gain as shown in Figure 28.

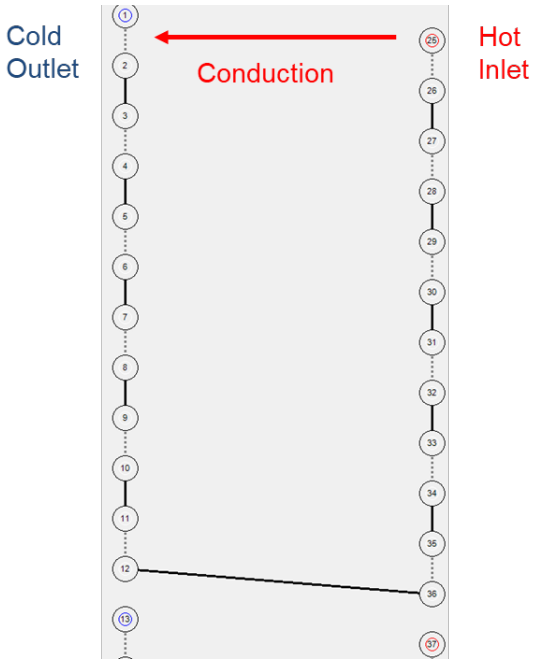

Figure 26: Counterflow circuitry with conductive heat transfer between banks

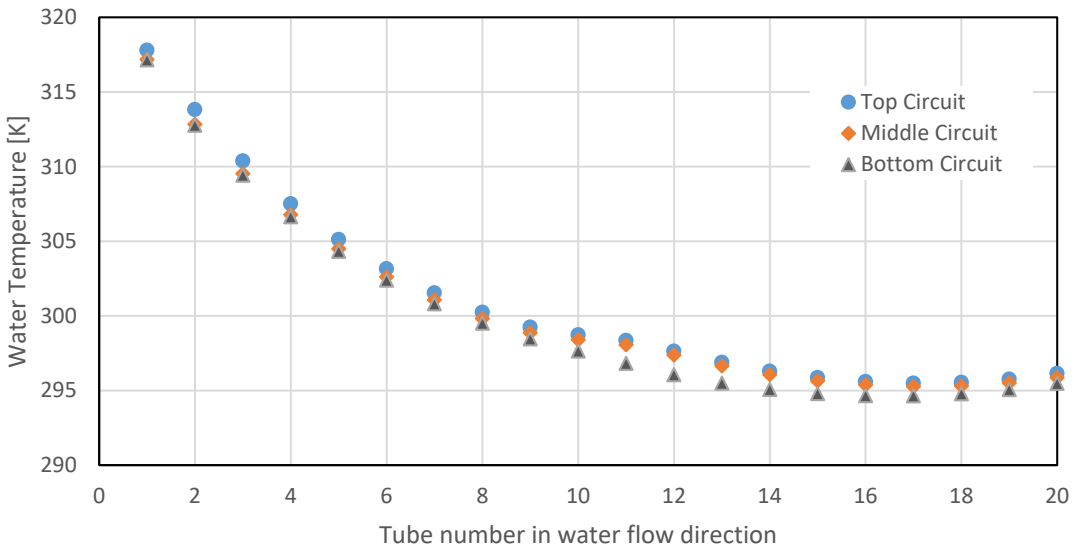

Figure 27: Average water temperature calculated using CoilDesigner conduction solver (Coil #8, Test #1)

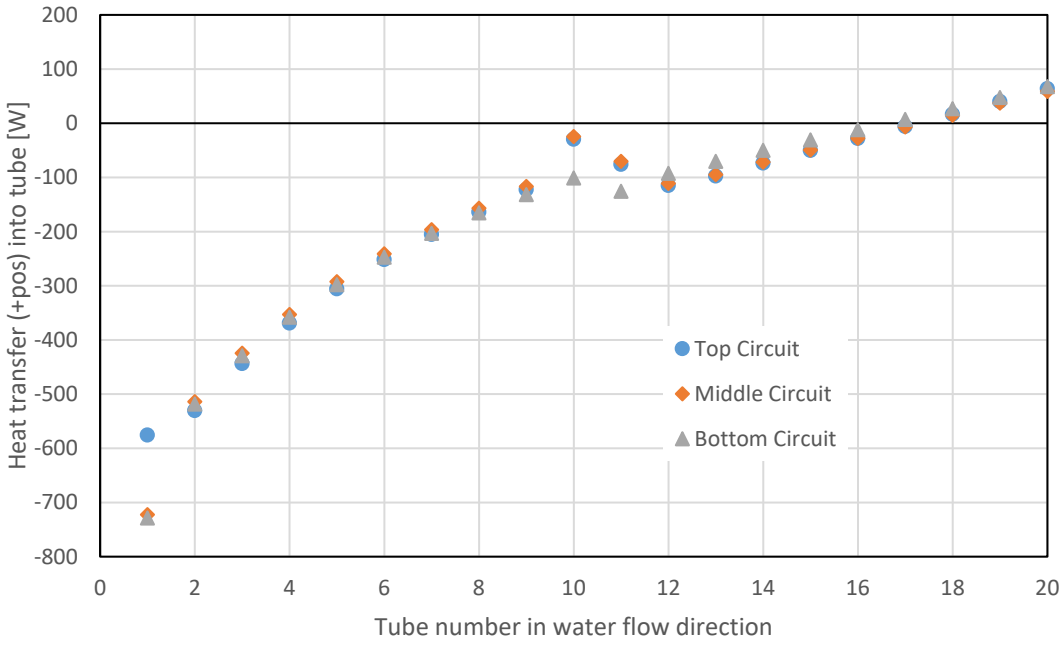

Figure 28: Net heat transfer by tube using CoilDesigner conduction solver (Coil #8, Test #1)

When data reduction is carried out using these results, the total heat rejection of the coil is attributed to the entire surface area of the heat exchanger, but because much of the first row of the coil is not effective in transferring heat, the apparent heat transfer coefficient is quite small. Results of this type with a high level of fin conduction are therefore not suitable for determining air-side heat transfer coefficients. Steps should be taken to identify and avoid these conditions when testing heat exchangers to determine air-side HTC. These findings indicate that the values of HTC derived from initial testing were flawed in some 2-row heat exchanger designs.

6.3.4 Additional testing

Initial testing conditions were established to ensure sufficiently turbulent flow inside the tubes, ensure adequate water-side temperature difference, and minimize refrigerant

resistance to the extent possible. The tests which were conducted utilized the maximum mass flow rate of the water pump to accomplish this, however, Section 6.3.3 indicated the insufficiency of the existing experimental setup to provide suitable experimental results for air-side data reduction. In the time since the initial testing conducted for this work, a larger water pump was acquired at the test facility and was utilized for limited repeat testing of coils where results were unsatisfactory.

It was first necessary to identify which heat exchanger tests were affected by this issue. By repeating data reduction with and without the fin conduction model, the most problematic tests could be identified; if the air-side HTC calculated with conduction was significantly different than the value without conduction, then this was taken as an indication that the initial test could be flawed. Analysis showed that the two-row slit fin heat exchangers were affected by this phenomenon due to their counterflow circuitry.

In order to demonstrate the effect of fin conduction on determining air-side HTCs, testing was repeated under conditions with nearly an order of magnitude higher water flow rates. This required the implementation of a new water pump, the addition of one Coriolis flow meter, and the modification of coil circuitries. Coils with 24 tubes and 2 circuits were modified to contain 12 circuits and coils with 30 tubes and 3 circuits were modified to contain 15 circuits. The new test conditions and circuitries significantly reduced the temperature difference between inlet and outlet tubes and the subsequent fin conduction between banks; this led to observations of higher HTCs for two-row coils than were previously possible with the original equipment and instrumentation.

Coils 1, 3, 4, 6, and 8 were re-tested with water flow rates of 0.8, 0.9, and 1.0 kg/s. The results showed significantly higher HTCs for the re-tested 2-row coils, while the 1-row

coil's HTC was nearly the same. The unmodified correlation significantly over-predicts HTC performance for all tests, but less so for coils 5-8. By applying a 0.678 correction factor to the HTC correlation, 25% of the HTC data can be predicted with 10% error or less and 86% of the results can be predicted with 20% error or less. Figure 29 shows the experimental HTCs plotted against the correlation predictions with and without the correction factor applied.

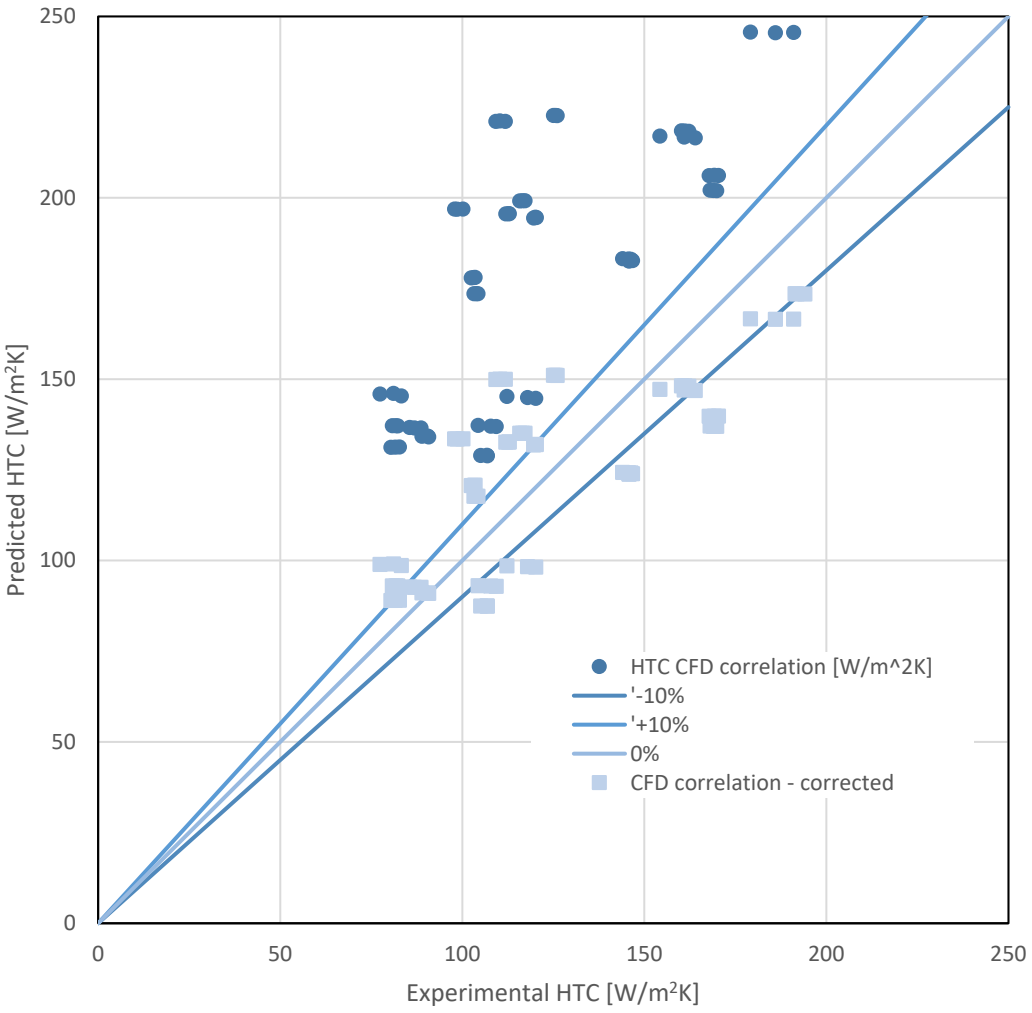

Figure 29:Predicted (Sarpotdar et al., 2016b) versus experimental air heat transfer coefficient for slit fin heat exchangers (including repeated tests)

6.4 Proposed new correlations

6.4.1 Louver fin

The analysis in section 6.2 and summary in Table 20 demonstrate the high degree of accuracy of predictions made by the CFD-based correlation when validated against experimental tests. The air pressure drop correlation is able to predict 68% and 100% of observed air pressure drop data with 10% and 20% error or less, respectively with the application of a 0.984 correction factor. A single correction factor of 0.776 applied to the air-side HTC correlation results in model predictions that match 58% and 100% of experimental data within 10 and 20%, respectively. These correlations provide satisfactory predictions of air-side performance for louver fin heat exchangers and the previously-published correlations (Sarpotdar et al., 2016a) are recommended for future use (with the addition of the recommended correction factors).

It should be noted that the discussion of fin conduction in section 6.3.3 is also applicable to the louver fin heat exchangers. The air-side HTCs were calculated for the louver fin test results using the fin conduction model; the calculated HTCs were nearly identical to the original results without the fin conduction model with the exception of coils 13 and 15. These heat exchangers had significantly different values of HTC when accounting for fin conduction. Re-testing these heat exchangers was not possible at the time of publication; if they are omitted from the experimental dataset, the correction factor becomes 0.816 and can predict 78% of the remaining data with 10% error or less and 100% of the data with 20% error or less.

Although heat exchangers with 3 mm and 4 mm tube diameters were not tested in this study, the performance of these correlations is expected to be similar across the entire 3-5

mm design space that was evaluated. While it cannot be confirmed until more testing of 3 and 4 mm heat exchangers is completed, it should be expected that these correlations can be used reliably to predict the performance of these designs.

6.4.2 Slit fin

As was observed for the louver fin, the tuned slit fin air-side pressure drop correlations developed from CFD simulations show excellent agreement with experimental observations, predicting 92% and 100% of experimental data with 10% and 20% error or less, respectively. A correction factor of 0.834 was required to achieve this level of fit and the modified correlation proposed in Appendix C can be recommended.

After retesting a sample of heat exchangers, the air-side heat transfer correlation was able to predict 25% and 86% of the HTC data with 10% and 20% error or less. A correction factor of 0.678 is recommended based on the completed 5 mm heat exchanger testing. Experimental results matched much more closely with observations for coils 5-8 than coils 1-4. The results show a substantial diversity in the performance of slit fin heat exchangers; coils 5-8 differ from the correlation by an average of 23%, while the average HTCs of coils 1-4 are nearly 43% lower than the predictions. It is possible that differences or defects in the manufacturing of some of these coils could be inhibiting their performance.

Table 20 shows the summary of the prediction accuracy of the correlations examined in this section. These findings are noteworthy because they show that models which were developed solely based on CFD simulations as source data are able to predict experimental observations in slit and louver fin heat exchangers with minimal

modification or tuning. Table 21 summarizes the correction factors recommended to minimize errors in predicting the experimental findings in this work.

Table 20: Summary of correlation predictions of experimental data

Correlation	% Air HTC data predicted within 10%	% Air HTC data predicted within 20%	% Air ΔP data predicted within 10%	% Air ΔP data predicted within 20%
Louver fin (Wang et al., 1999)	11.1	25.0	15.3	56.9
Louver fin (Sarpotdar et al., 2016a)*	62.5	98.6	68.1	100.0
Slit fin (Wang et al., 2001) **	33.3	56.9	0.0	4.2
Slit fin (Sarpotdar et al., 2016b)*, **	25.0	86.1	91.7	100.0

*after application of correction factor
**results after re-testing

Table 21: Recommended correction factors (conventional data reduction)

Correlation	Recommended HTC Correction Factor	Recommended ΔP Correction Factor
Louver fin (Sarpotdar et al., 2016a)	0.793	0.984
Slit fin (Sarpotdar et al., 2016b)	0.678	0.834

6.4.3 Data reduction including conduction effects

The analysis in section 6.3.3 illustrates the potential significance of conduction effects in calculating the heat transfer coefficient in some test conditions. An alternative approach to performing data reduction was implemented by iteratively solving for the value of air-side HTC that reproduces the observed average capacity from each experiment within a CoilDesigner model that includes fin conduction effects. For most data points, the HTC computed from this approach does not differ from the original value calculated neglecting

conduction effects by a substantial margin. However, the results are consistently different, indicating that the HTC, when accounting for conduction effects, does differ from the value calculated from the original CoilDesigner data reduction approach or even the simpler ε-NTU-based method described by Wang et al. (2000). Data reduction was repeated for all test points (following the re-testing of slit fin coils described in section 6.3.4) and Figure 30 shows a comparison of the HTCs calculated with the fin conduction model versus the previous values without fin conduction. Also included in the plot are the outlier results of coil 13 and 15 which exhibited significant conduction effects which produced poor reduced data, yet re-tests could not be conducted.

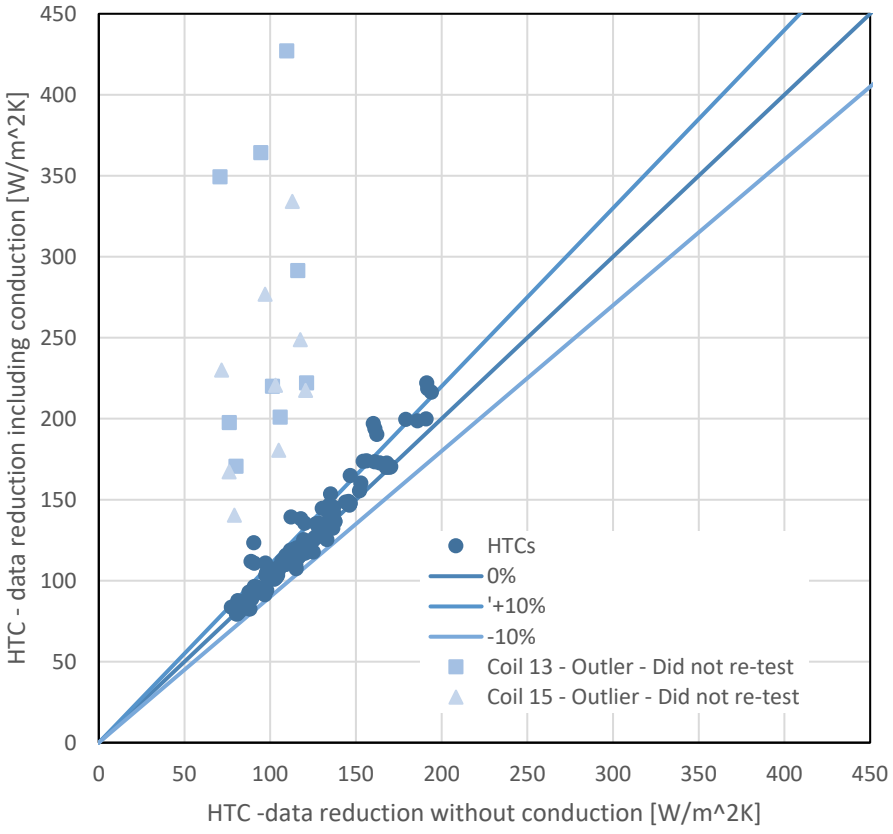

Figure 30: HTC calculated including conduction effects versus HTC calculated neglecting fin conduction

When seeking a correction factor for the heat transfer correlations, the prospect of applying a single correction factor to both correlations was evaluated. One major contributor to the deviation between CFD predictions and observed heat transfer performance is likely the thermal contact resistance between fin and tube. El Sherbini et al. (2003) summarized past research on thermal contact resistance in tube and fin heat exchangers and highlighted several publications that reported that fin contact resistance could contribute between roughly 10 and 50% of the overall thermal resistance of the studied heat exchangers. While it is a difficult quantity to measure directly, it is clear that contact resistance between fin and tube can contribute significantly to a heat exchanger's overall thermal resistance and the magnitude of this effect can vary depending on the quality of materials and manufacturing processes. Figure 31 shows a simple thermal circuit representation of the heat exchanger. The CFD-based correlation development approach lacks any modeling to predict the thermal contact resistance between fin and tube, and through experimental validation, this quantity is effectively incorporated into the correction factor applied to the CFD-based correlation. Because of different manufacturing processes and quality standards, it is possible that the heat exchangers tested as part of this effort had varying levels of contact resistance. It is proposed here that a single correction factor can be applied to both the louver and slit fin datasets to minimize the error in both. This correction factor would seek to express the average deviation between CFD prediction and observed heat transfer regardless of fin enhancement type.

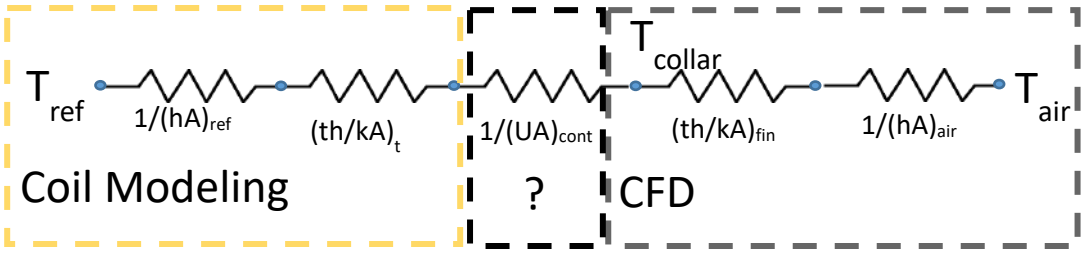

Figure 31: Simplified thermal circuit

Again, least squares regression was used to determine the value of correction factor that minimizes errors between the predicted HTC and observed HTC (calculated from this approach). A correction factor of 0.84 was found to minimize errors. When all slit and louver data points are included, 61% of points are predicted with 20% error or less and 49% of points are predicted with 10% error or less. However, coils 13 and 15 are clear outliers that should be re-tested when possible in future work. Coils 1-4 are also clearly outliers and may suffer from high thermal contact resistance between fin and tube due to manufacturing differences or defects. It should be noted that coils 1-4 were prototype coils produced by a manufacturer without mass-production tooling for smooth tube 5 mm heat exchangers and it is likely that the contact quality is not as high as coils produced using more robust expansion techniques. Coils 5-8 and 13-16 were produced with pressure expansion techniques and Coils 9-12 were produced by mechanical expansion by a capable manufacturer. All coils were manufactured as prototypes and there may be some possibility that production-scale heat exchangers could have different values of thermal contact resistance depending on the processes employed. When omitting coils 1-4 and 13 and 15, the louver and slit correlations with a 0.84 correction factor can predict 98% of points with 20% error or less and 78% of points with 10% error or less. Figure 32

shows a summary of all slit and louver fin results and identifies the outlier points that should be retested and those (1-4) with anomalously low performance, potentially due to poor fin-to-tube contact.

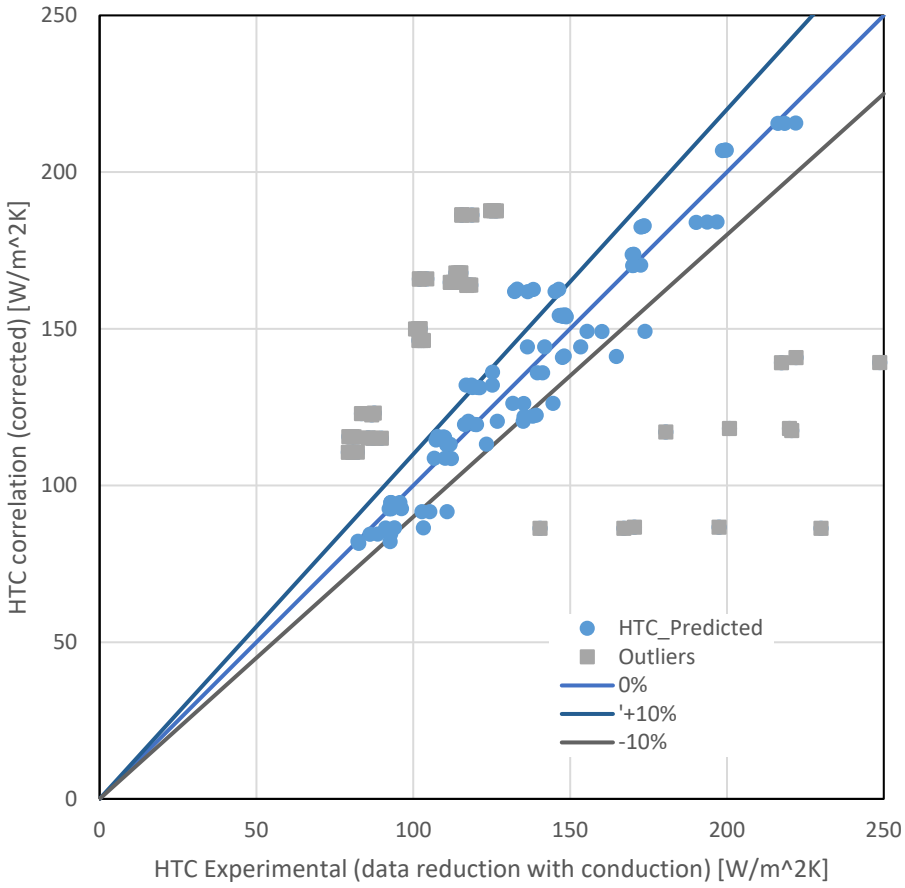

Figure 32: Comparison of tuned HTC predictions against experimental observations for both louver and slit datasets

7. Applications

7.1 Refrigerant validation

As described in section 5.6, additional tests were conducted using a louver fin heat exchanger with internally-enhanced tubes with three different refrigerants in condenser operating conditions. The purpose of these tests was to verify that the newly developed air-side correlations, in conjunction with the selected refrigerant-side correlations, were able to accurately predict the performance of complete heat exchangers with a variety of refrigerants in two-phase operating conditions. CoilDesigner was used to perform these simulations using the correlations outlined in Table 22. As shown in Figure 33, the predicted capacities match well with the experimentally-observed values. The total refrigerant pressure drops are also well-predicted, with 92% of all points predicted with 20% error or less as shown in Figure 34. As expected from the findings in section 6.2, and shown in Figure 35, the air-side pressure drop is well-predicted. Additional, Figure 36 shows that the heat exchanger models are able to accurately predict the degree of subcooling for the tested near-azeotropic mixture and refrigerants with temperature glide. Actual error bars are shown and the degree of uncertainty in subcooling comes mainly from the random component, caused by fluctuating readings, and the need to calculate refrigerant properties to find saturation temperatures.

Table 22: Correlations used for refrigerant validation

	Heat transfer	**Pressure drop**
Air-side	(Sarpotdar et al., 2016b) * 0.84 correction	(Sarpotdar et al., 2016b) * 0.984 correction
Single-phase refrigerant	(Ravigururajan and Bergles, 1985)	(Schlager et al., 1989)
Two-phase refrigerant	(Koyama and Yonemoto, 2006)	(Koyama and Yonemoto, 2006)

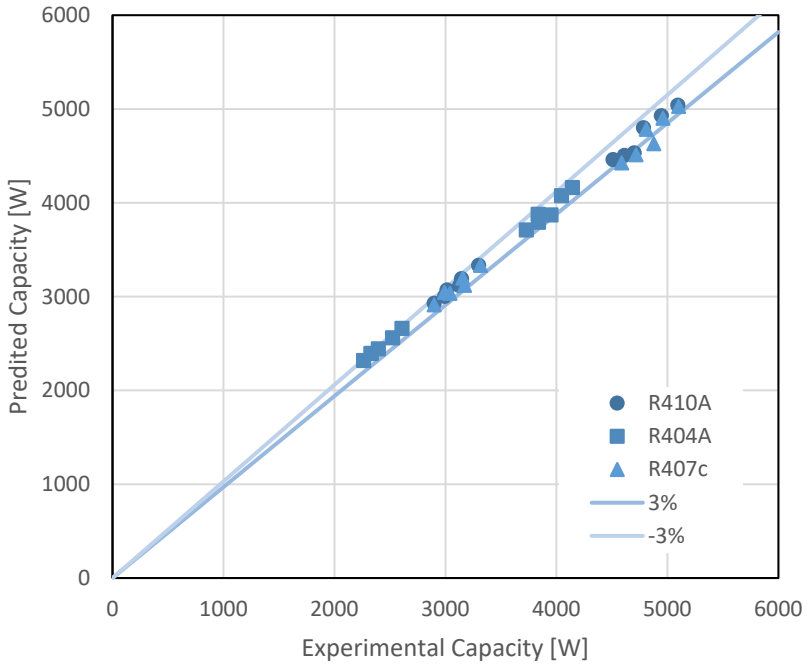

Figure 33: Simulated versus experimental capacity from condenser validation testing

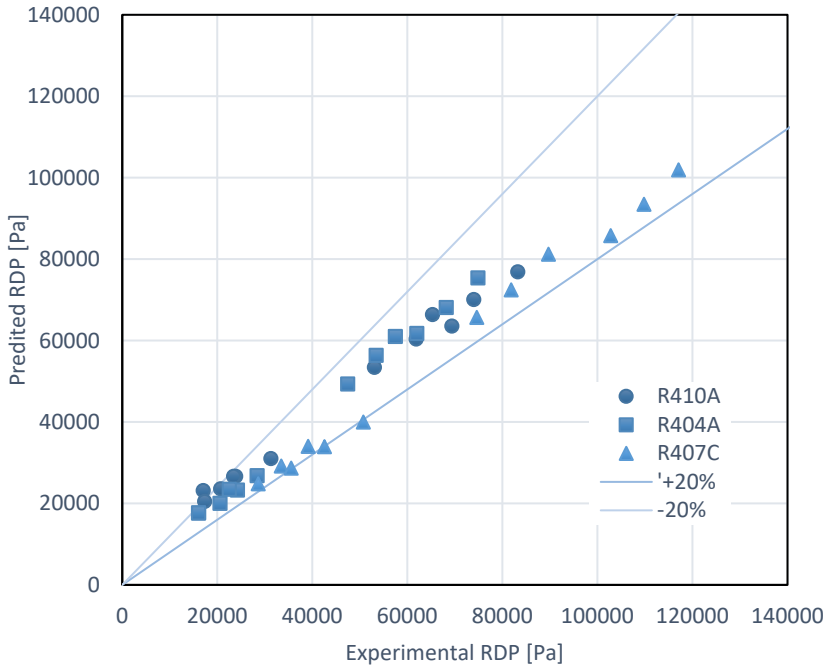

Figure 34: Simulated versus experimental refrigerant pressure drop from condenser validation testing

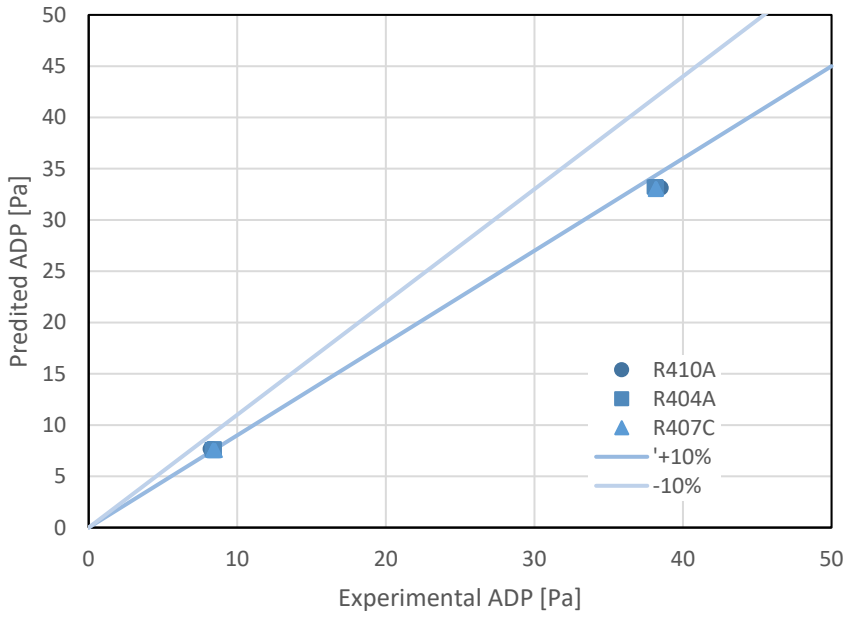

Figure 35: Simulated versus experimental air pressure drop from refrigerant testing

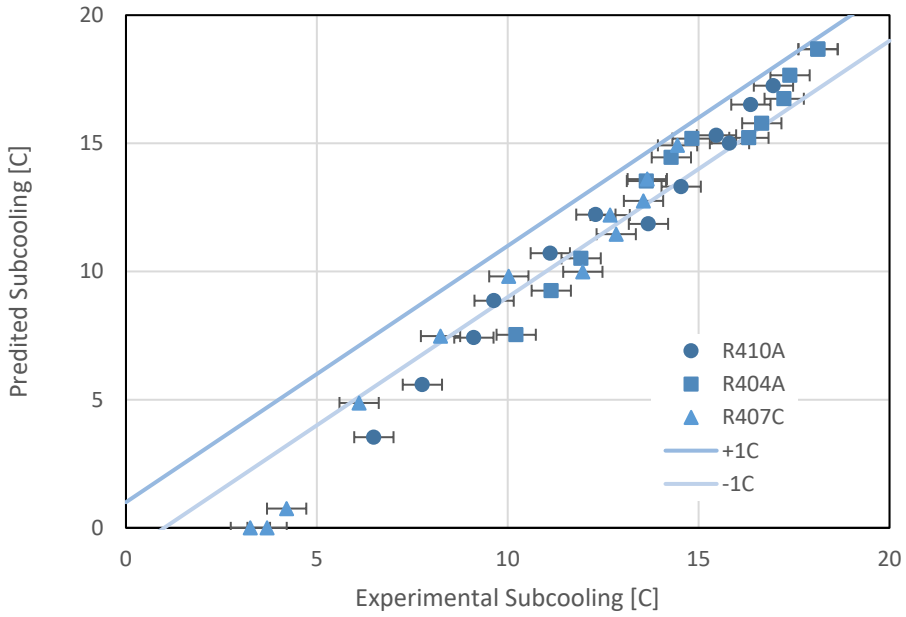

Figure 36: Simulated versus experimental subcooling from refrigerant validation testing

The purpose of this section is to succinctly illustrate that the combination of the new air-side correlations, existing correlations for refrigerant-side performance, and modeling software, such as CoilDesigner, can produce accurate simulations of an entire heat exchanger with two-phase refrigerant. The ability to accurately predict air pressure drop is critical for considering fan performance in the design of a heat exchanger and the accurate modeling of refrigerant pressure drop and subcooling is necessary to accurately model any vapor compression system. In this sense, a primary objective of this research has been satisfied by demonstrating the required tools to enable engineers to accurately model, design, and optimize these types of enhanced-fin heat exchangers with tube diameters of 5 mm and less.

7.2 Experimental validation at CEEE

During the course of this project, additional experiments were conducted by other researchers at CEEE (Huang and Gao, 2016). Two slit fin heat exchangers, one having 5 mm OD tubes and another have 4 mm tubes were tested with water as the working fluid to extract air-side performance information. These particular heat exchangers were constructed with internally-enhanced tubes; as such, data reduction is more difficult and less certain due to the lack of reliable correlations for tube-side performance. Additionally, the exact slit geometries (which are proprietary) differ from the geometry for which the CFD-based correlations were developed for; the 5 mm heat exchanger has a greater slit width, and the 4 mm heat exchanger has an asymmetrical slit arrangement. Both the Wilson plot method and the CoilDesigner data reduction tool were used to extract air-side heat transfer coefficients and the results varied significantly. Because of these challenges, these data are not used in the correlation tuning conducted in section

6.2, but are presented here as additional data points confirming the relative performance of the original CFD-based correlations in predicting geometries outside of the ranges for which they were developed. Figure 37 shows a comparison of the simulated and experimental air pressure drops for the tested 5 mm heat exchanger using the proposed correlation for slit fins as well as the existing correlation from Wang (2001). Figure 38 shows a comparison of the air-side heat transfer coefficients predicted with the new model versus the experimentally-observed heat transfer coefficients determined using the CoilDesigner data reduction approach and Wilson plot method. Figure 39 and Figure 40 show the same comparisons for the sample 4 mm heat exchanger. The results show that the new correlations provide predictions with less error than the existing models even for these fin geometries which are slightly outside of the correlation range.

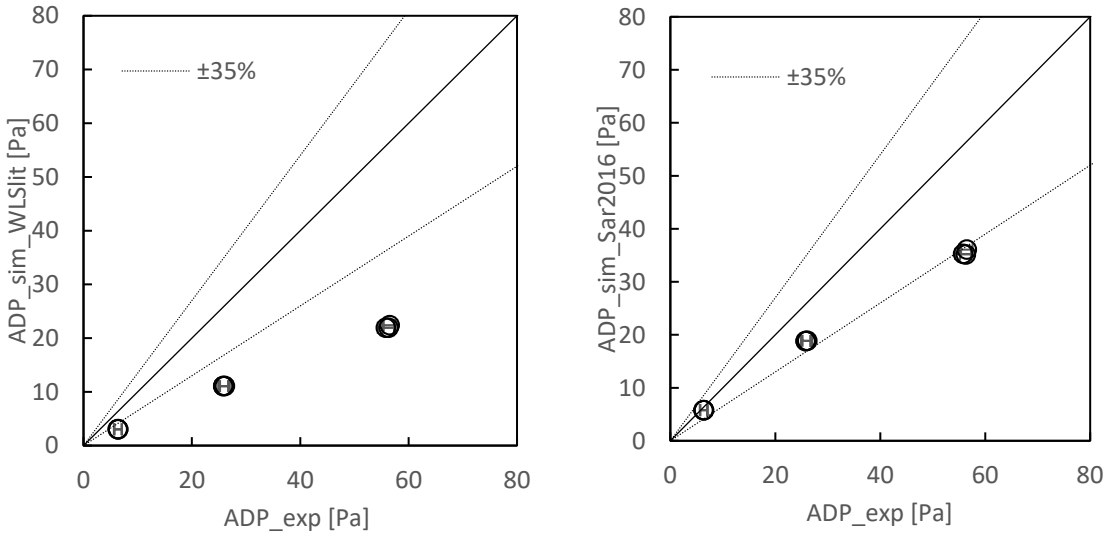

Figure 37: Comparison of simulated and experimental air pressure drop of 5 mm heat exchanger. Wang (2001) correlation (left), Sarpotdar (2016) correlation (right)

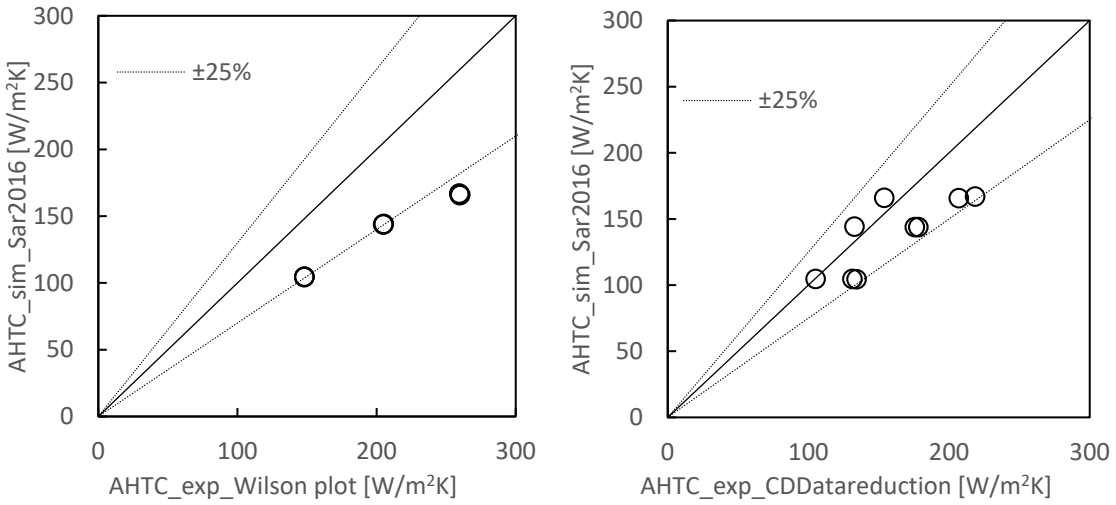

Figure 38: Comparison of simulated and experimental heat transfer coefficients of 5 mm heat exchanger. CoilDesigner data reduction (left), Wilson plot method (right)

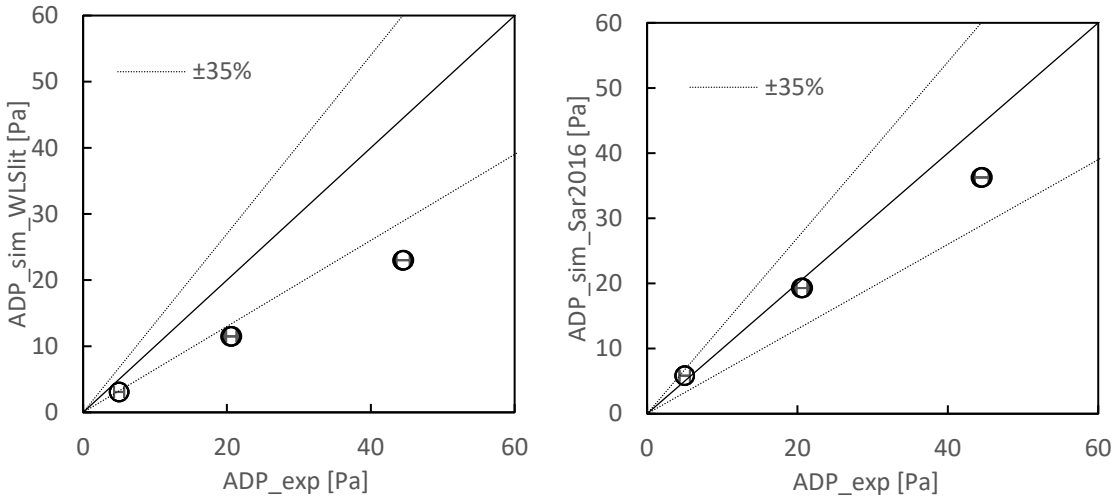

Figure 39: Comparison of simulated and experimental air pressure drop of 4 mm heat exchanger. Wang (2001) correlation (left), Sarpotdar (2016) correlation (right)

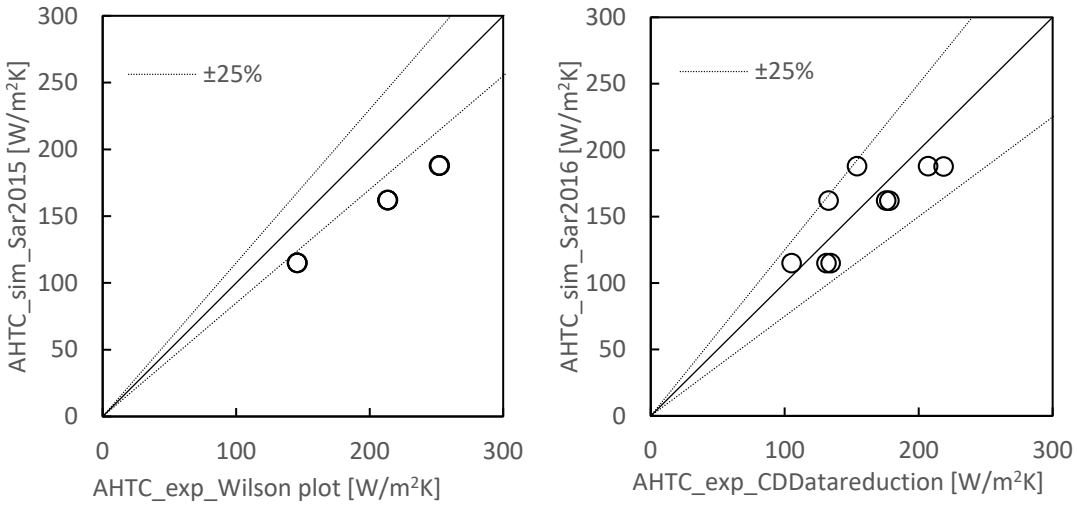

Figure 40: Comparison of simulated and experimental heat transfer coefficients of 4 mm heat exchanger. CoilDesigner data reduction (left), Wilson plot method (right)

7.3 Optimization study

A significant application of these new air-side heat transfer and pressure drop correlations is found in the design and optimization of new heat exchangers. The broad range for which these correlations were developed, allows for the assessment of performance of a wide range of designs which are not limited to the fin patterns currently available on the market. As such, conducting optimization studies of heat exchangers using these new correlations enables the design of new heat exchangers as well as new fin designs that will perform best under certain criteria.

One such example was prepared using these new air-side correlations and was described in Nasuta et al. (2017). In this study, a replacement condenser coil was sought for an existing 1-ton mini-split air conditioner system. This baseline system is summarized in Table 23. These optimization studies explored heat exchangers with tube diameters ranging from 3 to 9.52 mm and considered all variables outlined in Table 24. The

problem was defined such that the heat exchanger's operating conditions, performance, and face area would remain the same as the baseline, while several performance criteria were optimized, as summarized in Table 25. Heat exchanger models were programmatically constructed using CoilDesigner to create models for each candidate geometry. A custom software using a Multi-Objective Genetic Algorithm (MOGA) solver was used to carry out the optimization. Because of the wide range of tube diameters, different correlations are used for different tube diameters. Table 26 contains the selected correlations; all tubes are considered to be internally-enhanced, and for large diameter tubes, a 1.5x correction factor is applied to refrigerant heat transfer and pressure drop correlations for smooth tubes to approximate this difference. This correction factor was validated from experimental testing of the baseline unit (Li and et al., 2014).

Table 23: Baseline heat exchanger summary

Parameter	**Value**
Size: LxWxH [m / in]	0.76x0.26x0.58 / 29.9x10.2x22.8
Tubes	Copper microfin, 9.52 mm / 0.375 in
Fins	Aluminum, Wavy
Refrigerant	R410A
Heatload	4 kW / 1.14 R.T.
Air Pressure Drop	26 Pa
Estimated Condenser Charge	0.71 kg

Table 24: Optimization variables

Parameter	Value
P_l	$2xD_o$ to $4xD_o$
P_t	$1.1xP_l$ to $2xP_l$
N_B	1 to 6
FPI	14 to 40
S_h/L_p	$0.3xF_p$ to $0.7xF_p$/0.8 to 1.8 mm
# Tube banks	1 to 5
# Tubes per bank	16 to 32
# Circuits	All numbers evenly divisible by number of tubes per bank
N_{slits} / $N_{louvers}$	2 to 6 / 2 to 8

Table 25: Optimization constraints

Parameter	Value
$T_{in, ref}$	66.0°C / 150.8°F
$P_{in, ref}$	2726.8 kPa / 27.3 bar
$\dot{m}_{ref}$	20.1 g/s / 2.7 lbm/min
$T_{in, air}$	35°C / 95°F
$P_{in,}$ air	101.3 kPa / 14.7 PSI
Air Flow Rate	0.5 m^3/s / 1059.4 CFM
Face Area	0.4 m^2 / 4.3 ft^2
HX aspect ratio (Tube length/height)	<1.5
Subcooling	≥6°C / 10.8°F
Heat load	≥4 kW / 1.14 R.T.

Table 26: Correlation selection for optimization studies

Correlation Type	Small Diameter Tubes (3, 4, 5 mm)	Conventional tubes (7, 7.94, 9.52 mm)
Slit Fin: Air HTC / ΔP	Sarpotdar et al., 2016a	Wang et al., 2001
Louver Fin: Air HTC / ΔP	Sarpotdar et al., 2016b	Wang et al., 1999
Refrigerant single-phase HTC	Churchill, 1977	Gnielinski, 1976 x1.5 CF
Refrigerant single-phase ΔP	Churchill, 1977	Churchill, 1977 x1.5 CF
Refrigerant two-phase HTC	Yu et al., 1998	Shah, 2013 x1.5 CF
Refrigerant two-phase ΔP	Yu et al., 1998	Friedel, 1979 x1.5 CF

Within this framework, several optimization studies were conducted, considering different objectives important to heat exchanger design. Optimization was carried out on both louver and slit fin geometries. However, since the results are very similar, the only louver fin results are presented here.

A major factor in heat exchanger design is obviously cost, and as the popularity of aluminum microchannel heat exchangers increases and the global market for heat exchangers expands, tube-fin heat exchanger producers see increasing pressure to reduce costs to remain competitive. A key advantage of small-diameter tube fin heat exchangers is their increased material utilization and compactness; in other words, they can provide more heat transfer surface area per quantity of tube material compared to larger-diameter designs. This advantage can be seen in Figure 41, where Pareto-optimal heat exchanger designs show lower material costs as the tube diameter decreases. Here the “Raw Material Cost” is defined as the mass of aluminum and copper multiplied with their raw material costs at the time of writing (4.775 USD/kg for copper and 1.55 USD/kg for aluminum). This approach does not account for the more complex labor, tooling, and capital costs that are truly required to construct a heat exchanger because these parameters vary widely across manufacturers and locations, however, the raw material cost is representative of the total cost and provides a fair basis for comparison. Figure 41 shows the potential for reduced diameter designs to achieve a lower air-side pressure drop than the 26 Pa baseline, but also significantly reduce raw material costs while maintaining the same performance and face area. At a lower air-side pressure drop than the baseline, 5 and 3 mm designs have the potential to reduce raw material costs by roughly 50 and 70%, respectively. 5 mm and smaller designs appear to consistently cost

less than equivalent 7 mm designs and the plot also shows that from a raw material cost perspective, 3 mm designs still offer significant savings over 5 mm designs (approximately 30% lower). It is important to note that these designs with lower air flow rate will perform better than the baseline in an actual system; the lower friction resistance will result in some reduction of fan power and/or increase in volumetric air flow rate, thus increasing heat exchanger capacity and/or system COP.

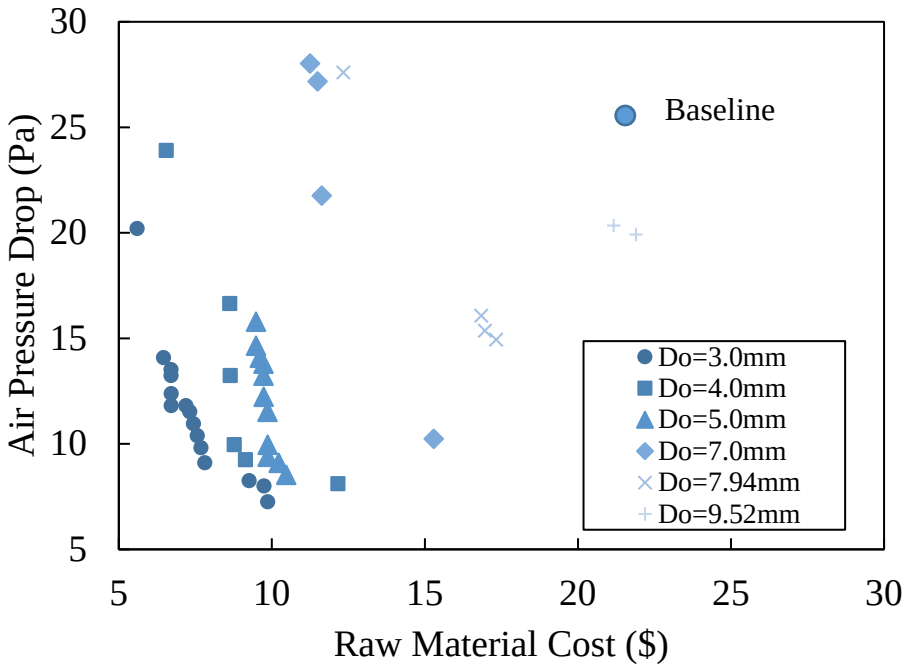

Figure 41: Pareto results, minimization of material cost and air pressure drop

Other major drivers in heat exchanger design include environmental impacts, safety, and regulatory conformity. As governments throughout the world seek to combat global climate change, new regulations seek to limit the greenhouse gas emissions of refrigerants by limiting the maximum allowable GWPs of working fluids. Many newer

fluids with lower GWP values also present other risks in terms of flammability or toxicity, so the refrigerant quantities are often also limited by safety regulations. It is therefore necessary to find solutions in heat exchanger design that can reduce the required refrigerant charge in order to enable these more environmentally-friendly fluids while meeting all safety requirements. Figure 42 shows the results of this optimization study seeking to minimize air pressure drop and refrigerant charge, this time using R32 (and appropriate operating conditions from experimentation) as the refrigerant. The findings are significant because R32, an A2L – or "mildly flammable" – refrigerant, is currently implemented in some countries, but limited due to safety concerns in others. The ability of small diameter heat exchangers to perform with equivalent capacity but drastically-reduced refrigerant charge may allow designers to safely implement new, more environmentally-friendly, refrigerants and mitigate their risks. The lower absolute quantity of refrigerant also means that the potential quantity of refrigerant that can be leaked, and subsequent global warming impact, will necessarily be reduced. The figure shows that 3, 4 and 5 mm designs can achieve equivalent performance with roughly an order of magnitude less refrigerant than the baseline heat exchanger. Even 7 mm designs have approximately twice the refrigerant charge of equivalent 5 mm designs, which should be expected from the ratios of internal volumes (comparing 7^2 and 5^2).

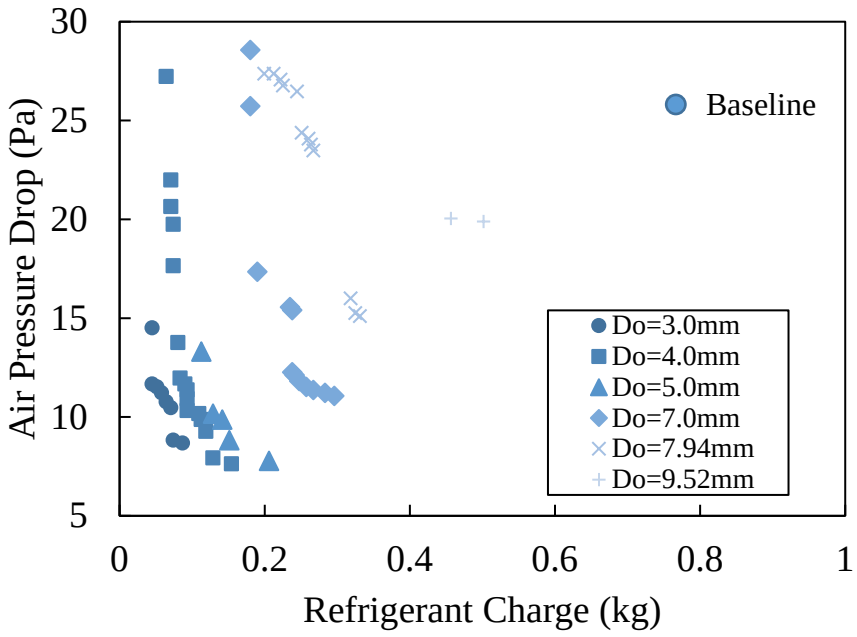

Figure 42: Pareto results, minimization of refrigerant charge and air pressure drop

8. Conclusions

The intended purpose of this research is to make several contributions towards the manner in which heat exchanger performance is characterized and to provide valid correlations for two particular tube-fin heat exchanger geometries. The work indicates that the CFD-based correlation development technique implemented by others in the past, for example Bacellar et al. (2014), is a suitable technique, verifiable by experiments, for these louver- and slit-fin geometries. The DOE sampling approach was successful in characterizing performance through a vast design space with only a limited number of CFD-simulations, and the proposed correlations were able to predict CFD source data with a high degree of accuracy, predicting 97+% of data with 20% error or less.

Experiments were conducted on 16 heat exchangers with 5 mm tubes and varying configurations of fin dimensions. Several data reduction approaches were utilized to extract heat transfer coefficients and dimensionless j- and f-factors from the experimental data; these comparisons served to highlight the limitations of each technique and provided validation of results by confirming that multiple techniques produce similar values. CoilDesigner was ultimately selected as an accurate tool for performing data reduction, accounting for the heat exchanger geometry and circuitry in detail.

Experimental results validated the accuracy of the CFD-based air-side pressure drop correlations, which matched 100% of louver fin and slit fin tests with 20% error or less with correction factors applied. These results are promising and show an equivalent or better level of fit than most experimentally-based correlations in the literature. Applying a single correction factor to the original CFD-based correlation for louver fins predicts 99% of experimentally-observed HTCs with 20% error or less, respectively. The

corrected correlation is able to predict 86% of slit fin heat transfer coefficients with 20% error or less. When HTCs are instead calculated using a new procedure that accounts for fin conduction and a single correction factor of 0.84 is applied to both slit- and louver-fin correlations, 61% of all data points are predicted with 20% error or less, but when outlier points are removed, 98% of the data can be predicted with 20% error or less.

When applied to modeling heat exchangers with two-phase refrigerant flow, the selected correlations were able to predict the performance of condensers with R410A, R404A, and R407C with a high degree of accuracy. This verification confirms that the recommended correlations can be used reliably by designers to evaluate the performance of small diameter slit and louver fin heat exchangers. Additionally, several optimization studies were conducted using these new correlations to identify heat exchanger designs that could minimize material costs and refrigerant charge. These studies highlight the potential benefits that can be realized through the reduction of tube diameter and show, for example, that an optimized 5 mm heat exchanger may have roughly 50% lower cost and 80+% less refrigerant charge than the 9.52 mm baseline heat exchanger.

9. Future work

The experimental verification conducted as part of this research focusses on heat exchanges with 5 mm OD tubes due to the absence of 3 mm and low availability of 4 mm heat exchangers at the time of writing. As these heat exchangers become more prevalent in the market, additional testing should be conducted to confirm the accuracy of these CFD-based correlations. Additional efforts should be considered to extend testing in the wet surface condition when condensing water covers the fin surfaces.

While the ranges of the proposed correlations are expansive, there are some other characteristics that do certainly have a major impact on the performance of the fins and were not fully included in this study. Expanding the design space to include a range of louver angles and slit widths as well as different fin thicknesses would broaden the applicability of the correlations and may result in new fin designs with greater performance than what is possible in the current designs space.

Additional studies should be conducted to better understand the number of CFD simulations required to develop suitable correlations and guidelines should be formed. The current process of CFD-based correlation development, while almost certainly less intensive than a purely experimental approach, is still highly computationally expensive and if the same quality of correlation can be developed from less data, the approach will be even more appealing. Conversely, as computational power continues to improve, conducting CFD simulations of fin performance will become increasingly accessible and future researchers will be less motivated by minimizing computational time and more willing to perform high-accuracy simulations of air-side or entire heat exchanger performance when evaluating new designs.

This work showed that the deviations between observed heat transfer coefficients and predictions may indicate that fin contact resistance plays a significant role in the performance of a heat exchanger which cannot be predicted through CFD tools. Additional research into the quantification of thermal contact resistance between fins and tubes in heat exchangers should be conducted. Current methods for measurement and correlations to predict fin contact resistance have unacceptably high uncertainties. If the CFD methodology is to be implemented for predicting heat transfer coefficients of tube-fin heat exchangers, researchers must develop a stronger understanding of the impact of contact resistance in order to predict the true performance of these types of heat exchangers.

At present, small diameter tube-fin heat exchangers present solutions to a number of problems faced by the industry. 5 mm heat exchangers are already being implemented widely and some manufacturers are beginning to introduce 4 mm designs. While this work aims to present the design tools necessary to implement these designs, there are still a number of manufacturing challenges that must be addressed. Reductions in tube diameter result in increasing refrigerant pressure drop per unit length and therefore require significant increases in the number of circuits within a heat exchanger. As designs with 5, 4 and 3 mm tubes are considered, manufacturers must find ways to construct coils with large numbers of circuits at a low cost, with a low rate of failure/leakage, and with uniform refrigerant distribution to each circuit. Fin collar diameters are limited by the tube hole diameter; a smaller diameter tube means that less material can be pressed to form a collar. The consequence of this limitation is that as tube diameters decrease, the fin density must increase. In order to maintain the same air pressure drop, it is desirable

to reduce the air velocity by increasing the coil face area, which can often be a challenge from a product development perspective. Placing tubes into fin sheets and expanding tubes also becomes increasingly difficult with reduced-diameter tubes. So while the benefits of reducing tube diameter are clear, and tools have been proposed for their design and simulation, the industry must address a number of manufacturing challenges before heat exchangers with tube diameters less than 5 mm see widespread adoption.

Nomenclature

OD	Outer diameter	m
A	Area	m^2
ADP	"Air delta P", pressure drop	Pa
Ch	Sh/Fp	-
Cl	Pl/Dn	-
Ct	Pt/Pl	-
Dc	Collar diameter	m
Dn	Nominal diameter	m
Do	Outer diameter	m
f	friction factor	-
Fp	Fin pitch (center to center distance between fins)	m
FPI	Fins per inch	-/in
Fsp	Fin spacing (distance between fin faces)	m
Ft	Fin thickness	m
G	Mass flux	kg/m^2s
h, HTC	Heat transfer coefficient	W/m^2K
j	j factor	-
k	Thermal conductivity	W/m-K
LMTD	Log mean temperature difference	K
Lp	Louver pitch	m
$\dot{m}$	Mass flow rate	kg/s

N	Number (of tube banks in airflow direction, if no subscript)	-
P	Pressure	Pa
Pd	Pattern depth	m
Pl	Longitudinal tube pitch	m
Pr	Prandtl number	-
Pt	Transverse tube pitch	m
$\dot{Q}$	Heat transfer rate	W
Re	Reynolds number	-
Sh	Slit height	m
T	Temperature	K
u	Velocity	m/s
U	Overall heat transfer coefficient	W/m^2K
Wl	Wavelength	m
δf	Fin thickness	m
η	Efficiency / effectiveness	-
η_0	Fin effectiveness	-
θ	Louver angle	degrees
ρ	Density	kg/m^3
σ	Contraction ratio	-

Subscripts

banks	tube banks
f	fin
i	inner
l	louvers
max	maximum
min	minimum
o	outer
s	slits
simple	simplified version of j and f factor using inlet thermodynamic properties
w	wall

Appendix A: Louver fin correlation code

```
   public double GetADP(UMDCEEE.CEEEHXTFMC.Correlations.AirHTCDPInputs airinputs)
        {

            double Pl = airinputs.TubeHorizontalSpacing;
            double Pt = airinputs.TubeVerticalSpacing;
            double N = airinputs.Columns;
            double Lp = airinputs.LouverPitch;
            UMDCEEE.Units.DimensionedValue valu = new UMDCEEE.Units.DimensionedValue("Value", 0.0);
            bool temp_ns = airinputs.UserParameters.TryGetValue("Nl", out valu);
            double Ns = valu.Value;
            double Ft = airinputs.FinThickness;
            double Fp = airinputs.FinSpacing + Ft;
            double Lh = Lp * Math.Sin(27 * 3.141592653589790000 / 180) * Math.Cos(27 * 3.141592653589790000 /
180) + (0.000125);
            double Rows = airinputs.Rows;
            double fins = (airinputs.TubeLength / Fp);
            double Dc = airinputs.TubeOD + 2.0 * airinputs.FinThickness;
            double area_fin = ((Pt / 2 * Pl * N) - (3.141592653589790000 / 4 * Dc * Dc) / 2 * N) * 2 + 2 * (Pt /
2 * Ft);
            double area_tube = 3.141592653589790000 * Dc * N * (Fp - Ft) / 2;
            double area_totalsurfacearea = area_fin + area_tube;//(airinputs.FinArea + airinputs.TubeArea) /
            double FPM = 1 / Fp;
            double Height = airinputs.FaceArea / airinputs.TubeLength;
            double Width = airinputs.TubeLength;
            double X_diag = Math.Sqrt(Pt * Pt / 4 + Pl * Pl);
            double two_a = (Pt - Dc) - ((Pt - Dc) * Ft * FPM);
            double two_b = ((X_diag - Dc) - (Pt - Dc) * Ft * FPM) * 2;
            double c = two_a;
            if (two_b < two_a)
            {
                c = two_b;
            }
            double min_free_flow_area_Shekhar = (((Height / Pt) - 1) * c + (Pt - Dc) - (Pt - Dc) * Ft * FPM) *
Width;
            //Min Area Caculations-End
            double Area_min = min_free_flow_area_Shekhar / Rows / fins / 2;
            double Area_Frontal = Pt / 2 * Fp;
            double Sigma = Area_min / Area_Frontal;
            double u_max = airinputs.AirAvgVelocity / Sigma;
            double rho_in = airinputs.AirDensity;
            double Re_Dc_MaxV = rho_in * u_max * Dc / airinputs.AirViscosity;
            double Depth_HX = Pl * N;
            double Dh = 4 * Area_min * Depth_HX / area_totalsurfacearea;
            double Xl = 0.5 * Math.Pow(Pt * Pt / 4 + Pl * Pl, 0.5);
            double Req = 1.27 * (Pt / 2) / (Dc / 2) * Math.Pow(Xl / (Pt / 2) - 0.3, 0.5);
            double phi = (Req - 1) * (1 + 0.35 * Math.Log(Req));
            double G_c = u_max * rho_in;
            double f_simplelog1 = -815760.33488704;
            double f_simplelog2 = Math.Log(Pl) * -1013669.28781209;
            double f_simplelog3 = Math.Log(Pt) * -1345777.74292259;
            double f_simplelog4 = Math.Log(N) * -1345602.68063008;
            double f_simplelog5 = Math.Log(Lp) * -364221.902609561;
            double f_simplelog6 = Math.Log(Ns) * -173875.825256107;
            double f_simplelog7 = Math.Log(Fp) * -1344974.33608404;
            double f_simplelog8 = Math.Log(Lh) * 2617.19789112508;
            double f_simplelog9 = Math.Log(Dc) * 483.197355613171;
            double f_simplelog10 = Math.Log(Dh) * 1344955.24773289;
            double f_simplelog11 = Math.Log(area_totalsurfacearea) * 1345602.40091377;
            double f_simplelog12 = Math.Log(Area_min) * 13.423204051482;
            double f_simplelog13 = Math.Log(Re_Dc_MaxV) * -2.29231399573514;
            double f_simplelog14 = Math.Log(Sigma) * -1345307.13319948;
            double f_simplelog15 = Math.Log(phi) * 309.11386829997;
            double f_simplelog16 = Math.Log(Pl) * Math.Log(Lp) * -521591.61576759;
            double f_simplelog17 = Math.Log(Pl) * Math.Log(Ns) * -250824.761248093;
            double f_simplelog18 = Math.Log(Pl) * Math.Log(Re_Dc_MaxV) * -0.561652794109108;
            double f_simplelog19 = Math.Log(Pl) * Math.Log(phi) * 2.94069014358154;
            double f_simplelog20 = Math.Log(Pt) * Math.Log(N) * -479302.99085586;
            double f_simplelog21 = Math.Log(Pt) * Math.Log(Lp) * -521647.13023717;
            double f_simplelog22 = Math.Log(Pt) * Math.Log(Ns) * -250814.801164953;
            double f_simplelog23 = Math.Log(Pt) * Math.Log(Fp) * -479331.362019013;
            double f_simplelog24 = Math.Log(Pt) * Math.Log(Lh) * 70.0900211475239;
            double f_simplelog25 = Math.Log(Pt) * Math.Log(Dh) * 479330.208530486;
            double f_simplelog26 = Math.Log(Pt) * Math.Log(area_totalsurfacearea) * 479302.936983934;
            double f_simplelog27 = Math.Log(Pt) * Math.Log(Re_Dc_MaxV) * -0.425470491629325;
            double f_simplelog28 = Math.Log(Pt) * Math.Log(Sigma) * -479313.770026838;
```

```
            double f_simplelog29 = Math.Log(N) * Math.Log(Lp) * -521716.365948558;
            double f_simplelog30 = Math.Log(N) * Math.Log(Ns) * -250824.801977549;
            double f_simplelog31 = Math.Log(N) * Math.Log(Fp) * -479333.638651077;
            double f_simplelog32 = Math.Log(N) * Math.Log(Lh) * 158.494622059558;
            double f_simplelog33 = Math.Log(N) * Math.Log(Dc) * -8.44234782771136;
            double f_simplelog34 = Math.Log(N) * Math.Log(Dh) * 479333.520457786;
            double f_simplelog35 = Math.Log(N) * Math.Log(area_totalsurfacearea) * 479301.272506505;
            double f_simplelog36 = Math.Log(N) * Math.Log(Re_Dc_MaxV) * -0.421940657278265;
            double f_simplelog37 = Math.Log(N) * Math.Log(Sigma) * -479306.779047871;
            double f_simplelog38 = Math.Log(Lp) * Math.Log(Ns) * 3.09124696669282;
            double f_simplelog39 = Math.Log(Lp) * Math.Log(Fp) * -521962.525531339;
            double f_simplelog40 = Math.Log(Lp) * Math.Log(Lh) * 194.501561717711;
            double f_simplelog41 = Math.Log(Lp) * Math.Log(Dc) * -204.699481136264;
            double f_simplelog42 = Math.Log(Lp) * Math.Log(Dh) * 521960.241376619;
            double f_simplelog43 = Math.Log(Lp) * Math.Log(area_totalsurfacearea) * 521716.817311239;
            double f_simplelog44 = Math.Log(Lp) * Math.Log(Re_Dc_MaxV) * 0.0266395847925328;
            double f_simplelog45 = Math.Log(Lp) * Math.Log(Sigma) * -521811.414035691;
            double f_simplelog46 = Math.Log(Lp) * Math.Log(phi) * -134.206445355139;
            double f_simplelog47 = Math.Log(Ns) * Math.Log(Fp) * -250817.209728926;
            double f_simplelog48 = Math.Log(Ns) * Math.Log(Lh) * -3.80683876233717;
            double f_simplelog49 = Math.Log(Ns) * Math.Log(Dc) * -0.23707483211039;
            double f_simplelog50 = Math.Log(Ns) * Math.Log(Dh) * 250827.344548505;
            double f_simplelog51 = Math.Log(Ns) * Math.Log(area_totalsurfacearea) * 250824.80642749;
            double f_simplelog52 = Math.Log(Ns) * Math.Log(Area_min) * -10.0743991360318;
            double f_simplelog53 = Math.Log(Ns) * Math.Log(Re_Dc_MaxV) * 0.0875763792954198;
            double f_simplelog54 = Math.Log(Ns) * Math.Log(Sigma) * -250816.460279823;
            double f_simplelog55 = Math.Log(Fp) * Math.Log(Lh) * 463.920196222731;
            double f_simplelog56 = Math.Log(Fp) * Math.Log(Dc) * -36.1483908150303;
            double f_simplelog57 = Math.Log(Fp) * Math.Log(Dh) * 479373.557435568;
            double f_simplelog58 = Math.Log(Fp) * Math.Log(area_totalsurfacearea) * 479334.06628623;
            double f_simplelog59 = Math.Log(Fp) * Math.Log(Sigma) * -479306.053688274;
            double f_simplelog60 = Math.Log(Fp) * Math.Log(phi) * -38.2118653618422;
            double f_simplelog61 = Math.Log(Lh) * Math.Log(Dc) * 259.849958299261;
            double f_simplelog62 = Math.Log(Lh) * Math.Log(Dh) * -459.898029055765;
            double f_simplelog63 = Math.Log(Lh) * Math.Log(area_totalsurfacearea) * -159.058633609663;
            double f_simplelog64 = Math.Log(Lh) * Math.Log(Sigma) * 272.460429753476;
            double f_simplelog65 = Math.Log(Lh) * Math.Log(phi) * 170.895432506583;
            double f_simplelog66 = Math.Log(Dc) * Math.Log(Dh) * 36.6127424275103;
            double f_simplelog67 = Math.Log(Dc) * Math.Log(area_totalsurfacearea) * 8.62176321997616;
            double f_simplelog68 = Math.Log(Dc) * Math.Log(Re_Dc_MaxV) * -0.204280764853943;
            double f_simplelog69 = Math.Log(Dc) * Math.Log(phi) * -9.93228659002375;
            double f_simplelog70 = Math.Log(Dh) * Math.Log(area_totalsurfacearea) * -479333.974460417;
            double f_simplelog71 = Math.Log(Dh) * Math.Log(Re_Dc_MaxV) * 0.227348862308172;
            double f_simplelog72 = Math.Log(Dh) * Math.Log(Sigma) * 479309.359926494;
            double f_simplelog73 = Math.Log(Dh) * Math.Log(phi) * 39.3472389795062;
            double f_simplelog74 = Math.Log(area_totalsurfacearea) * Math.Log(Re_Dc_MaxV) * 0.410577562650643;
            double f_simplelog75 = Math.Log(area_totalsurfacearea) * Math.Log(Sigma) * 479307.145169789;
            double f_simplelog76 = Math.Log(Re_Dc_MaxV) * Math.Log(Sigma) * -0.182038472932637;
            double f_simplelog77 = Math.Log(Sigma) * Math.Log(phi) * -19.0629730027725;
            double f_simplelog78 = Math.Log(Pl) * Math.Log(Pl) * 239648.267640287;
            double f_simplelog79 = Math.Log(Pt) * Math.Log(Pt) * -239655.068016596;
            double f_simplelog80 = Math.Log(N) * Math.Log(N) * -239650.607771909;
            double f_simplelog81 = Math.Log(Lp) * Math.Log(Lp) * -229.191255863403;
            double f_simplelog82 = Math.Log(Ns) * Math.Log(Ns) * 0.115797101976652;
            double f_simplelog83 = Math.Log(Fp) * Math.Log(Fp) * -239687.862324651;
            double f_simplelog84 = Math.Log(Dc) * Math.Log(Dc) * -12.8648689704997;
            double f_simplelog85 = Math.Log(Dh) * Math.Log(Dh) * -239687.050122179;
            double f_simplelog86 = Math.Log(area_totalsurfacearea) * Math.Log(area_totalsurfacearea) * -
239650.635334316;
            double f_simplelog87 = Math.Log(Re_Dc_MaxV) * Math.Log(Re_Dc_MaxV) * 0.105780310972096;
            double f_simplelog88 = Math.Log(Sigma) * Math.Log(Sigma) * -239638.755173034;
            double f_simplelogsum = f_simplelog1 + f_simplelog2 + f_simplelog3 + f_simplelog4 + f_simplelog5 +
f_simplelog6 + f_simplelog7 + f_simplelog8 + f_simplelog9 + f_simplelog10 + f_simplelog11 +
          f_simplelog12 + f_simplelog13 + f_simplelog14 + f_simplelog15 + f_simplelog16 + f_simplelog17 +
f_simplelog18 + f_simplelog19 + f_simplelog20 + f_simplelog21 + f_simplelog22 + f_simplelog23 +
          f_simplelog24 + f_simplelog25 + f_simplelog26 + f_simplelog27 + f_simplelog28 + f_simplelog29 +
f_simplelog30 + f_simplelog31 + f_simplelog32 + f_simplelog33 + f_simplelog34 + f_simplelog35 +
          f_simplelog36 + f_simplelog37 + f_simplelog38 + f_simplelog39 + f_simplelog40 + f_simplelog41 +
f_simplelog42 + f_simplelog43 + f_simplelog44 + f_simplelog45 + f_simplelog46 + f_simplelog47 +
          f_simplelog48 + f_simplelog49 + f_simplelog50 + f_simplelog51 + f_simplelog52 + f_simplelog53 +
f_simplelog54 + f_simplelog55 + f_simplelog56 + f_simplelog57 + f_simplelog58 + f_simplelog59 +
          f_simplelog60 + f_simplelog61 + f_simplelog62 + f_simplelog63 + f_simplelog64 + f_simplelog65 +
f_simplelog66 + f_simplelog67 + f_simplelog68 + f_simplelog69 + f_simplelog70 + f_simplelog71 +
          f_simplelog72 + f_simplelog73 + f_simplelog74 + f_simplelog75 + f_simplelog76 + f_simplelog77 +
f_simplelog78 + f_simplelog79 + f_simplelog80 + f_simplelog81 + f_simplelog82 + f_simplelog83 +
          f_simplelog84 + f_simplelog85 + f_simplelog86 + f_simplelog87 + f_simplelog88;

            double f = Math.Exp(f_simplelogsum);
```

```
            double DP = (f * area_totalsurfacearea / (Area_min)) * (Math.Pow(G_c, 2.0) / (2.0 * rho_in));
//simplified expression without iteration
            return DP;

        }


        public double GetAHTC(UMDCEEE.CEEEHXTFMC.Correlations.AirHTCDPInputs airinputs)
        {

            double Pl = airinputs.TubeHorizontalSpacing;
            double Pt = airinputs.TubeVerticalSpacing;
            double N = airinputs.Columns;
            double Lp = airinputs.LouverPitch;
            UMDCEEE.Units.DimensionedValue valu = new UMDCEEE.Units.DimensionedValue("Value", 0.0);
            bool temp_ns = airinputs.UserParameters.TryGetValue("Nl", out valu);
            double Ns = valu.Value;

            double Ft = airinputs.FinThickness;
            double Fp = airinputs.FinSpacing + Ft;
            double Lh = Lp * Math.Sin(27 * 3.141592653589790000 / 180) * Math.Cos(27 * 3.141592653589790000 /
180) + (0.000125);
            double Rows = airinputs.Rows;
            double fins = (airinputs.TubeLength / Fp);
            double Dc = airinputs.TubeOD + 2.0 * airinputs.FinThickness;
            double area_fin = ((Pt / 2 * Pl * N) - (3.141592653589790000 / 4 * Dc * Dc) / 2 * N) * 2 + 2 * (Pt /
2 * Ft);
            double area_tube = 3.141592653589790000 * Dc * N * (Fp - Ft) / 2;
            double area_totalsurfacearea = area_fin + area_tube;
            double FPM = 1 / Fp;
            double Height = airinputs.FaceArea / airinputs.TubeLength;
            double Width = airinputs.TubeLength;
            double X_diag = Math.Sqrt(Pt * Pt / 4 + Pl * Pl);
            double two_a = (Pt - Dc) - ((Pt - Dc) * Ft * FPM);
            double two_b = ((X_diag - Dc) - (Pt - Dc) * Ft * FPM) * 2;

            double c = two_a;
            if (two_b < two_a)
            {
                c = two_b;
            }
            double min_free_flow_area_Shekhar = (((Height / Pt) - 1) * c + (Pt - Dc) - (Pt - Dc) * Ft * FPM) *
Width;
            //Min Area Caculations-End
            double Area_min = min_free_flow_area_Shekhar / Rows / fins / 2;
            double Area_Frontal = Pt / 2 * Fp;
            double Sigma = Area_min / Area_Frontal;
            double u_max = airinputs.AirAvgVelocity / Sigma;
            double rho_in = airinputs.AirDensity;
            double Re_Dc_MaxV = rho_in * u_max * Dc / airinputs.AirViscosity;
            double Depth_HX = Pl * N;
            double Dh = 4 * Area_min * Depth_HX / area_totalsurfacearea;
            double G_c = u_max * rho_in;
            double Pr = airinputs.AirSpecificHeat * airinputs.AirViscosity / airinputs.AirConductivity;

            double Xl = 0.5 * Math.Pow(Pt * Pt / 4 + Pl * Pl, 0.5);
            double Req = 1.27 * (Pt / 2) / (Dc / 2) * Math.Pow(Xl / (Pt / 2) - 0.3, 0.5);
            double phi = (Req - 1) * (1 + 0.35 * Math.Log(Req));

            double neta1 = -12868725.2433763;
            double neta2 = Math.Log(Pl) * -18565659.0112163;
            double neta3 = Math.Log(Pt) * -18565604.1786456;
            double neta4 = Math.Log(N) * -18565647.4819432;
            double neta5 = Math.Log(Lp) * 4437161.05821925;
            double neta6 = Math.Log(Ns) * 48210.2110600247;
            double neta7 = Math.Log(Fp) * -18565563.2379018;
            double neta8 = Math.Log(Lh) * -5521760.42376142;
            double neta9 = Math.Log(Dc) * 15.6744733896143;
            double neta10 = Math.Log(Dh) * 18565617.0971958;
            double neta11 = Math.Log(area_totalsurfacearea) * 18565652.2834347;
            double neta12 = Math.Log(Area_min) * -133017.443343003;
            double neta13 = Math.Log(Re_Dc_MaxV) * 54749.092282147;
            double neta14 = Math.Log(Sigma) * -18129911.7092101;
            double neta15 = Math.Log(phi) * 9.31796998616484;
            double neta16 = Math.Log(Pl) * Math.Log(Lp) * 6401525.77628698;
            double neta17 = Math.Log(Pl) * Math.Log(Ns) * 69546.2508242001;
            double neta18 = Math.Log(Pl) * Math.Log(Lh) * -7966266.51840767;
```

```
            double neta19 = Math.Log(Pl) * Math.Log(Dc) * 3.41449990601487;
            double neta20 = Math.Log(Pl) * Math.Log(Area_min) * -191823.845650411;
            double neta21 = Math.Log(Pl) * Math.Log(Re_Dc_MaxV) * 78990.7690650583;
            double neta22 = Math.Log(Pl) * Math.Log(Sigma) * 628530.840244192;
            double neta23 = Math.Log(Pl) * Math.Log(phi) * 3.47679954026221;
            double neta24 = Math.Log(Pt) * Math.Log(Lp) * 6401523.91133061;
            double neta25 = Math.Log(Pt) * Math.Log(Ns) * 69543.2052214506;
            double neta26 = Math.Log(Pt) * Math.Log(Fp) * 14.6794156029264;
            double neta27 = Math.Log(Pt) * Math.Log(Lh) * -7966264.16576323;
            double neta28 = Math.Log(Pt) * Math.Log(Dc) * -2.43865183976936;
            double neta29 = Math.Log(Pt) * Math.Log(area_totalsurfacearea) * -2.06494609694094;
            double neta30 = Math.Log(Pt) * Math.Log(Area_min) * -191833.162197914;
            double neta31 = Math.Log(Pt) * Math.Log(Re_Dc_MaxV) * 78990.6294677191;
            double neta32 = Math.Log(Pt) * Math.Log(Sigma) * 628523.383786794;
            double neta33 = Math.Log(N) * Math.Log(Lp) * 6401525.1668951;
            double neta34 = Math.Log(N) * Math.Log(Ns) * 69546.250388997;
            double neta35 = Math.Log(N) * Math.Log(Fp) * 2.27170684135554;
            double neta36 = Math.Log(N) * Math.Log(Lh) * -7966265.77006362;
            double neta37 = Math.Log(N) * Math.Log(Dc) * 0.0287579522998578;
            double neta38 = Math.Log(N) * Math.Log(Dh) * -2.45527002811045;
            double neta39 = Math.Log(N) * Math.Log(area_totalsurfacearea) * 0.0227224631503323;
            double neta40 = Math.Log(N) * Math.Log(Area_min) * -191823.618094194;
            double neta41 = Math.Log(N) * Math.Log(Re_Dc_MaxV) * 78990.490389871;
            double neta42 = Math.Log(N) * Math.Log(Sigma) * 628532.390008747;
            double neta43 = Math.Log(Lp) * Math.Log(Ns) * -0.725575324081059;
            double neta44 = Math.Log(Lp) * Math.Log(Fp) * 6401512.7952845;
            double neta45 = Math.Log(Lp) * Math.Log(Lh) * -0.852339807896888;
            double neta46 = Math.Log(Lp) * Math.Log(Dh) * -6401513.17381744;
            double neta47 = Math.Log(Lp) * Math.Log(area_totalsurfacearea) * -6401526.30491028;
            double neta48 = Math.Log(Lp) * Math.Log(Re_Dc_MaxV) * 0.921561498016026;
            double neta49 = Math.Log(Lp) * Math.Log(Sigma) * 6401519.98263144;
            double neta50 = Math.Log(Ns) * Math.Log(Fp) * 69543.6000034099;
            double neta51 = Math.Log(Ns) * Math.Log(Lh) * 0.898048743220976;
            double neta52 = Math.Log(Ns) * Math.Log(Dh) * -69546.6851769345;
            double neta53 = Math.Log(Ns) * Math.Log(area_totalsurfacearea) * -69546.2451751534;
            double neta54 = Math.Log(Ns) * Math.Log(Area_min) * 3.07463216193912;
            double neta55 = Math.Log(Ns) * Math.Log(Re_Dc_MaxV) * -0.0170831498922733;
            double neta56 = Math.Log(Ns) * Math.Log(Sigma) * 69543.4750553705;
            double neta57 = Math.Log(Ns) * Math.Log(phi) * -0.039650104433712;
            double neta58 = Math.Log(Fp) * Math.Log(Lh) * -7966249.47557364;
            double neta59 = Math.Log(Fp) * Math.Log(Dh) * -19.0981084017171;
            double neta60 = Math.Log(Fp) * Math.Log(area_totalsurfacearea) * -4.02533618343807;
            double neta61 = Math.Log(Fp) * Math.Log(Area_min) * -191825.896382285;
            double neta62 = Math.Log(Fp) * Math.Log(Re_Dc_MaxV) * 78990.01396144;
            double neta63 = Math.Log(Fp) * Math.Log(Sigma) * 628529.558948703;
            double neta64 = Math.Log(Lh) * Math.Log(Dh) * 7966249.80712876;
            double neta65 = Math.Log(Lh) * Math.Log(area_totalsurfacearea) * 7966267.20777591;
            double neta66 = Math.Log(Lh) * Math.Log(Re_Dc_MaxV) * -1.16422508678719;
            double neta67 = Math.Log(Lh) * Math.Log(Sigma) * -7966258.42544289;
            double neta68 = Math.Log(Lh) * Math.Log(phi) * -0.0912952115032578;
            double neta69 = Math.Log(Dc) * Math.Log(Re_Dc_MaxV) * -0.459323730232368;
            double neta70 = Math.Log(Dc) * Math.Log(phi) * -2.32638461344203;
            double neta71 = Math.Log(Dh) * Math.Log(area_totalsurfacearea) * 2.11916523713542;
            double neta72 = Math.Log(Dh) * Math.Log(Area_min) * 191820.553959153;
            double neta73 = Math.Log(Dh) * Math.Log(Re_Dc_MaxV) * -78989.9904841306;
            double neta74 = Math.Log(Dh) * Math.Log(Sigma) * -628544.203733193;
            double neta75 = Math.Log(area_totalsurfacearea) * Math.Log(Area_min) * 191825.671797689;
            double neta76 = Math.Log(area_totalsurfacearea) * Math.Log(Re_Dc_MaxV) * -78990.5196678448;
            double neta77 = Math.Log(area_totalsurfacearea) * Math.Log(Sigma) * -628534.212108985;
            double neta78 = Math.Log(Area_min) * Math.Log(Sigma) * -191805.502446343;
            double neta79 = Math.Log(Area_min) * Math.Log(phi) * -0.253477247912346;
            double neta80 = Math.Log(Re_Dc_MaxV) * Math.Log(Sigma) * 78990.3438117407;
            double neta81 = Math.Log(Re_Dc_MaxV) * Math.Log(phi) * -0.349301272031211;
            double neta82 = Math.Log(Sigma) * Math.Log(phi) * 2.14235196424352;
            double neta83 = Math.Log(Pl) * Math.Log(Pl) * -1.90160746060201;
            double neta84 = Math.Log(Pt) * Math.Log(Pt) * 10.6715988482634;
            double neta85 = Math.Log(Ns) * Math.Log(Ns) * -0.0228136607611045;
            double neta86 = Math.Log(Fp) * Math.Log(Fp) * 12.5257838025938;
            double neta87 = Math.Log(Dh) * Math.Log(Dh) * 12.2122283370594;
            double neta88 = Math.Log(Sigma) * Math.Log(Sigma) * 628518.229883001;
            double neta89 = Math.Log(phi) * Math.Log(phi) * -1.6782190856396;


            double netasum = neta1 + neta2 + neta3 + neta4 + neta5 + neta6 + neta7 + neta8 + neta9 + neta10 +
neta11 + neta12 + neta13 + neta14 + neta15 + neta16 + neta17 + neta18 + neta19 + neta20 + neta21 + neta22 +
neta23 + neta24 + neta25 + neta26 + neta27 + neta28 + neta29 + neta30 + neta31 + neta32 + neta33 + neta34 +
neta35 + neta36 + neta37 + neta38 + neta39 + neta40 + neta41 + neta42 + neta43 + neta44 + neta45 + neta46 +
neta47 + neta48 + neta49 + neta50 + neta51 + neta52 + neta53 + neta54 + neta55 + neta56 + neta57 + neta58 +
neta59 + neta60 + neta61 + neta62 + neta63 + neta64 + neta65 + neta66 + neta67 + neta68 + neta69 + neta70 +
```

```
neta71 + neta72 + neta73 + neta74 + neta75 + neta76 + neta77 + neta78 + neta79 + neta80 + neta81 + neta82 +
neta83 + neta84 + neta85 + neta86 + neta87 + neta88 + neta89;

            double neta_correlation = Math.Exp(netasum);
            // H T C    C A L C U L A T I O N S

            double j_simplelog1 = -3217786.22453845;
            double j_simplelog2 = Math.Log(Pl) * -4643227.18575148;
            double j_simplelog3 = Math.Log(Pt) * -4643603.4143226;
            double j_simplelog4 = Math.Log(N) * -4643111.10169104;
            double j_simplelog5 = Math.Log(Lp) * -86.4348099798031;
            double j_simplelog6 = Math.Log(Ns) * -0.953010348856323;
            double j_simplelog7 = Math.Log(Fp) * -4642797.65839097;
            double j_simplelog8 = Math.Log(Lh) * -436235.649233502;
            double j_simplelog9 = Math.Log(Dc) * 91.5408189430598;
            double j_simplelog10 = Math.Log(Dh) * 4641953.24389938;
            double j_simplelog11 = Math.Log(area_totalsurfacearea) * 4643125.60753054;
            double j_simplelog12 = Math.Log(Area_min) * 474.417027718359;
            double j_simplelog13 = Math.Log(Re_Dc_MaxV) * -3.0270821002864;
            double j_simplelog14 = Math.Log(Sigma) * -4643074.10062615;
            double j_simplelog15 = Math.Log(phi) * 63.7023220555819;
            double j_simplelog16 = Math.Log(neta_correlation) * -50.7931602860337;
            double j_simplelog17 = Math.Log(Pl) * Math.Log(Ns) * 1.79387845257246;
            double j_simplelog18 = Math.Log(Pl) * Math.Log(Lh) * -629519.442314844;
            double j_simplelog19 = Math.Log(Pl) * Math.Log(Dc) * -80.7473593389511;
            double j_simplelog20 = Math.Log(Pl) * Math.Log(Dh) * -534.631059666487;
            double j_simplelog21 = Math.Log(Pl) * Math.Log(area_totalsurfacearea) * 9.78532292231181;
            double j_simplelog22 = Math.Log(Pl) * Math.Log(Re_Dc_MaxV) * 3.69378937938928;
            double j_simplelog23 = Math.Log(Pl) * Math.Log(phi) * -12.0748126508112;
            double j_simplelog24 = Math.Log(Pt) * Math.Log(N) * -49.2971491070941;
            double j_simplelog25 = Math.Log(Pt) * Math.Log(Lp) * -11.1450052251599;
            double j_simplelog26 = Math.Log(Pt) * Math.Log(Ns) * 1.52635139649896;
            double j_simplelog27 = Math.Log(Pt) * Math.Log(Fp) * -759.215213643526;
            double j_simplelog28 = Math.Log(Pt) * Math.Log(Lh) * -629504.211243779;
            double j_simplelog29 = Math.Log(Pt) * Math.Log(Dc) * -91.9803531243105;
            double j_simplelog30 = Math.Log(Pt) * Math.Log(Dh) * 128.356830857079;
            double j_simplelog31 = Math.Log(Pt) * Math.Log(area_totalsurfacearea) * 48.9549342597284;
            double j_simplelog32 = Math.Log(Pt) * Math.Log(Area_min) * 93.5378471834916;
            double j_simplelog33 = Math.Log(Pt) * Math.Log(Re_Dc_MaxV) * 3.13233689777716;
            double j_simplelog34 = Math.Log(Pt) * Math.Log(Sigma) * -529.052046173429;
            double j_simplelog35 = Math.Log(Pt) * Math.Log(phi) * -21.5283398951988;
            double j_simplelog36 = Math.Log(Pt) * Math.Log(neta_correlation) * -8.06380130175587;
            double j_simplelog37 = Math.Log(N) * Math.Log(Lh) * -629516.440324098;
            double j_simplelog38 = Math.Log(N) * Math.Log(Dc) * -48.2121788549437;
            double j_simplelog39 = Math.Log(N) * Math.Log(Dh) * -573.967569111329;
            double j_simplelog40 = Math.Log(N) * Math.Log(area_totalsurfacearea) * -10.0176143362261;
            double j_simplelog41 = Math.Log(N) * Math.Log(Area_min) * 45.3350188168664;
            double j_simplelog42 = Math.Log(N) * Math.Log(Re_Dc_MaxV) * -0.127908506892957;
            double j_simplelog43 = Math.Log(N) * Math.Log(neta_correlation) * -41.4151228623828;
            double j_simplelog44 = Math.Log(Lp) * Math.Log(Fp) * -115.416420076013;
            double j_simplelog45 = Math.Log(Lp) * Math.Log(Dh) * 119.761953505347;
            double j_simplelog46 = Math.Log(Lp) * Math.Log(Re_Dc_MaxV) * 0.141408244269906;
            double j_simplelog47 = Math.Log(Lp) * Math.Log(Sigma) * -81.4238789892555;
            double j_simplelog48 = Math.Log(Lp) * Math.Log(neta_correlation) * 0.921127169350298;
            double j_simplelog49 = Math.Log(Ns) * Math.Log(Lh) * 0.068970115204343;
            double j_simplelog50 = Math.Log(Ns) * Math.Log(Dc) * -3.32183130744739;
            double j_simplelog51 = Math.Log(Ns) * Math.Log(area_totalsurfacearea) * -0.0625621682449373;
            double j_simplelog52 = Math.Log(Ns) * Math.Log(Re_Dc_MaxV) * 0.105399456367645;
            double j_simplelog53 = Math.Log(Ns) * Math.Log(Sigma) * 1.03810317200366;
            double j_simplelog54 = Math.Log(Ns) * Math.Log(phi) * -2.12971282121861;
            double j_simplelog55 = Math.Log(Ns) * Math.Log(neta_correlation) * 0.660103163883099;
            double j_simplelog56 = Math.Log(Fp) * Math.Log(Lh) * -629369.621859025;
            double j_simplelog57 = Math.Log(Fp) * Math.Log(Area_min) * 665.155310336052;
            double j_simplelog58 = Math.Log(Fp) * Math.Log(Sigma) * -976.790669103759;
            double j_simplelog59 = Math.Log(Fp) * Math.Log(phi) * 7.47267066033452;
            double j_simplelog60 = Math.Log(Fp) * Math.Log(neta_correlation) * -27.493806106375;
            double j_simplelog61 = Math.Log(Lh) * Math.Log(Dc) * 4.9859506097265;
            double j_simplelog62 = Math.Log(Lh) * Math.Log(Dh) * 629364.59114238;
            double j_simplelog63 = Math.Log(Lh) * Math.Log(area_totalsurfacearea) * 629516.40404567;
            double j_simplelog64 = Math.Log(Lh) * Math.Log(Sigma) * -629415.075120887;
            double j_simplelog65 = Math.Log(Lh) * Math.Log(phi) * 3.65282676588757;
            double j_simplelog66 = Math.Log(Dc) * Math.Log(Dh) * 11.4127378130943;
            double j_simplelog67 = Math.Log(Dc) * Math.Log(area_totalsurfacearea) * 48.795681335653;
            double j_simplelog68 = Math.Log(Dc) * Math.Log(Re_Dc_MaxV) * -7.06275929217822;
            double j_simplelog69 = Math.Log(Dc) * Math.Log(phi) * 18.8867271794211;
            double j_simplelog70 = Math.Log(Dc) * Math.Log(neta_correlation) * -74.8642343154216;
            double j_simplelog71 = Math.Log(Dh) * Math.Log(area_totalsurfacearea) * 564.170295758917;
            double j_simplelog72 = Math.Log(Dh) * Math.Log(Area_min) * -662.441267957619;
            double j_simplelog73 = Math.Log(Dh) * Math.Log(neta_correlation) * 26.5354169426133;
```

```
            double j_simplelog74 = Math.Log(area_totalsurfacearea) * Math.Log(Area_min) * -35.4613366909185;
            double j_simplelog75 = Math.Log(area_totalsurfacearea) * Math.Log(neta_correlation) *
40.0599010032903;
            double j_simplelog76 = Math.Log(Area_min) * Math.Log(Sigma) * 438.668372919593;
            double j_simplelog77 = Math.Log(Re_Dc_MaxV) * Math.Log(Sigma) * 1.98373984110075;
            double j_simplelog78 = Math.Log(Re_Dc_MaxV) * Math.Log(phi) * -4.48371977574494;
            double j_simplelog79 = Math.Log(Re_Dc_MaxV) * Math.Log(neta_correlation) * 1.60608879552036;
            double j_simplelog80 = Math.Log(Sigma) * Math.Log(phi) * 16.2567224337724;
            double j_simplelog81 = Math.Log(phi) * Math.Log(neta_correlation) * -50.447406905026;
            double j_simplelog82 = Math.Log(Pt) * Math.Log(Pt) * -92.4998382825307;
            double j_simplelog83 = Math.Log(N) * Math.Log(N) * 10.0627305554213;
            double j_simplelog84 = Math.Log(Fp) * Math.Log(Fp) * -601.379446157448;
            double j_simplelog85 = Math.Log(Dc) * Math.Log(Dc) * 27.1120519957628;
            double j_simplelog86 = Math.Log(Dh) * Math.Log(Dh) * 599.09261913114;
            double j_simplelog87 = Math.Log(Re_Dc_MaxV) * Math.Log(Re_Dc_MaxV) * 0.0885784513892449;
            double j_simplelog88 = Math.Log(Sigma) * Math.Log(Sigma) * -379.32816828361;

            double j_simple_log_sum = j_simplelog1 + j_simplelog2 + j_simplelog3 + j_simplelog4 + j_simplelog5 +
j_simplelog6 + j_simplelog7 + j_simplelog8 + j_simplelog9 + j_simplelog10 + j_simplelog11 + j_simplelog12 +
j_simplelog13 + j_simplelog14 +
            j_simplelog15 + j_simplelog16 + j_simplelog17 + j_simplelog18 + j_simplelog19 + j_simplelog20 +
j_simplelog21 + j_simplelog22 + j_simplelog23 + j_simplelog24 + j_simplelog25 + j_simplelog26 + j_simplelog27 +
j_simplelog28 + j_simplelog29 +
            j_simplelog30 + j_simplelog31 + j_simplelog32 + j_simplelog33 + j_simplelog34 + j_simplelog35 +
j_simplelog36 + j_simplelog37 + j_simplelog38 + j_simplelog39 + j_simplelog40 + j_simplelog41 + j_simplelog42 +
j_simplelog43 + j_simplelog44 +
            j_simplelog45 + j_simplelog46 + j_simplelog47 + j_simplelog48 + j_simplelog49 + j_simplelog50 +
j_simplelog51 + j_simplelog52 + j_simplelog53 + j_simplelog54 + j_simplelog55 + j_simplelog56 + j_simplelog57 +
j_simplelog58 + j_simplelog59 +
            j_simplelog60 + j_simplelog61 + j_simplelog62 + j_simplelog63 + j_simplelog64 + j_simplelog65 +
j_simplelog66 + j_simplelog67 + j_simplelog68 + j_simplelog69 + j_simplelog70 + j_simplelog71 + j_simplelog72 +
j_simplelog73 + j_simplelog74 +
            j_simplelog75 + j_simplelog76 + j_simplelog77 + j_simplelog78 + j_simplelog79 + j_simplelog80 +
j_simplelog81 + j_simplelog82 + j_simplelog83 + j_simplelog84 + j_simplelog85 + j_simplelog86 + j_simplelog87 +
j_simplelog88;
            double j_simple = Math.Exp(j_simple_log_sum);

            double HTC = j_simple * airinputs.AirDensity * u_max * airinputs.AirSpecificHeat / Math.Pow(Pr,
0.6666666666667);
            return HTC;

        }
```

Appendix B: Slit HTC correlation code

```
        public double GetAHTC(UMDCEEE.CEEEHXTFMC.Correlations.AirHTCDPInputs airinputs)
        {
            double Pl = airinputs.TubeHorizontalSpacing;
            double Pt = airinputs.TubeVerticalSpacing;
            double N = airinputs.Columns;
            double Sh = airinputs.SlitHeight;
            double Ns = airinputs.SlitCount;//????? airinputs.LouverCount;//?????

            UMDCEEE.Units.DimensionedValue valu = new UMDCEEE.Units.DimensionedValue("Value", 0.0);
            //bool temp_ns = airinputs.UserParameters.TryGetValue("Nl", out valu);
            double Ft = airinputs.FinThickness;
            double Fp = airinputs.FinSpacing + Ft;
            double Rows = airinputs.Rows;
            double fins = (airinputs.TubeLength / Fp);
            double Dc = airinputs.TubeOD + 2.0 * airinputs.FinThickness;
            double area_fin = ((Pt / 2 * Pl * N) - (3.141592653589790000 / 4 * Dc * Dc) / 2 * N) * 2 + 2 * (Pt /
2 * Ft);
            double area_tube = 3.141592653589790000 * Dc * N * (Fp - Ft) / 2;
            double area_totalsurfacearea = area_fin + area_tube;//(airinputs.FinArea + airinputs.TubeArea) /
Rows / fins/2; //external tube surface area
            //Min Area Caculations -Start
            //double F_p = F_s + airinputs.FinThickness;
            //double Ft = airinputs.FinThickness;
            double FPM = 1 / Fp;
            double Height = airinputs.FaceArea / airinputs.TubeLength;
            double Width = airinputs.TubeLength;
            double X_diag = Math.Sqrt(Pt * Pt / 4 + Pl * Pl);

            double two_a = (Pt - Dc) - ((Pt - Dc) * Ft * FPM);
            double two_b = ((X_diag - Dc) - (Pt - Dc) * Ft * FPM) * 2;

            double c = two_a;
            if (two_b < two_a)
            {
                c = two_b;
            }
            double min_free_flow_area_Shekhar = (((Height / Pt) - 1) * c + (Pt - Dc) - (Pt - Dc) * Ft * FPM) *
Width;
            //Min Area Caculations-End
            double Area_min = min_free_flow_area_Shekhar / Rows / fins / 2;
            double Area_Frontal = Pt / 2 * Fp;
            double Sigma = Area_min / Area_Frontal;

            double u_max = airinputs.AirAvgVelocity / Sigma;
            //double cp_m=airinputs.AirSpecificHeat;
            //double Pr=cp_m*airinputs.AirViscosity/airinputs.AirConductivity;
            double rho_in = airinputs.AirDensity;//airprops.rho_TPRH(airinputs.AirTemperature, 1.01325e5, 0,
UMDCEEE.Units.UnitSystem.SI);
            double Re_Dc_MaxV = rho_in * u_max * Dc / airinputs.AirViscosity;
            double Depth_HX = Pl * N;
            double Dh = 4 * Area_min * Depth_HX / area_totalsurfacearea;
            double Xl = 0.5 * Math.Pow(Pt * Pt / 4 + Pl * Pl, 0.5);
            double Req = 1.27 * (Pt / 2) / (Dc / 2) * Math.Pow(Xl / (Pt / 2) - 0.3, 0.5);
            double phi = (Req - 1) * (1 + 0.35 * Math.Log(Req));
            double G_c = u_max * rho_in;
            double Pr = airinputs.AirSpecificHeat * airinputs.AirViscosity / airinputs.AirConductivity;

            double netalog1 = 17942179.3978034;
            double netalog2 = Math.Log(Dc) * 59.4279581980059;
            double netalog3 = Math.Log(Pl) * 24580093.9305892;
            double netalog4 = Math.Log(Pt) * 27721182.2564473;
            double netalog5 = Math.Log(N) * 27544156.2718623;
            double netalog6 = Math.Log(Sh) * 0.95185621479249;
            double netalog7 = Math.Log(Ns) * 1809158.82065876;
            double netalog8 = Math.Log(Fp) * 27721201.9754496;
```

```
            double netalog9 = Math.Log(Area_min) * -177037.880592169;
            double netalog10 = Math.Log(area_totalsurfacearea) * -26062145.4509486;
            double netalog11 = Math.Log(Sigma) * 30685238.1134226;
            double netalog12 = Math.Log(phi) * 2.58317400016547;
            double netalog13 = Math.Log(Dh) * -24580116.8167669;
            double netalog14 = Math.Log(Re_Dc_MaxV) * -2.07107911928566;
            double netalog15 = Math.Log(Dc) * Math.Log(N) * 37.1312281423879;
            double netalog16 = Math.Log(Dc) * Math.Log(Sh) * 1.7820443486625;
            double netalog17 = Math.Log(Dc) * Math.Log(Fp) * 48.2679367033805;
            double netalog18 = Math.Log(Dc) * Math.Log(area_totalsurfacearea) * -37.0848473668585;
            double netalog19 = Math.Log(Dc) * Math.Log(Sigma) * 53.3046007187191;
            double netalog20 = Math.Log(Dc) * Math.Log(phi) * 47.990064613833;
            double netalog21 = Math.Log(Dc) * Math.Log(Dh) * -50.0947590337132;
            double netalog22 = Math.Log(Dc) * Math.Log(Re_Dc_MaxV) * -0.628176693319208;
            double netalog23 = Math.Log(Pl) * Math.Log(N) * -25.1458967673448;
            double netalog24 = Math.Log(Pl) * Math.Log(Sh) * -1.06815850822648;
            double netalog25 = Math.Log(Pl) * Math.Log(Ns) * 1305031.45923255;
            double netalog26 = Math.Log(Pl) * Math.Log(area_totalsurfacearea) * 2138113.92285421;
            double netalog27 = Math.Log(Pl) * Math.Log(phi) * -23.7709524709937;
            double netalog28 = Math.Log(Pl) * Math.Log(Dh) * 4276214.52988118;
            double netalog29 = Math.Log(Pl) * Math.Log(Re_Dc_MaxV) * 0.291657049776574;
            double netalog30 = Math.Log(Pt) * Math.Log(N) * 4276183.58368063;
            double netalog31 = Math.Log(Pt) * Math.Log(Sh) * -0.695340858887539;
            double netalog32 = Math.Log(Pt) * Math.Log(Fp) * 4276214.44245284;
            double netalog33 = Math.Log(Pt) * Math.Log(area_totalsurfacearea) * -2138094.86315253;
            double netalog34 = Math.Log(Pt) * Math.Log(Re_Dc_MaxV) * 1.12837652344882;
            double netalog35 = Math.Log(N) * Math.Log(Ns) * 1305031.52995596;
            double netalog36 = Math.Log(N) * Math.Log(Fp) * 4276213.85078563;
            double netalog37 = Math.Log(N) * Math.Log(area_totalsurfacearea) * -2138088.71037093;
            double netalog38 = Math.Log(N) * Math.Log(Sigma) * 4276214.82245309;
            double netalog39 = Math.Log(N) * Math.Log(phi) * -0.00162636735822511;
            double netalog40 = Math.Log(N) * Math.Log(Re_Dc_MaxV) * -0.0264186327915285;
            double netalog41 = Math.Log(Sh) * Math.Log(Ns) * -0.0155109200519322;
            double netalog42 = Math.Log(Sh) * Math.Log(Fp) * -0.43030031638354;
            double netalog43 = Math.Log(Sh) * Math.Log(Sigma) * -0.977396523924845;
            double netalog44 = Math.Log(Sh) * Math.Log(phi) * 1.30096588644953;
            double netalog45 = Math.Log(Sh) * Math.Log(Re_Dc_MaxV) * -0.0151020273918269;
            double netalog46 = Math.Log(Ns) * Math.Log(Fp) * 0.841833527419966;
            double netalog47 = Math.Log(Ns) * Math.Log(Area_min) * 1305031.66979429;
            double netalog48 = Math.Log(Ns) * Math.Log(area_totalsurfacearea) * -1305031.52872855;
            double netalog49 = Math.Log(Ns) * Math.Log(phi) * 0.0647602470181208;
            double netalog50 = Math.Log(Ns) * Math.Log(Dh) * -1305032.45464571;
            double netalog51 = Math.Log(Ns) * Math.Log(Re_Dc_MaxV) * -0.0174339232033777;
            double netalog52 = Math.Log(Fp) * Math.Log(area_totalsurfacearea) * -2138124.92949053;
            double netalog53 = Math.Log(Fp) * Math.Log(phi) * 22.6485575331487;
            double netalog54 = Math.Log(Area_min) * Math.Log(Sigma) * 4276212.15950653;
            double netalog55 = Math.Log(Area_min) * Math.Log(phi) * -23.9913407546967;
            double netalog56 = Math.Log(Area_min) * Math.Log(Re_Dc_MaxV) * -0.979451337162224;
            double netalog57 = Math.Log(area_totalsurfacearea) * Math.Log(Sigma) * -2138126.06875628;
            double netalog58 = Math.Log(area_totalsurfacearea) * Math.Log(Dh) * -2138088.92361933;
            double netalog59 = Math.Log(Sigma) * Math.Log(phi) * 23.0505567708678;
            double netalog60 = Math.Log(Sigma) * Math.Log(Dh) * 7.04236815598826;
            double netalog61 = Math.Log(Sigma) * Math.Log(Re_Dc_MaxV) * 0.484246702052249;
            double netalog62 = Math.Log(phi) * Math.Log(Re_Dc_MaxV) * -0.428720088596288;
            double netalog63 = Math.Log(Dh) * Math.Log(Re_Dc_MaxV) * 1.05609005361066;
            double netalog64 = Math.Log(Dc) * Math.Log(Dc) * 37.0619722732384;
            double netalog65 = Math.Log(Pl) * Math.Log(Pl) * -2138104.79453111;
            double netalog66 = Math.Log(Pt) * Math.Log(Pt) * 2138104.00230376;
            double netalog67 = Math.Log(N) * Math.Log(N) * 2138088.77008549;
            double netalog68 = Math.Log(Sh) * Math.Log(Sh) * 0.25431737503859;
            double netalog69 = Math.Log(Fp) * Math.Log(Fp) * 2138109.67414588;
            double netalog70 = Math.Log(Sigma) * Math.Log(Sigma) * -2138107.30478262;
            double netalog71 = Math.Log(phi) * Math.Log(phi) * 15.1315485858389;
            double netalog72 = Math.Log(Dh) * Math.Log(Dh) * -2138109.45007103;
            double netalog73 = Math.Log(Re_Dc_MaxV) * Math.Log(Re_Dc_MaxV) * 0.0215584692929149;

            double netalogsum = netalog1 + netalog2 + netalog3 + netalog4 + netalog5 + netalog6 + netalog7 +
netalog8 + netalog9 + netalog10 + netalog11 + netalog12 + netalog13 + netalog14 + netalog15 + netalog16 +
```

```
netalog17 + netalog18 + netalog19 + netalog20 + netalog21 + netalog22 + netalog23 + netalog24 + netalog25 +
netalog26 + netalog27 + netalog28 + netalog29 + netalog30 + netalog31 + netalog32 + netalog33 + netalog34 +
netalog35 + netalog36 + netalog37 + netalog38 + netalog39 + netalog40 + netalog41 + netalog42 + netalog43 +
netalog44 + netalog45 + netalog46 + netalog47 + netalog48 + netalog49 + netalog50 + netalog51 + netalog52 +
netalog53 + netalog54 + netalog55 + netalog56 + netalog57 + netalog58 + netalog59 + netalog60 + netalog61 +
netalog62 + netalog63 + netalog64 + netalog65 + netalog66 + netalog67 + netalog68 + netalog69 + netalog70 +
netalog71 + netalog72 + netalog73;
            double neta_corr =Math.Exp(netalogsum);

            double j_simple_log1 = 80532114.2483677;
            double j_simple_log2 = Math.Log(Dc) * 272.235067496045;
            double j_simple_log3 = Math.Log(Pl) * 128165505.726041;
            double j_simple_log4 = Math.Log(Pt) * 149273733.158203;
            double j_simple_log5 = Math.Log(N) * 135010031.641474;
            double j_simple_log6 = Math.Log(Sh) * 13636736.3739449;
            double j_simple_log7 = Math.Log(Ns) * 3.63773799616712;
            double j_simple_log8 = Math.Log(Fp) * 149274034.837135;
            double j_simple_log9 = Math.Log(Area_min) * -16545344.3996564;
            double j_simple_log10 = Math.Log(area_totalsurfacearea) * -137291555.761334;
            double j_simple_log11 = Math.Log(Sigma) * 149273936.139906;
            double j_simple_log12 = Math.Log(phi) * 183.131491513323;
            double j_simple_log13 = Math.Log(Dh) * -132728584.193002;
            double j_simple_log14 = Math.Log(Re_Dc_MaxV) * -6665545.41733133;
            double j_simple_log15 = Math.Log(neta_corr) * -40343585.1024629;
            double j_simple_log16 = Math.Log(Dc) * Math.Log(Ns) * -3.55959802723662;
            double j_simple_log17 = Math.Log(Dc) * Math.Log(Fp) * 318.776636980344;
            double j_simple_log18 = Math.Log(Dc) * Math.Log(Area_min) * -11.4255934777327;
            double j_simple_log19 = Math.Log(Dc) * Math.Log(area_totalsurfacearea) * 2.2500361963408;
            double j_simple_log20 = Math.Log(Dc) * Math.Log(Sigma) * 349.437695309574;
            double j_simple_log21 = Math.Log(Dc) * Math.Log(Dh) * -318.945522343899;
            double j_simple_log22 = Math.Log(Dc) * Math.Log(Re_Dc_MaxV) * -4.01888102850257;
            double j_simple_log23 = Math.Log(Pl) * Math.Log(Sh) * 19673650.6203763;
            double j_simple_log24 = Math.Log(Pl) * Math.Log(Ns) * 1.60081865132162;
            double j_simple_log25 = Math.Log(Pl) * Math.Log(Area_min) * -3291476.73293169;
            double j_simple_log26 = Math.Log(Pl) * Math.Log(phi) * 11.4702587754243;
            double j_simple_log27 = Math.Log(Pl) * Math.Log(Dh) * 3291518.00624478;
            double j_simple_log28 = Math.Log(Pl) * Math.Log(Re_Dc_MaxV) * -4808169.63015303;
            double j_simple_log29 = Math.Log(Pl) * Math.Log(neta_corr) * -29101782.8324584;
            double j_simple_log30 = Math.Log(Pt) * Math.Log(N) * 3291351.08117879;
            double j_simple_log31 = Math.Log(Pt) * Math.Log(Sh) * 19673650.9386528;
            double j_simple_log32 = Math.Log(Pt) * Math.Log(Ns) * 1.94551603829848;
            double j_simple_log33 = Math.Log(Pt) * Math.Log(Area_min) * -62.4142968755059;
            double j_simple_log34 = Math.Log(Pt) * Math.Log(area_totalsurfacearea) * 195.627689413277;
            double j_simple_log35 = Math.Log(Pt) * Math.Log(Re_Dc_MaxV) * 3.37498740361868;
            double j_simple_log36 = Math.Log(Pt) * Math.Log(neta_corr) * -33.0760114228539;
            double j_simple_log37 = Math.Log(N) * Math.Log(Sh) * 19673650.8424306;
            double j_simple_log38 = Math.Log(N) * Math.Log(Fp) * 3291547.75665301;
            double j_simple_log39 = Math.Log(N) * Math.Log(area_totalsurfacearea) * -6582830.21315843;
            double j_simple_log40 = Math.Log(N) * Math.Log(Sigma) * 3291567.57426615;
            double j_simple_log41 = Math.Log(N) * Math.Log(phi) * 1.18292863770038;
            double j_simple_log42 = Math.Log(N) * Math.Log(Dh) * -3291514.11156333;
            double j_simple_log43 = Math.Log(N) * Math.Log(Re_Dc_MaxV) * -4808171.35907932;
            double j_simple_log44 = Math.Log(N) * Math.Log(neta_corr) * -29101779.8775928;
            double j_simple_log45 = Math.Log(Sh) * Math.Log(Fp) * 19673651.4245086;
            double j_simple_log46 = Math.Log(Sh) * Math.Log(area_totalsurfacearea) * -19673650.8347381;
            double j_simple_log47 = Math.Log(Sh) * Math.Log(Sigma) * 19673650.7724948;
            double j_simple_log48 = Math.Log(Sh) * Math.Log(Dh) * -19673651.2612372;
            double j_simple_log49 = Math.Log(Ns) * Math.Log(Fp) * 5.91966623115747;
            double j_simple_log50 = Math.Log(Ns) * Math.Log(Sigma) * 5.04417428146911;
            double j_simple_log51 = Math.Log(Ns) * Math.Log(phi) * -2.48344353816151;
            double j_simple_log52 = Math.Log(Ns) * Math.Log(Dh) * -5.83856283717319;
            double j_simple_log53 = Math.Log(Fp) * Math.Log(phi) * 196.464693856572;
            double j_simple_log54 = Math.Log(Fp) * Math.Log(Dh) * -164.780046282166;
            double j_simple_log55 = Math.Log(Fp) * Math.Log(neta_corr) * 4.25066727832751;
            double j_simple_log56 = Math.Log(Area_min) * Math.Log(area_totalsurfacearea) * -3291546.72909644;
            double j_simple_log57 = Math.Log(Area_min) * Math.Log(Dh) * 101.053389558153;
            double j_simple_log58 = Math.Log(Area_min) * Math.Log(Re_Dc_MaxV) * -4808172.76476217;
            double j_simple_log59 = Math.Log(Area_min) * Math.Log(neta_corr) * -29101744.9639954;
```

```
            double j_simple_log60 = Math.Log(area_totalsurfacearea) * Math.Log(Sigma) * -20.319157452861;
            double j_simple_log61 = Math.Log(area_totalsurfacearea) * Math.Log(Dh) * 3291513.23653443;
            double j_simple_log62 = Math.Log(area_totalsurfacearea) * Math.Log(Re_Dc_MaxV) * 4808171.29007918;
            double j_simple_log63 = Math.Log(area_totalsurfacearea) * Math.Log(neta_corr) * 29101779.0374533;
            double j_simple_log64 = Math.Log(Sigma) * Math.Log(phi) * 215.031152727372;
            double j_simple_log65 = Math.Log(Sigma) * Math.Log(Dh) * -33.6946332106141;
            double j_simple_log66 = Math.Log(phi) * Math.Log(Dh) * -205.121992217758;
            double j_simple_log67 = Math.Log(phi) * Math.Log(Re_Dc_MaxV) * -2.23851228811571;
            double j_simple_log68 = Math.Log(Dh) * Math.Log(Re_Dc_MaxV) * 4808173.12570148;
            double j_simple_log69 = Math.Log(Dh) * Math.Log(neta_corr) * 29101743.3651972;
            double j_simple_log70 = Math.Log(Re_Dc_MaxV) * Math.Log(neta_corr) * 0.522541619764479;

            double j_simple_log71 = Math.Log(Dc) * Math.Log(Dc) * 10.7093449301768;
            double j_simple_log72 = Math.Log(Pl) * Math.Log(Pl) * -3291421.26901198;
            double j_simple_log73 = Math.Log(N) * Math.Log(N) * 3291415.78826394;
            double j_simple_log74 = Math.Log(Fp) * Math.Log(Fp) * 62.4507604144673;
            double j_simple_log75 = Math.Log(area_totalsurfacearea) * Math.Log(area_totalsurfacearea) *
3291414.53865191;
            double j_simple_log76 = Math.Log(Sigma) * Math.Log(Sigma) * -55.7887738687927;
            double j_simple_log77 = Math.Log(phi) * Math.Log(phi) * -5.39275212863774;
            double j_simple_log78 = Math.Log(Re_Dc_MaxV) * Math.Log(Re_Dc_MaxV) * 0.0376132150756312;
            double j_simple_log79 = Math.Log(neta_corr) * Math.Log(neta_corr) * -1.89603742613159;


            double j_simple_log_sum = j_simple_log1 + j_simple_log2 + j_simple_log3 + j_simple_log4 +
j_simple_log5 + j_simple_log6 + j_simple_log7 + j_simple_log8 + j_simple_log9 + j_simple_log10 + j_simple_log11
+ j_simple_log12 + j_simple_log13 + j_simple_log14 + j_simple_log15 + j_simple_log16 + j_simple_log17 +
j_simple_log18 + j_simple_log19 + j_simple_log20 + j_simple_log21 + j_simple_log22 + j_simple_log23 +
j_simple_log24 + j_simple_log25 + j_simple_log26 + j_simple_log27 + j_simple_log28 + j_simple_log29 +
j_simple_log30 + j_simple_log31 + j_simple_log32 + j_simple_log33 + j_simple_log34 + j_simple_log35 +
j_simple_log36 + j_simple_log37 + j_simple_log38 + j_simple_log39 + j_simple_log40 + j_simple_log41 +
j_simple_log42 + j_simple_log43 + j_simple_log44 + j_simple_log45 + j_simple_log46 + j_simple_log47 +
j_simple_log48 + j_simple_log49 + j_simple_log50 + j_simple_log51 + j_simple_log52 + j_simple_log53 +
j_simple_log54 + j_simple_log55 + j_simple_log56 + j_simple_log57 + j_simple_log58 + j_simple_log59 +
j_simple_log60 + j_simple_log61 + j_simple_log62 + j_simple_log63 + j_simple_log64 + j_simple_log65 +
j_simple_log66 + j_simple_log67 + j_simple_log68 + j_simple_log69 + j_simple_log70 + j_simple_log71 +
j_simple_log72 + j_simple_log73 + j_simple_log74 + j_simple_log75 + j_simple_log76 + j_simple_log77 +
j_simple_log78 + j_simple_log79;
            double j_simple = Math.Exp(j_simple_log_sum);
            double HTC = j_simple * airinputs.AirDensity * u_max * airinputs.AirSpecificHeat / Math.Pow(Pr,
0.6666666666667);

            return HTC;
        }
```

Appendix C: Modified Slit fin DP correlation

```
    double Pl = airinputs.TubeHorizontalSpacing;
            double Pt = airinputs.TubeVerticalSpacing;
            double N = airinputs.Columns;
            double Sh = airinputs.SlitHeight;
            double Ns = airinputs.SlitCount;
            double Ft = airinputs.FinThickness;
            double Fp = airinputs.FinSpacing + Ft;
            double Rows = airinputs.Rows;
            double fins = (airinputs.TubeLength / Fp);
            double Dc = airinputs.TubeOD + 2.0 * airinputs.FinThickness;
            double area_fin = ((Pt / 2 * Pl * N) - (3.141592653589790000 / 4 * Dc * Dc) / 2 * N) * 2 + 2 * (Pt /
2 * Ft);
            double area_tube = 3.141592653589790000 * Dc * N * (Fp - Ft) / 2;
            double area_totalsurfacearea = area_fin + area_tube;
            double FPM = 1 / Fp;
            double Height = airinputs.FaceArea / airinputs.TubeLength;
            double Width = airinputs.TubeLength;
            double X_diag = Math.Sqrt(Pt * Pt / 4 + Pl * Pl);
            double two_a = (Pt - Dc) - ((Pt - Dc) * Ft * FPM);
            double two_b = ((X_diag - Dc) - (Pt - Dc) * Ft * FPM) * 2;
            double c = two_a;
            if (two_b < two_a)
            {
                c = two_b;
            }
            double min_free_flow_area_OTS = (((Height / Pt) - 1) * c + (Pt - Dc) - (Pt - Dc) * Ft * FPM) *
Width;
            //Min Area Caculations-End
            double Area_min = min_free_flow_area_OTS / Rows / fins / 2;
            double Area_Frontal = Pt / 2 * Fp;
            double Sigma = Area_min / Area_Frontal;
            double u_max = airinputs.AirAvgVelocity / Sigma;
            double rho_in = airinputs.AirDensity;
            double Re_Dc_MaxV = rho_in * u_max * Dc / airinputs.AirViscosity;
            double Depth_HX = Pl * N;
            double Dh = 4 * Area_min * Depth_HX / area_totalsurfacearea;
            double Xl = 0.5 * Math.Pow(Pt * Pt / 4 + Pl * Pl, 0.5);
            double Req = 1.27 * (Pt / 2) / (Dc / 2) * Math.Pow(Xl / (Pt / 2) - 0.3, 0.5);
            double phi = (Req - 1) * (1 + 0.35 * Math.Log(Req));
            double G_c = u_max * rho_in;


          double f_simplelog1 =  9.57655362393778730000000000;
            double f_simplelog2 = Math.Log(Dc) * 0.49001686400881722000000000;
            double f_simplelog3 = Math.Log(Pl) * -0.08820407806899437100000000;
            double f_simplelog4 = Math.Log(Pt) * -0.07071586732786344600000000;
            double f_simplelog5 = Math.Log(N) * 0.08580095140774812700000000;
            double f_simplelog6 = Math.Log(Sh) * -1.19008716550821680000000000;
            double f_simplelog7 = Math.Log(Ns) * -0.95434198351847177000000000;
            double f_simplelog8 = Math.Log(Fp) * 2.77251742645646490000000000;
            double f_simplelog9 = Math.Log(Re_Dc_MaxV) * -1.19807363525699650000000000;
            double f_simplelog10 = Math.Log(Dc) * Math.Log(Pl) * -0.18292595479673554000000000;
            double f_simplelog11 = Math.Log(Dc) * Math.Log(Pt) * 0.57764897838606610000000000;
            double f_simplelog12 = Math.Log(Dc) * Math.Log(N) * 0.05652843890559729200000000;
            double f_simplelog13 = Math.Log(Dc) * Math.Log(Ns) * -0.14461295650727943000000000;
            double f_simplelog14 = Math.Log(Dc) * Math.Log(Fp) * -0.09542197222128837000000000;
            double f_simplelog15 = Math.Log(Dc) * Math.Log(Re_Dc_MaxV) * -0.06801573226582848000000000;
            double f_simplelog16 = Math.Log(Pl) * Math.Log(N) * -0.01569432416936200300000000;
            double f_simplelog17 = Math.Log(Pl) * Math.Log(Sh) * -0.04490654977892477600000000;
            double f_simplelog18 = Math.Log(Pl) * Math.Log(Ns) * -0.09085588621173659700000000;
            double f_simplelog19 = Math.Log(Pl) * Math.Log(Fp) * -0.09348416386626622100000000;
            double f_simplelog20 = Math.Log(Pl) * Math.Log(Re_Dc_MaxV) * -0.11416568619876205000000000;
            double f_simplelog21 = Math.Log(Pt) * Math.Log(Sh) * -0.17928373971065767000000000;
            double f_simplelog22 = Math.Log(Pt) * Math.Log(Ns) * 0.09897802608589605100000000;
            double f_simplelog23 = Math.Log(Pt) * Math.Log(Fp) * -0.07049598401315838900000000;
            double f_simplelog24 = Math.Log(Pt) * Math.Log(Re_Dc_MaxV) * -0.05396153703084426900000000;
            double f_simplelog25 = Math.Log(N) * Math.Log(Sh) * 0.01635373936302218100000000;
            double f_simplelog26 = Math.Log(N) * Math.Log(Ns) * 0.01213468694673214400000000;
            double f_simplelog27 = Math.Log(N) * Math.Log(Fp) * -0.05145325472847782400000000;
            double f_simplelog28 = Math.Log(N) * Math.Log(Re_Dc_MaxV) * -0.01729479701296401600000000;
            double f_simplelog29 = Math.Log(Sh) * Math.Log(Ns) * 0.08312664348457410300000000;
            double f_simplelog30 = Math.Log(Sh) * Math.Log(Fp) * 1.52490760226788870000000000;
            double f_simplelog31 = Math.Log(Sh) * Math.Log(Re_Dc_MaxV) * 0.04548813266682727500000000;
            double f_simplelog32 = Math.Log(Ns) * Math.Log(Fp) * -0.09854500569494510600000000;
            double f_simplelog33 = Math.Log(Ns) * Math.Log(Re_Dc_MaxV) * 0.04027280911409156900000000;
```

```
            double f_simplelog34 = Math.Log(Fp) * Math.Log(Re_Dc_MaxV) * 0.15562374127850595000000000;
            double f_simplelog35 = Math.Log(Dc )* Math.Log(Dc) * -0.12441925235277188000000000;
            double f_simplelog36 = Math.Log(Pl)* Math.Log(Pl) * 0.19238868743590706000000000;
            double f_simplelog37 = Math.Log(Pt) * Math.Log(Pt) * -0.25068868842959702000000000;
            double f_simplelog38 = Math.Log(Sh) * Math.Log(Sh) * -0.69121157926251642000000000;
            double f_simplelog39 = Math.Log(Ns) * Math.Log(Ns) * 0.08498761727245654500000000;
            double f_simplelog40 = Math.Log(Fp) * Math.Log(Fp) * -0.44791694001349291000000000;
            double f_simplelog41 = Math.Log(Re_Dc_MaxV) * Math.Log(Re_Dc_MaxV) * 0.06281211510127858400000000;

            double f_simplelogsum = f_simplelog1 + f_simplelog2 + f_simplelog3 + f_simplelog4 + f_simplelog5 +
f_simplelog6 + f_simplelog7 + f_simplelog8 + f_simplelog9 + f_simplelog10 + f_simplelog11 +
           f_simplelog12 + f_simplelog13 + f_simplelog14 + f_simplelog15 + f_simplelog16 + f_simplelog17 +
f_simplelog18 + f_simplelog19 + f_simplelog20 + f_simplelog21 + f_simplelog22 + f_simplelog23 +
           f_simplelog24 + f_simplelog25 + f_simplelog26 + f_simplelog27 + f_simplelog28 + f_simplelog29 +
f_simplelog30 + f_simplelog31 + f_simplelog32 + f_simplelog33 + f_simplelog34 + f_simplelog35 +
           f_simplelog36 + f_simplelog37 + f_simplelog38 + f_simplelog39 + f_simplelog40 + f_simplelog41;
double f = Math.Exp(f_simplelogsum);
            double DP = (f * area_totalsurfacearea / (Area_min)) * (Math.Pow(G_c, 2.0) / (2.0 * rho_in));
//simplified expression without iteration
            return DP;
```

Appendix D: Slit Experimental Data HTC Summary

Coil#	Test#	ReDc	HTC CFD correlation [W/m^2K]	HTCconductionAvgHeatload [W/m^2K]	HTC_no_conduction [W/m^2K]
1	1	1265.691986	195.5219	111.8223306	111.98
1	2	1266.786841	195.5782	112.823237	112.76
1	3	1267.053191	195.5806	113.7299662	112.98
1	4	1954.112924	222.6726	124.7182827	125.09
1	5	1953.882943	222.6693	125.6755232	125.64
1	6	1952.457353	222.6284	126.5266928	126.08
1	7	527.8449115	136.6515	85.73205025	85.573
1	8	526.9934027	136.542	87.13928169	86.915
1	9	526.7766734	136.5185	89.85427298	88.695
2	1	1307.004201	196.8687	102.0750335	100.23
2	2	1306.367902	196.8363	101.9965232	98.631
2	3	1306.995238	196.8579	104.3672641	97.926
2	4	2021.416816	221.0497	118.7082032	111.86
2	5	2025.848451	221.1602	115.4969413	110.36
2	6	2020.437164	221.0141	115.5108505	109.26
2	7	553.6829716	145.343	86.79054893	83.309
2	8	559.9227165	146.027	87.60608066	81.144
2	9	558.4739176	145.8579	83.52688049	77.475
3	1	1237.86224	173.519	101.8266128	103.26
3	2	1237.925716	173.5143	102.58425	103.89
3	3	1238.531691	173.531	103.2736433	104.37
3	4	1909.359875	194.4066	117.0988755	119.64
3	5	1918.857646	194.597	117.8342724	120.12
3	6	1915.913249	194.5199	118.3963991	120.38
3	7	514.7648786	131.1926	79.33278442	80.435
3	8	515.2222255	131.2314	80.79506841	81.648
3	9	515.6060407	131.2662	82.2250348	82.754
4	1	1263.618973	178.0196	102.2659065	103.55
4	2	1262.640712	177.9834	101.6056553	103.22
4	3	1260.765111	177.9134	100.7957225	102.49
4	4	1953.437786	199.1551	115.210187	117.26
4	5	1953.216436	199.1391	114.4286589	116.55
4	6	1953.053041	199.1299	113.6508707	115.83
4	7	527.7038263	137.0848	81.17841792	82.313
4	8	528.2893738	137.1327	80.56241375	81.821
4	9	528.1327053	137.1167	79.51533002	80.85
5	1	1392.687343	183.2094	148.4105221	144.06
5	2	1389.752018	183.1144	147.4069274	145.69
5	3	1387.254615	183.0257	146.6007746	146.36
5	4	2165.744446	202.0861	172.5359156	168.1
5	5	2158.531544	201.9737	170.2707599	169.01
5	6	2155.625699	201.929	169.9965194	169.92
5	7	571.370977	137.2053	107.8394713	104.38
5	8	569.2627683	137.0217	109.6182705	107.88
5	9	568.02489	136.9174	110.0164102	109.35
6	1	1349.801599	182.5215	148.8085962	145.82
6	2	1352.679753	182.6697	148.122697	145.89
6	3	1352.858261	182.6791	147.6662334	146.79
6	4	2078.208924	206.0667	169.8285331	167.83
6	5	2081.989989	206.1464	170.3132108	169.25
6	6	2081.484788	206.1362	170.3177841	170.4
6	7	566.9013107	128.8554	112.2194958	106.92
6	8	567.8333403	128.9587	110.2335927	106.81
6	9	567.7100311	128.9422	106.7363943	105.09
7	1	1433.887506	216.9759	173.6703245	154.31
7	2	1429.057835	216.7215	173.3584106	160.99
7	3	1425.331843	216.5082	172.6225633	164
7	4	2226.276991	245.6628	199.5014482	179.2
7	5	2217.845838	245.4625	198.6209385	186.02
7	6	2212.63556	245.5595	199.8295338	191.05
7	7	587.4728308	145.23	139.2240178	112.29

7	8	585.1261976	144.896	138.1279746	117.98
7	9	583.7375772	144.7005	135.3640708	120.21
8	1	1412.328249	218.4208	196.9002068	160.23
8	2	1411.848177	218.3816	193.7525704	161.17
8	3	1410.476079	218.2865	190.2582371	162.26
8	4	2172.306768	255.8744	221.9838454	191.43
8	5	2170.642777	255.7837	218.4772704	191.99
8	6	2169.431307	255.7578	216.3116114	194.11
8	7	589.2571462	134.2734	123.3528419	90.54
8	8	588.9271454	134.2238	111.7833398	88.953
8	9	587.9024381	134.0595	110.6907668	90.825

Appendix E: Louver Experimental Data HTC Summary

Coil#	Test#	ReDc	HTC CFD correlation [W/m^2K]	HTCconductionAvgHeatload [W/m^2K]	HTC_no_conduction [W/m^2K]
9	1	1313.49533	141.6791	120.2344039	116.68
9	2	1314.765495	141.7339	116.3862512	115.93
9	3	1315.405488	141.7584	119.6963772	114.8
9	4	2035.890374	171.1489	136.4490063	137.84
9	5	2034.824541	171.1071	141.9626207	137.03
9	6	2034.497442	171.0924	153.4334583	135.34
9	7	557.3548734	100.1899	86.22487294	86.406
9	8	557.5793479	100.2102	88.67105048	89.298
9	9	557.3487566	100.1807	92.82042801	87.738
10	1	1306.079647	135.8453	107.3289216	115.23
10	2	1311.09291	136.0442	109.5863018	115.07
10	3	1311.081199	136.0347	110.1469689	114.2
10	4	2035.57779	161.3229	139.5702558	135.89
10	5	2035.5565	161.2882	141.2802042	134.5
10	6	2044.675723	161.5645	125.2970862	133.14
10	7	568.2292729	97.5039	82.42822496	88.223
10	8	557.3046627	96.7256	82.67714943	87.834
10	9	566.9429701	97.38	92.67971871	88.392
11	1	1343.536501	149.7504	131.7719756	128.5
11	2	1341.82021	149.6783	135.280644	128.8
11	3	1343.944184	149.7577	144.6047011	130.49
11	4	2074.766642	176.9774	155.4617234	152.19
11	5	2074.245287	176.9526	160.1998114	152.93
11	6	2074.787172	176.9701	173.9451504	156.32
11	7	570.3979539	108.688	102.8111663	98.968
11	8	570.8227891	108.7039	105.3146806	98.18
11	9	571.4067134	108.7381	110.8394484	97.323
12	1	1340.394675	142.9548	126.8261451	127.28
12	2	1339.890863	142.9383	135.0994569	126.9
12	3	1340.010382	142.9205	117.6322622	125.2
12	4	2063.39282	167.0952	147.6149593	146.46
12	5	2078.040001	167.5045	164.7881639	146.81
12	6	2083.976631	167.6702	148.1489624	145.24
12	7	572.8597964	102.5879	94.04426435	98.03
12	8	573.1621757	102.5967	103.2590658	97.466
12	9	572.6561321	102.5554	91.24104942	96.923
13	1	1346.112148	140.2047	200.8487384	105.92
13	2	1346.176775	140.1946	219.9871821	101.45
13	3	1350.51772	140.2995	364.1445339	94.582
13	4	2088.040171	167.0702	222.0566556	121.32
13	5	2085.353032	166.9738	291.4082225	116.19
13	6	2085.093146	166.9723	427.0284115	109.73
13	7	570.5416642	102.8246	170.564506	80.175
13	8	570.6297504	102.8197	197.5237523	76.263
13	9	571.4807279	102.8552	349.2595843	70.815
14	1	1289.384752	156.6248	116.9028102	120.5
14	2	1289.698858	156.6383	118.6080466	120.26
14	3	1290.315994	156.6642	125.2690135	119.63
14	4	1994.803648	192.0078	136.5292947	137.79
14	5	1997.474896	192.086	145.2427904	137.04
14	6	1996.608542	192.0835	132.3335821	136.62
14	7	546.8713212	112.158	92.87800241	93.826
14	8	546.9556173	112.1608	92.93691466	93.317
14	9	547.1362518	112.1669	95.78919307	92.873
15	1	1340.634661	138.8944	180.5626591	105
15	2	1354.222953	139.4265	220.6780876	103.06
15	3	1341.157594	138.9074	276.8468638	97.034
15	4	2074.92064	165.133	217.441172	120.65
15	5	2075.825926	165.1581	248.7520469	117.6
15	6	2076.424093	165.1769	334.1655824	112.88
15	7	568.7202031	102.3926	140.4835939	79.107

15	8	569.0222044	102.401	167.1977129	76.049
15	9	569.3997425	102.4179	230.0276712	71.675
16	1	1293.381787	155.6568	121.2408965	118.45
16	2	1294.697619	155.7264	118.9280304	117.69
16	3	1295.19902	155.747	120.5232911	116.31
16	4	1996.203249	192.8498	138.3406111	136.34
16	5	1998.32936	192.9626	133.1698463	135.65
16	6	1997.59204	192.918	146.4099196	134.3
16	7	549.1450167	109.7978	92.37392021	92.192
16	8	549.5449113	109.8225	93.02624049	91.437
16	9	549.9481122	109.8443	96.27609048	90.789

Appendix F: Slit Experimental Data DP Summary

Coil#	*Test#*	*ReDc*	*ADP Experiment [Pa]*	*ADP Correlation [Pa]*
1	1	1303.159822	54.63	67.5391
1	2	1302.735529	54.55	67.4972
1	3	1302.612082	54.53	67.4627
1	4	2017.062244	105.77	128.3456
1	5	2014.558378	105.59	128.1309
1	6	2016.289535	105.39	128.2637
1	7	552.3493383	16.42	20.5093
1	8	552.7498564	16.43	20.5173
1	9	552.2641846	16.39	20.4879
2	1	1307.004201	32	34.5996
2	2	1306.367902	31.88	34.5704
2	3	1306.995238	31.79	34.5889
2	4	2021.416816	62.62	66.0634
2	5	2025.848451	62.64	66.2687
2	6	2020.437164	62.52	65.9991
2	7	553.6829719	9.14	10.3831
2	8	559.9227156	9.13	10.5344
2	9	558.4739184	9.09	10.4947
3	1	1262.350123	36.64	43.2652
3	2	1263.193465	36.53	43.29
3	3	1262.431858	36.48	43.2552
3	4	1951.924425	73.82	83.8073
3	5	1951.211401	73.7	83.7823
3	6	1960.10265	73.68	84.361
3	7	536.2277203	10.03	12.6493
3	8	537.0554782	10	12.6515
3	9	537.3836146	9.99	12.6255
4	1	1275.36508	20.45	24.1632
4	2	1275.288502	20.4	24.1469
4	3	1276.840541	20.32	24.1846
4	4	1970.394295	41.51	46.8635
4	5	1971.168782	41.45	46.8906
4	6	1968.925963	41.38	46.816
4	7	542.2230637	5.25	7.045
4	8	543.0012465	5.25	7.056
4	9	544.9579634	5.23	7.0882
5	1	1390.48286	28.37318954	31.9673
5	2	1387.229505	28.52715271	31.8709
5	3	1384.183243	28.5722622	31.7812
5	4	2156.962887	54.6904315	61.2936
5	5	2151.339748	54.89182934	61.0395
5	6	2149.041651	54.90592461	60.9389
5	7	568.6689337	8.235286332	9.1923
5	8	566.7855719	8.334974647	9.1527
5	9	565.7432897	8.328514214	9.1303
6	1	1393.907934	47.66556063	61.3443
6	2	1386.720213	47.94680894	60.8881
6	3	1387.283038	48.20259709	60.9115
6	4	2174.035707	91.51561987	118.3414
6	5	2165.439089	91.70279942	117.6554
6	6	2161.665014	91.7910531	117.3645
6	7	560.1463289	15.03169021	17.3591
6	8	557.4169567	15.17063668	17.2492
6	9	555.6420418	15.16933511	17.1796
7	1	1433.887506	44.09271341	55.9107
7	2	1429.057835	44.30621565	55.6293
7	3	1425.331842	44.42851007	55.3888
7	4	2226.276992	80.58803785	104.7396
7	5	2217.84584	80.89403643	104.2134
7	6	2212.63556	81.30221399	104.1769
7	7	587.4728302	14.48783496	16.825
7	8	585.1261968	14.63024285	16.7418

7	9	583.7375773	14.68506407	16.6951
8	1	2163.442867	159.5	189.0594
8	2	2161.984817	159.09	188.8522
8	3	2162.481073	158.74	188.8721
8	4	1446.354393	92.17	107.2124
8	5	1446.203582	91.89	107.1684
8	6	1449.828556	91.69	107.4902
8	7	613.1621771	30.88	34.2609
8	8	613.8073694	30.73	34.2846
8	9	614.2141267	30.42	34.2997

Appendix G: Louver Experimental Data DP Summary

Coil#	Test#	ReDc	ADP Experiment [Pa]	ADP Correlation [Pa]
9	1	1313.49533	18.61	20.4573
9	2	1314.765495	18.54	20.4873
9	3	1315.405488	18.5	20.4998
9	4	2035.890374	38.83	42.8418
9	5	2034.824541	38.78	42.7996
9	6	2034.497442	38.67	42.7839
9	7	557.3548734	4.61	5.4233
9	8	557.5793479	4.61	5.4279
9	9	557.3487566	4.58	5.4196
10	1	1306.079647	35.28	38.6815
10	2	1311.09291	35.28	38.9162
10	3	1311.081199	35.13	38.901
10	4	2035.57779	72.92	81.4573
10	5	2035.5565	72.87	81.3974
10	6	2044.675723	72.68	82.0273
10	7	568.2292729	9.18	10.7312
10	8	557.3046627	9.19	10.4257
10	9	566.9429701	9.15	10.6745
11	1	1343.536501	26.57	27.706
11	2	1341.82021	26.53	27.6511
11	3	1343.944184	26.41	27.7087
11	4	2074.766642	53.83	56.1095
11	5	2074.245287	53.75	56.0722
11	6	2074.787172	53.62	56.0959
11	7	570.3979539	7.18	7.7596
11	8	570.8227891	7.15	7.7621
11	9	571.4067134	7.2	7.7704
12	1	1340.394675	50.83	53.2975
12	2	1339.890863	50.71	53.2734
12	3	1340.010382	50.59	53.233
12	4	2063.39282	102.14	106.7956
12	5	2078.040001	102.04	108.0292
12	6	2083.976631	101.72	108.5327
12	7	572.8597964	14.44	15.2225
12	8	573.1621757	14.44	15.2223
12	9	572.6561321	14.31	15.2002
13	1	1346.112148	44.27	40.3665
13	2	1346.176775	44.08	40.3486
13	3	1350.51772	44.02	40.4341
13	4	2088.040171	85.34	80.8112
13	5	2085.353032	85.08	80.6209
13	6	2085.093146	84.99	80.6242
13	7	570.5416642	13.2	11.6516
13	8	570.6297504	13.3	11.6474
13	9	571.4807279	13.35	11.6606
14	1	1289.384752	23.03	19.2292
14	2	1289.698858	22.96	19.2343
14	3	1290.315994	22.96	19.244
14	4	1994.803648	47.52	39.3982
14	5	1997.474896	47.45	39.4306
14	6	1996.608542	47.39	39.4469
14	7	546.8713212	5.77	5.2839
14	8	546.9556173	5.73	5.2843
14	9	547.1362518	5.77	5.285
15	1	1340.634661	40.6	39.5209
15	2	1354.222953	40.46	40.139
15	3	1341.157594	40.29	39.5326
15	4	2074.92064	79.43	79.6533
15	5	2075.825926	79.27	79.6984
15	6	2076.424093	79.17	79.7343
15	7	568.7202031	11.66	11.2396
15	8	569.0222044	11.66	11.2418

15	9	569.3997425	11.59	11.2487
16	1	1293.381787	22.31	19.0556
16	2	1294.697619	22.27	19.084
16	3	1295.19902	22.25	19.0907
16	4	1996.203249	46.45	39.0648
16	5	1998.32936	46.37	39.1418
16	6	1997.59204	46.38	39.1087
16	7	549.1450167	5.58	5.1998
16	8	549.5449113	5.47	5.2043
16	9	549.9481122	5.52	5.208

References

Abdelaziz, O., Aute, V., Azarm, S., and Radermacher, R. (2010). Approximation-Assisted Optimization for Novel Compact Heat Exchanger Designs. HVAC&R Research *16*, 707–728.

AHRI (2001). Standard 410-2001: Forced-Circulation Air-Cooling and Air-Heating Coils.

ANSI/ASHRAE (1992). Standard 41.2: Standard Methods for Laboratory Airflow Measurement.

ANSI/ASHRAE (2016). Standard 33-2016: Methods of Testing Forced-Circulation Air-Cooling and Air-Heating Coils.

Aute, V., Saleh, K., Abdelaziz, O., Azarm, S., and Radermacher, R. (2013). Cross-validation based single response adaptive design of experiments for Kriging metamodeling of deterministic computer simulations. Struct Multidisc Optim *48*, 581–605.

Bacellar, D., Aute, V., and Radermacher, R. (2014). CFD-Based Correlation Development For Air Side Performance Of Finned And Finless Tube Heat Exchangers With Small Diameter Tubes. (Purdue University), p.

Bacellar, D., Aute, V., and Radermacher, R. (2015). CFD-BASED CORRELATION DEVELOPMENT FOR AIR SIDE PERFORMANCE OF SMALL DIAMETER TUBE-FIN HEAT EXCHANGERS WITH WAVY FINS. The 24th IIR International Congress of Refrigeration.

Bacellar, D., Aute, V., and Radermacher, R. (2016a). CFD-Based Correlation Development for Air Side Performance of Wavy Fin Tube Heat Exchangers using Small Diameter Tubes. p.

Bacellar, D., Aute, V., Huang, Z., and Radermacher, R. (2016b). Airside friction and heat transfer characteristics for staggered tube bundle in crossflow configuration with diameters from 0.5 mm to 2.0 mm. International Journal of Heat and Mass Transfer *98*, 448–454.

Bestani, A., Mitra, N.K., and Fiebig, M. (1990). Numerical simulation of flow field in a fin tube heat exchanger. ASME Journal of Fluids Engineering *101*, 91–96.

Cavallini, A., Censi, G., Del Col, D., Doretti, L., Longo, G.A., Rossetto, L., and Zilio, C. (2003). Condensation inside and outside smooth and enhanced tubes — a review of recent research. International Journal of Refrigeration *26*, 373–392.

Churchill, S.W. (1977). Frictional Equation Spans all Fluid Flow Regimes. Chem. Eng. *84*, 91–92.

ElSherbini, A.I., Jacobi, A.M., and Hrnjak, P.S. (2003). Experimental investigation of thermal contact resistance in plain-fin-and-tube evaporators with collarless fins. International Journal of Refrigeration *26*, 527–536.

Fernández-Seara, J., Uhía, F.J., Sieres, J., and Campo, A. (2007). A general review of the Wilson plot method and its modifications to determine convection coefficients in heat exchange devices. Applied Thermal Engineering *27*, 2745–2757.

Friedel, L. (1979). Improved Friction Pressure Drop Correlations for Horizontal and Vertical Two Phase Pipe Flow. European Two Phase Flow Group Meeting, Ispra, Italy Paper E2.

Gao, Y. (2013). FIN DESIGN FOR FIN-AND-TUBE HEAT EXCHANGER WITH MICROGROOVE SMALL DIAMETER TUBES FOR AIR CONDITIONER. 4th IIR Conference on Thermophysical Properties and Transfer Processes of Refrigerants, Delft, The Netherlands.

Gnielinski, V. (1976). New Equations for Heat and MAss Transfer in Turbulent Pipe and Channel Flow. International Chemical Engineering *16*, 359–368.

Huang, Z., and Gao, L. (2016). ICA Coil Testing.

Huang, X., Ding, G., Hu, H., Zhu, Y., Gao, Y., and Deng, B. (2010). Condensation heat transfer characteristics of R410A–oil mixture in 5 mm and 4 mm outside diameter horizontal microfin tubes. Experimental Thermal and Fluid Science *34*, 845–856.

Jang, J.-Y., and Chen, C.-C. (2015). Optimization of louvered-fin heat exchanger with variable louver angles. Applied Thermal Engineering *91*, 138–150.

Kim, N.H., Youn, B., and Webb, R.L. (1999). Air-Side Heat Transfer and Friction Correlations for Plain Fin-and-Tube Heat Exchangers With Staggered Tube Arrangements. J. Heat Transfer *121*, 662–667.

Klein, S.A. (2017). Engineering Equation Solver (FChart Software).

Kline, S.J., and McClintock, F.A. (1953). Describing Uncertainties in Single-Sample Experiments. Mechanical Engineering *3*, 3–8.

Kong, Y.Q., Yang, L.J., Du, X.Z., and Yang, Y.P. (2016). Air-side flow and heat transfer characteristics of flat and slotted finned tube bundles with various tube pitches. International Journal of Heat and Mass Transfer *99*, 357–371.

Koyama, S., and Yonemoto, R. (2006). Experimental Study on Condensation of Pure Refrigerants in Horizontal Micro-Fin Tube – Proposal of Correlations for Heat Transfer Coefficient and Frictional Pressure Drop. (Purdue University), p.

Li, S., and et al. (2014). Third Group Final Report: Abroad Intensive Training at CEEE.

Liebenberg, L., and Meyer, J. (2006). The characterization of flow regimes with power spectral density distributions of pressure fluctuations during condensation in smooth and micro-fin tubes. Experimental Thermal and Fluid Science *31*, 127–140.

Lophaven, S.N., Nielsen, H.B., and Søndergaard, J. (2002). DACE – A MATLAB Kriging Toolbox.

Lucon, O., Ürge-Vorsatz, D., Zain Ahmed, A., Akbari, H., Bertoldi, P., Cabeza, L.F., Eyre, N., Gadgil, A., Harvey, L.D.D., Jiang, Y., et al. (2014). Buildings. In Climate Change 2014: Mitigation of Climate Change. Contribution of Working Group III to the Fifth Assessment Report of the Intergovernmental Panel on Climate Change [Edenhofer, O., R. Pichs-Madruga, Y. Sokona, E. Farahani, S. Kadner, K. Seyboth, A. Adler, I. Baum, S. Brunner, P. Eickemeier, B. Kriemann, J. Savolainen, S. Schlömer, C. von Stechow, T. Zwickel and J.C. Minx (Eds.)]. Cambridge University Press, Cambridge, United Kingdom and New York, NY, USA., p.

MathWorks Inc. (2016). MATLAB (Natick, Massachusetts, United States.).

Miyara, A., Nonaka, K., and Taniguchi, M. (2000). Condensation heat transfer and flow pattern inside a herringbone-type micro-fin tube. International Journal of Refrigeration *23*, 141–152.

Nasuta, D., Sarpotdar, S., and Martin, C. (2017). Comparative Study of Optimized Small Diameter Tube-Fin Heat Exchangers Vs. Traditional, Larger Diameter Tube-Fin Heat Exchanger Designs. (Las Vegas, NV), p.

Ravigururajan, T.S., and Bergles, A.E. (1985). General Correlations for Pressure Drop and Heat Transfer for Single-Phase Turbulent Flow in Internally Ribbed Tubes. Augmentation of Heat Transfer in Energy Systems, ASME HTD *52*, 9–20.

Roache, P.J. (1997). Quantification of Uncertainty in Computational Fluid Dynamics. Annual Review of Fluid Mechanics *29*, 123.

Sarpotdar, S., Nasuta, D., and Aute, V. (2016a). CFD-Based Airside Heat Transfer and Pressure Drop Correlation Development for Small Diameter (3 mm to 5 mm) Louver Fin Heat Exchangers. 16th International Refrigeration and Air Conditioning Conference at Purdue, July 11-14, 2016.

Sarpotdar, S., Nasuta, D., and Aute, V. (2016b). CFD Based Comparison of Slit Fin and Louver Fin Performance for Small Diameter (3mm to 5 mm) Heat Exchangers. 16th International Refrigeration and Air Conditioning Conference at Purdue, July 11-14, 2016.

Schlager, L.M., Pate, M.B., and Bergles, A.E. (1989). Heat transfer and pressure drop during evaporation and condensation of R22 in horizontal micro-fin tubes. International Journal of Refrigeration *12*, 6–14.

Shah, M.M. (2013). General Correlation For Heat Transfer During Condensation in Plain Tubes: Further Development and Verification. ASHRAE Annual Conference.

Shah, M.M. (2014). Evaluation of a method for predicting heat transfer during boiling of mixtures in plain tubes. 15th International Heat Transfer Conference, IHTC-15, Kyoto, Japan.

Shewry, M.C., and Wynn, H.P. (1987). Maximum entropy sampling. Journal of Applied Statistics *14*, 165–170.

Singh, V. (2009). DEVELOPMENT OF AN ADVANCED HEAT EXCHANGER MODEL FOR STEADY STATE AND FROSTING CONDITIONS.

Sun, L., and Zhang, C.-L. (2014). Evaluation of elliptical finned-tube heat exchanger performance using CFD and response surface methodology. International Journal of Thermal Sciences *75*, 45–53.

Taler, D., and Ocłoń, P. (2014). Determination of heat transfer formulas for gas flow in fin-and-tube heat exchanger with oval tubes using CFD simulations. Chemical Engineering and Processing: Process Intensification *83*, 1–11.

US Energy Information Administration (2009). Residential Energy Consumption Survey, Table CE3.1 Household Site End-Use Consumption in the U.S., Totals and Averages, 2009.

US EPA (2013). Inventory of U.S. Greenhouse Gas Emissions and Sings: 1990-2011.

Wang, C.-C., and Chi, K.-Y. (2000). Heat transfer and friction characteristics of plain fin-and-tube heat exchangers, part I: new experimental data. International Journal of Heat and Mass Transfer *43*, 2681–2691.

Wang, C.-C., Lee, C.-J., Chang, C.-T., and Lin, S.-P. (1999). Heat transfer and friction correlation for compact louvered fin-and-tube heat exchangers. International Journal of Heat and Mass Transfer *42*, 1945–1956.

Wang, C.-C., Webb, R., and Chi, K.-Y. (2000). Data reduction for air-side performance of fin-and-tube heat exchangers. Experimental Thermal and Fluid Science *21*, 218–226.

Wang, C.-C., Lee, W.-S., and Sheu, W.-J. (2001). A comparative study of compact enhanced fin-and-tube heat exchangers. International Journal of Heat and Mass Transfer *44*, 3565–3573.

Wang, C.-C., Hwang, Y.-M., and Lin, Y.-T. (2002). Empirical correlations for heat transfer and flow friction characteristics of herringbone wavy fin-and-tube heat exchangers. International Journal of Refrigeration *25*, 673–680.

Wilson, E.E. (1915). A basis of rational design of heat transfer apparatus. ASME Journal of Heat Transfer *37*, 47–70.

Wu, Z., and Wu, Y. (2013). Convective Vaporization in Micro-fin Tubes of Different Geometries. Experimental Thermal and Fluid Science *44*, 398–408.

Wu, W., Ding, G., Zheng, Y., and Song, J. (2012). Principle of Designing Fin-and-Tube Heat Exchanger With Smaller Tube for Air Condition. International Refrigeration and Air Conditioning Conference at Purdue.

Wu, Z., Sunden, B., Wadeker, V., and Li, W. (2015). Heat Transfer Correlations for Single-Phase Flow, Condensation, and Boiling in Microfin Tubes. Heat Transfer Engineering *36*, 582–595.

Xie, G., Wang, Q., and Sunden, B. (2009). Parametric study and multiple correlations on air-side heat transfer and friction characteristics of fin-and-tube heat exchangers with large number of large-diameter tube rows. Applied Thermal Engineering *29*, 1–16.

Yu, J., and Koyama, S. (1998). Condensation Heat Transfer of Pure Refrigerants in Microfin Tubes. Proceedings of the International Refrigeration Conference, Purdue, West Lafayette, In.